A Systems Approach to Elucidate Personalized Mechanistic Complexities of Antibody-Fc Receptor Activation Post-vaccination

by

Melissa Marie Lemke

A dissertation submitted in partial fulfillment
of the requirements for the degree of
Doctor of Philosophy
(Biomedical Engineering)
in the University of Michigan
2022

Doctoral Committee:

Assistant Professor Kelly B. Arnold
Professor Kathleen Collins
Professor Santiago Schnell, University of Notre Dame
Associate Professor Ariella Shikanov

Melissa Marie Lemke

lemkem@umich.edu

ORCID iD: 0000-0003-1860-4550

Dedication

This dissertation is dedicated to my family, specifically: Theresa, Mark, Jessica, Joan, Margret, Harry, John, and Max.

Acknowledgments

I want to thank:

- My committee, for being there to push and support me past milestones
- Dr. Kelly Arnold, for being there to see me through it all
- Dr. Amy Chung, for being there at midnight meetings
- Katy, for being there in our office until *the dark days* (but also always)
- Kat, for being there to *brighten* the *days* again
- Christina, for being there through flamingo frenzies and puppy playdates
- Suzie, for being there at 8 am and 2 pm every - single - day for weeks
- Robby, for being there to keep the fridge stocked
- Tiff, for being there to keep me up too late and keep me sane
- Ashley, for being there like nothing has changed when everything always will
- Maekena, for being there to look at me sideways
- Olive, for being there… right there, following me, everywhere, all the time
- Phil, for being there to take Olive on her morning walks so I can sleep in
- My mom and dad, for being there since the beginning

  and
- Jess, for showing up late but being worth the wait

Table of Contents

Dedication ii

Acknowledgments iii

List of Tables ix

List of Figures x

Abstract xiii

Chapter 1 Introduction 1

1.1 The emerging threat of antigenically variable viruses 1

1.2 Only one of many HIV vaccine trials has been moderately protective at 31% efficacy 4

1.3 Fc-mediated cellular immunity has been linked with protection in HIV vaccine trials 7

1.4 Systems serology combining diverse datasets has highlighted a relationship between ADCC and IgGs in protective vaccine responses 8

1.5 Mechanistic modeling will give new insight into personalized differences in Fc-mediated vaccine responses 10

1.6 Structure of thesis 12

Chapter 2 A Systems Approach to Elucidate Personalized Mechanistic Complexities of Antibody-Fc Receptor Activation Post-vaccination 15

2.1 Abstract 16

2.2 Introduction 16

2.3 Results 18

2.3.1 Model predictions of IgG-FcR complex formation validated in an Fc multiplex assay 18

2.3.2 Sensitivity analysis highlights the importance of IgG1 and IgG3 for HIV env activation of FcγRIIIa 21

2.3.3 Model reveals personalized differences in the benefit of increasing IgG1 22

2.3.4 Experimental validation of IgG1 sensitivity predictions 25

2.3.5 IgG1 allotype may significantly influence IgG-FcR complex formation 26

2.3.6 IgG1 binding affinity for FcR is important for increasing FcγRIIIa complex formation broadly across a population 28

2.3.7 The model reveals synergistic effects of combined changes in IgG1 concentration and IgG1 FcγRIIIa binding affinity 31

2.4 Discussion 33

2.4.1 Limitations of the study 35

2.5 STAR Methods 35

2.5.1 Key Resources Table 35

2.5.2 Resource Availability 36

2.5.3 Experimental Model and Subject Details 37

2.5.4 Method Details 37

Chapter 3 A Quantitative Approach to Unravel the Role of Host Genetics in IgG-FcγR Complex Formation after Vaccination 47

3.1 Abstract 48

3.2 Introduction 48

3.3 Materials and Methods 50

3.3.1 Evaluating combined IgG1 concentration and affinity parameter changes 51

3.3.2 Evaluating Boosting of IgG1 concentrations in individuals with different FcγRIIIa polymorphisms 52

3.3.3 Simulating IgG1 allotypes and glycosylation 52

3.3.4 Determining preferred boosting method in IgG1 allotypes 54

3.3.5 Evaluating mixed allotype populations 54

3.4 Results 55

3.4.1 Synergism between IgG1 concentration and IgG1 affinity 55

3.4.2 FcR polymorphism influences FcγR activation after boosting 56

3.4.3 The G1m-1,3 IgG1 allotype is not predicted to be sensitive to IgG1 Fc glycosylation modifications 58

3.4.4 IgG1 allotype determines whether vaccine boosts that increase IgG1 concentration vs. boost that increase IgG1 affinity would be more effective for improving FcR activation.... 60

3.4.5 Amount of G1m-1,3 allotype in a population determines whether boosting IgG1 antibody titers will be effective 62

3.5 Discussion 64

3.6 Conflict of Interest 67

3.7 Author Contributions 67

3.8 Funding 67

3.9 Acknowledgments 67

3.10 Data Availability Statement 68

3.11 Ethics Statement 68

Chapter 4 Draft Notes on Unpublished Work 69

4.1 HIV-specific Antibody Fc Receptor Interactions 69

4.1.1 Introduction 69

4.1.2 Methods 69

4.1.3 Results 69

4.1.4 Limitations 70

4.1.5 Future Directions 70

4.2 Non-HIV-specific and HIV-specific Antibody Fc Receptor Interactions 71

4.2.1 Introduction 71

4.2.2 Methods 72

4.2.3 Results 73
4.2.4 Limitations 77
4.2.5 Future Directions 77
4.3 SARS-CoV-2-specific Antibody Fc Receptor Interactions 78
4.3.1 Introduction 78
4.3.2 Methods 78
4.3.3 Results 79
4.3.4 Limitations 85
4.3.5 Future Directions 85
4.4 SARS-CoV-2-specific Neutralizing Antibody Interactions 85
4.4.1 Introduction 85
4.4.2 Methods 86
4.4.3 Results 88
4.4.4 Limitations 90
4.4.5 Future Directions 90
Chapter 5 Discussion 91
5.1 Scientific contributions 91
5.2 Model identified effects of personal variability on FcR activation 92
5.2.1 Importance and limitations of IgG1 concentration 92
5.3 Model predicted effects of host genetics on FcR activation 95
5.3.1 Impacts of synergy between IgG1 concentration and affinity to FcR 95
5.3.2 Vulnerable individuals, populations, and interventions 99
5.4 Limitations 101
5.4.1 Accuracy of the model 101
5.4.2 Relative personalized concentrations and antibody decay 104

5.4.3 Lack of genetic data and affinity interventions 104

5.5 Future directions 106

5.5.1 Personalized antibodies over time and in competition 106

5.5.2 More genetic factors and experimental validation 107

5.6 Overall conclusions 108

Appendix 110

Appendix A Supplemental Materials: A systems approach to elucidate personalized mechanistic complexities of antibody-Fc receptor activation post-vaccination 111

Bibliography 122

List of Tables

Table 2-1 Key Resources Table 36

Table 4-1 Affinity parameters 73

Table 4-2 Concentration parameters 73

Table 4-3 Parameters 79

Table 4-4 Sensitivity ranges for parameters 79

Table 4-5 Parameter table 86

Table 4-6 ACE2-RBD affinities to different variants 86

Table 4-7 Ab-RBD kon affinities to different variants 87

Table 4-8 Antibody-RBD koff affinities to different RBD variants 87

Table A-1 Affinities of IgG subtypes to FcRIIa and FcRIIIa polymorphisms 111

Table A-2 Fold change in IgG affinity to FcR with changes in Fc glycosylation, related to Figure 2.7. 111

List of Figures

Figure 1-1 Mechanistic modeling approach 14

Figure 1-1 Mechanistic modeling approach 15

Figure 2-2 Model schematic 19

Figure 2-3 Model validation and global sensitivity analysis for HIV env and RV144 samples 21

Figure 2-4 Combined changes in IgG subclass concentrations identifies an optimal range of antigen-specific IgG1 and IgG3 23

Figure 2-5 Experimental validation of IgG1 sensitivity 25

Figure 2-6 IgG1 concentration differences resulting from Gm allotype are predicted to significantly alter FcR complex formation 27

Figure 2-7 Personalized, single-parameter sensitivity analysis illustrates universal sensitivity of IgG1 affinity for FcγR 29

Figure 2-8 Combined changes in IgG1 concentration and IgG1 Fc binding result in synergistic changes in complex formation 32

Figure 3-1 Model schematic 51

Figure 3-2 Landscape illustrating the relationships between IgG1 concentration and IgG1- FcγR affinity across the physiological landscape of parameters (2500 unique parameter combinations) 55

Figure 3-3 FcγR polymorphisms have a greater influence on complex formation after IgG1 boosting. 57

Figure 3-4 Glycosylation differentially impacts IgG1 allotypes. 59

Figure 3-5 IgG1 allotype determines whether boosting IgG1 concentration or boosting IgG1 affinity (k_{on} IgG1- FcγR) would be most effective for increasing complex formation. 61

Figure 3-6 In mixed allotype populations, the benefit of boosting IgG1 concentration vs. IgG1 affinity is dependent on the presence of the G1m-1,3 allotype. 63

Figure 4-1 Antibody decay after vaccination reduces complex formation sooner for those with G1m-1,3 allotype. 69

Figure 4-2 Amount of G1m-1,3 allotype in a population determines when an affinity boost is more influential than a concentration boost. 70

Figure 4-3 Model Schematic 72

Figure 4-4 The presence of non-specific IgG interferes with complex formation in multiple epitopes 75

Figure 4-5 Model predicted percent of maximum complex formation compared to experimental 76

Figure 4-6 Measured and predicted complex formation with and without IgGn 77

Figure 4-7 Model schematic 78

Figure 4-8 SARS-CoV-2 initial FcR validations using the DRASTIC cohort 81

Figure 4-9 IgG1 vs IgG3 initial concentration landscapes 82

Figure 4-10 Global sensitivity 82

Figure 4-11 P-values from Mann-Whitney tests of IgG concentration data separating groups 83

Figure 4-12 P-values from Mann-Whitney tests of experimental FcR complex concentration data separating groups 84

Figure 4-13 Model Schematic 86

Figure 4-14 Model vs experimental results for two neutralizing antibodies. 89

Figure A-1 Extracellular IgGs activate Fc effector functions via FcRs 112

Figure A-2 Model validation with log-log least-squares fit (A). Model validation for A244 in FcγRIIIa-F158 and FcγRIIa-H131 (B-C), and BaL in FcγRIIIa-V158, FcγRIIIa-F158 and FcγRIIa-H131 (D-F). 113

Figure A-3 Global sensitivity analysis for FcγRIIIa-F158 (A-B), FcγRIIa-H131 (C-D), and FcγRIIa-R131 (E-F) 114

Figure A-4 Global sensitivity analysis with a cooperativity constant for FcγRIIIa-V158 (A-B), FcγRIIIa-F158 (C-D), FcγRIIa-H131 (E-F), and FcγRIIa-R131 (G-H). 117

Figure A-5 Alternative IgG1 vs IgG3 landscapes (A-B), and direct comparison of the predicted and measured fold change in complex formation after addition of IgG1 (C-D). 118

Figure A-6 Personalized single-parameter sensitivity analyses for FcγRIIIa-F158 (A), FcγRIIa-H131 (B), and FcγRIIa-R131 (C). 119

Figure A-7 Comparison of IgG subtypes and glycosylation regions and complex formation at baseline in different FcγR classes and polymorphism. 120

Abstract

One of the most significant challenges to current human healthcare is the emergence of antigenically variable viruses that evade traditional vaccination approaches. Human immunodeficiency virus (HIV) is one such virus that emerged over 30 years ago and still has no effective vaccine. Like many other antigenically variable viruses, after infection, HIV quickly mutates to evade broadly neutralizing antibodies that bind tightly to key sites to prevent infection. Over 250 clinical trials have been performed to date to develop an effective HIV vaccine, with only one providing moderate protection; the RV144 Thai trial, estimated to be 31% effective but has not been replicated in other populations. Rather than broadly neutralizing antibodies, the trial identified IgG antibodies with the capacity to induce Fc effector functions as a correlate of protection. These functions are triggered by less specific antibodies that bind HIV antigen and Fc receptors on the surface of innate immune cells to form immune complexes to activate protective cellular functions. Understanding how to increase the formation of IgG-FcR complexes may improve vaccine efficacy, but variation in IgG and FcR features across individuals suggests that protective mechanisms need to be understood on a personalized basis. There are multiple subclasses of protective IgGs, each having different concentrations and affinities to FcRs in different individuals. Genetics can also play a role, with FcR polymorphisms changing FcR binding affinity and IgG1 allotypes changing IgG subclass concentrations. Mechanistic ordinary differential equation (ODE) modeling of this system offers the opportunity to account for these factors on a personalized basis and deconvolve which are most influential and determine how to improve protection universally.

We developed an ODE model of IgG-FcγRIIIa immune complex formation to elucidate how personalized variability in IgG subclass concentration and genetic factors may contribute to complex formation after vaccination. We validated the model with RV144 plasma samples and used it to discover new mechanisms that underpin complex formation. This enabled the identification of genetic and post-translational features that influenced complex formation and suggested the best interventions on a personalized basis. For example, although IgG3 was

associated with protection in RV144 and has the highest affinity to FcγRIIIas, the model suggested that IgG1 may play a more essential role, though it also may be highly variable; due to high IgG1 concentration variability across individuals. The model identified RV144 vaccinees who were predicted to be sensitive, insensitive, or negatively affected by increases in HIV-specific IgG1, which was validated experimentally with the addition of HIV-specific IgG1 monoclonal antibodies to vaccine samples. The model also gave important insights into how to maximize IgG-FcγRIIIa complex formation in different genetic backgrounds. We found that individuals with certain IgG1 allotypes were predicted to be more responsive to vaccine adjuvant strategies that increase antibody affinity (e.g., glycosylation modifications) compared to other allotypes, which were predicted to be more responsive to vaccine boosting regimens that increase IgG1 antibody concentration. Finally, simulations in mixed-allotype populations suggest that the benefit of boosting IgG1 concentration versus IgG1 affinity may depend upon the frequency of a specific IgG1 allotype (G1m-1,3) in the population. Overall we believe that this approach represents a valuable tool that will help understand the role of personalized immune mechanisms in response to vaccination and address challenges related to under-represented genetic populations in vaccine trials.

Chapter 1 Introduction

1.1 The emerging threat of antigenically variable viruses

Antigenically variable viruses pose a critical threat to human health as they mutate rapidly and evade the immune system and traditional vaccination approaches. The SARS-CoV-2 virus is an example that has recently risen to the forefront of public attention during the COVID-19 pandemic, which has killed nearly 5 million people worldwide over two years and caused massive economic shutdowns and psychological damage[1]. However, this threat has long been present as demonstrated by other viruses, including seasonal influenza, which requires annual vaccinations and kills 291,000-646,000 people globally each year[2] and the human immunodeficiency virus (HIV), which has no effective vaccine and has claimed a total of 36.3 million lives since its emergence in 1981[3].

Globally, HIV/AIDS is the second most fatal infectious disease[4] with 680,000 deaths and 1,500,000 new infections in 2020[5]. HIV is most often spread through sexual contact but can also spread by needle sharing in injecting drug users or parent-to-child through pregnancy, birth, and breastfeeding. HIV infection leads to systemic T-cell destruction, which weakens the immune system to other opportunistic infections and leaves patients vulnerable to cancers and direct and systemic damage to many essential organs such as the heart, brain, and gut[6]. Clinically, HIV infection presents as lymphadenopathy (enlarged lymph nodes) and mononucleosis-like symptoms such as fever, diarrhea, and transient meningoencephalitis (inflammation in the brain causing cognitive and behavior changes, pains in neck and head, and seizure)[6]. HIV infection progresses to AIDS when a patients' CD4+ T cell count is below 200, or an AIDS-related infection or disease occurs. AIDS induces a gradual and chronic decline in immune system function leading to a high risk of contracting life-threatening infections (i.e., SARS-CoV-2) and cancers.

At the beginning of the global epidemic, AIDS was a death sentence, but now, of the 37,700,000 people living with HIV/AIDS globally, 73% are receiving treatment in the form of antiretroviral therapy (ART)5, which can reduce the chances of transmission to a sexual partner by 96% when started within four years[7,8]. With the introduction and iteration of more effective and less toxic antiretrovirals over the last 33 years[9–11], AIDS-related deaths have been reduced by 64% since their peak in 2004[5], but there is still no cure. Despite the effectiveness of ART, without a cure, prevention is an essential arm in the containment of the virus.

There are two main prevention methods: (1) "treatment as prevention," where HIV-positive patients can protect their HIV-negative sexual partners by keeping their viral loads undetectable through treatment, and (2) pre-exposure prophylaxis (PrEP), an oral or topical medication that can be taken by HIV-negative people at high risk of infection. As mentioned above, treatment as prevention is highly effective in many cases, but 10%-40% of HIV-positive individuals are unresponsive to ART treatment[12–14], immunological non-responders (INRs)[12,15–17], leading to more rapid disease progression and death. In these cases, treatment as prevention would have a much lower likelihood of protecting partners and preventing spread. In addition, studies have suggested that protection requires a 95% adherence rate to ART[18], and there are many physical, social, and economic reasons why this is difficult, including specific drug side-effects, limited doctor-patient time and attention, and family and social pressures[19]. There are new drug trials aimed at reducing the logistical burdens a daily pill can take. For instance, a study on a long-lasting injectable drug in Spain and the US found that women - traditionally reported to have lower adherence - mentioned feeling empowered by this long-term regularly scheduled injection over having to remember a daily pill[20]. All those within the study mentioned work, social obligations, exercise, and travel as primary areas of improvement with this long-term option[20]. However, women more often mentioned the mental burden of coordinating these with their caretaking duties of children, elderly parents, and ailing partners[20].

Researchers have performed clinical trials of oral PrEP in transwomen and men who have sex with men (MSM)[21,22], heterosexual men and women[23,24], and injecting drug users[25]. Efficacy rates are high among MSM, and many public health campaigns for PrEP target MSM, but awareness among injecting drug users is of concern[26] and highly variable efficacy in women[23,24].

Many continue to support the global guideline that PrEP is equally effective, over 90%[24], in women as long as they are adherent, and their low adherence levels cause lower overall efficacy[27,28]. However, in these cited trials, adherence was measured through blood levels of PrEP drugs, which does not account for differences in the pharmacokinetics of PrEP in the blood and metabolism by microbes in the female reproductive tract[29–34]. Additionally, this conversation in the clinical trial and public health space has neglected women who have sex with women (WSW) and women who have sex with both women and men (WSWM)[35,36], but a review of the impact of stigma for WSW and MSM in sub-Saharan Africa is in preparation[37].

The UN's Joint Program on ending HIV/AIDS (UNAIDS) in 2017 proposed a "90-90-90" target to help downgrade the crisis from a global epidemic[38]. This target would require 90% of HIV-positive individuals to know their status, 90% of those to be receiving treatment, and 90% of those to have undetectable viral loads, meaning 73% of HIV-positive people globally would have undetectable viral loads[38]. However, in 2020 73% of people living with HIV were accessing treatment, leaving at least 10,179,000 people living with HIV to continue transmitting the virus[5]. A universal prevention technique is needed to protect HIV-negative people, especially from these undiagnosed newly infected individuals. On top of that, only 10% of individuals eligible for PrEP use in the US are accessing it, and this percentage is potentially lower in other countries[39]. The cost of treatments alongside the PrEP prevention method should be a significant consideration as most people living with HIV live in low- and middle-come countries[5]. Accounting for ART for all those already living with HIV, the new infections expected each year, and PrEP for all those at high risk, the estimated cost for low and middle-income countries from 2016-2030 is $350 billion[40]. Promisingly a vaccine that is only 50% effective could reduce millions of new infections annually[41], and this long-term protection approach would improve PrEP's short-term protection in terms of cost, convenience, and adherence for those willing to adhere to it. While this solution will need to be implemented alongside ART and PrEP to achieve the broadest reach[42] – especially if the vaccine is only 50% effective - it is most likely essential to end the global epidemic[43].

1.2 Only one of many HIV vaccine trials has been moderately protective at 31% efficacy

The search for a vaccine against HIV began over 30 years ago[44], and to date, over 250 clinical trials have been run[45], with only one trial – RV144 – showing significant efficacy of 60% after one year and 31% at 3.5 years post-vaccination[46,47]. Most successful vaccines that have irradicated diseases like measles, mumps, and rubella work by introducing a piece of the pathogen, an inactivated virus, or a similar but less dangerous pathogen to the immune system and allowing the body to develop antibodies against the pathogen that can be elicited when an actual infection arises. In these cases, the antibodies developed are neutralizing antibodies that bind tightly to the pathogen on a site that prevents it from infecting the host, such as binding to the portion of a virus used to enter a host cell. Inducing broadly neutralizing antibodies that can neutralize a wide range of mutated viruses has long been the goal in developing vaccines against highly mutagenic viruses like HIV and influenza. The induction of broadly neutralizing antibodies has proven problematic in viruses that mutate rapidly and are present in many hosts simultaneously, multiplying this mutation probability[48], as in influenza, where vaccine efficacy rates vary from 19% to 60%[49]. An added complication in HIV infection is the presence of many different mutations of the virus both during transmission as well the acute infection period, meaning, for example, that even if a vaccination protects against 90% of the mutants present, the other 10% of virions can still thrive and mutate further[50].

Three major approaches to vaccinate against HIV have been used: (1) elicit neutralizing antibodies with recombinant envelope proteins, (2) use a viral vector to induce CD8+ T cell response, and (3) the only successful approach, use a heterologous prime-boost regimen to induce humoral and cell-mediated immune responses[51].

The phase III VAX trials from 1998-2003 were examples of the first approach, where priming and boosting used the same antigens. VAX003 was performed in Thailand, where HIV clades B and E are prevalent, and mainly enrolled injecting drug users (IDUs), 93% of whom were male. VAX004 was performed primarily in North America, where HIV clade B is prevalent, on MSM. Both trials used an AIDSVAX antigen that consists of a recombinant version of the HIV envelope protein gp120 (of the HIV subtype prevalent in the region), with boosts at months 1, 6, 12, 18, 24, and 36. Neither trial showed efficacy, but secondary analysis suggests that boosting

may promote IgG2 and IgG4 over IgG1 and IgG3 antibody subclasses, which are the subclasses with lower binding to Fc receptors on immune cells[52–55]. Additionally, these studies found antibody-dependent cellular cytotoxicity (ADCC) peaked after 3-4 immunizations and then declined after 5-7 immunizations[56].

The RV trials in Thailand starting in 2003 exemplify the heterologous prime-boost approach that aims to induce humoral and cellular immunity. The RV144 trial ended in 2009 is the only known prophylactic HIV vaccine trial proven to protect against infection, with 60.5% efficacy at 12 months[47] and 31% efficacy at 3.5 years[46]. This trial enrolled 16,402 men and women who were primarily heterosexual. Boosting occurred at months 1, 3, and 6, and all four immunizations contained ALVAC-HIV (vCP1521) – a live attenuated canarypox virus expressing HIV DNA, but the last two also contained the same AIDSVAX B/E in VAX003. The primary factors correlated with protection were the binding of IgG to the V1V2 region of the env protein and low levels of IgA binding to env[57]. Secondary analysis suggests that high levels of IgA may interfere with protective antibodies because in those vaccinees with lower env-specific IgA, IgG avidity, antibody-dependent cellular cytotoxicity (ADCC), neutralizing antibodies, and env-specific CD4+ T cells were also correlated with protection[57]. Additionally, follow-up studies found that depletion of env-specific IgG3 reduced Fc effector functions like[52]. Notably, IgG3 decreased over time (>80% at two weeks to 3% by week 52) just as efficacy decreased (60% at one year and 31.5% at 3.5 years)[57] and other vaccine trials were then designed to replicate results in other populations and promote lasting efficacy.

RV305 and RV306 are follow-up phase II trials to induce lasting immunity, which tested further boosting regimens after the original RV144 regimen. RV305 enrolled 162 enrollees from RV144 and boosted them with the same antigens 6 and 8 years after their RV144 regimen[58]. This protocol induced higher humoral responses than after RV144, but they quickly declined and did not increase after the second boost[58]. Secondary analysis suggested that boosting increased C1C2 specific monoclonal antibodies mediating ADCC, and crystallography showed these antibodies were binding to gp120 on the HIV env protein[59]. RV306 enrolled 367 HIV vaccine naïve participants of low risk and split them into four groups[60]. All groups received the original RV144 regimen at months 0, 1, 3, and 6. Group 1 received no additional boost. Group 2 received

AIDSVAX B/E and ALVAC-HIV (vCP1521) at month 12. Group 3 received AIDSVAX at month 12. Group 4a received AIDSVAX & ALVAC-HIV at month 15, and group 4b at month 18. Analysis for this trial is ongoing, but preliminary results show that all groups with an additional boost (2, 3, 4a & 4b) have higher peak plasma IgG binding titers for gp70 V1V2 than group 1, and increased polyfunctionality – multiple mechanisms of protection[60]. Boosting at month 12 did not increase gp120 specific antibodies but boosting at months 15 and 18 did increase gp120 specific antibody titers, and plasma IgG responses were significantly higher after months 15 and 18 boosts as well[60]. Neither of these studies was testing for efficacy.

Another series of follow-up trials based on RV144 was initiated in South Africa in 2015, starting with the phase ½ HVTN100 trial. This trial, which tested for safety and tolerability, enrolled low-risk males and females and followed the RV144 regimen at months 0, 1, 3, and 6 with an added boost at month 12 of both antigens. The antigens were adapted to express HIV-1 antigens from the strain circulating in South Africa (clade C), with ALVAC-HIV [vCP2438] administered at every immunization and a bivalent subtype C gp120 recombinant protein co-administered at months 3, 6, and 12[61]. The vaccine adjuvant was also changed from alum to MF59 to increase immunogenicity[61]. Results were promising with all gp120 specific IgG titers being significantly higher than in RV144 by 3.6-8.8-fold, and while the IgG response to V1V2 was lower here than in RV144 yet still higher than the estimated threshold to give the vaccine 50% efficacy[61], though efficacy was not explicitly evaluated in this trial.

HVTN702 is the phase III trial testing the efficacy of HVTN100's regimen. 5,407 HIV vaccine naïve men and women were enrolled starting in 2016 and given the same five immunizations listed for HVTN100. Surprisingly, after the promise of HVTN100, HVTN702 was stopped on January 23rd, 2020, after an interim analysis by an independent safety monitoring board (DSMB) found no increase in protection with the vaccine (129 HIV infections in 2694 vaccine recipients and 123 infections in the 2689 placebo recipients)[62,63]. The analysis is ongoing, and data is still being collected from all participants already immunized. Follow-up analyses to determine why HVTN100 results did not translate into a successful HVTN702 trial are expected.

New vaccine approaches like mosaic vaccines based on engineered immunogens that represent multiple strains and antigens and mRNA vaccines, which have experienced a recent boost in confidence with the success of COVID-19 vaccines, are also being explored. However, none have shown efficacy like the heterologous prime-boost regimen as of yet[51].

1.3 Fc-mediated cellular immunity has been linked with protection in HIV vaccine trials

Although neutralizing antibodies are the most common correlate of protection in regular vaccine regimens today[64,65], analysis of HIV vaccines points to the importance of a polyfunctional immune response requiring multiple protection mechanisms[52]. As mentioned above, HIV and influenza are viruses that mutate rapidly to escape any highly specific antibodies produced to target them[64–67], making the induction of neutralizing antibodies more difficult than in more stable viruses we have eradicated like smallpox. A polyfunctional antibody response could include neutralizing antibodies but does not depend on them alone to protect the vaccinee from the virus. Instead, it includes several antibody-mediated mechanisms of protection[52,68], most notably, antibody-dependent cellular cytotoxicity (ADCC) and antibody-dependent phagocytosis (ADCP). ADCC works by activating the Fc receptors (FcRs) on natural killer (NK) cells to secrete cytotoxic factors, whereas ADCP triggers phagocytosis in macrophages. Fc-mediated functions like ADCC and ADCP have been implicated as protective against multiple mutagenic viruses like tuberculosis[69], Ebola[70], influenza71, and HIV[72].

Both ADCC and ADCP are triggered by the formation of immune complexes. Whereas a broadly neutralizing antibody binds to a specific site on the antigen that can block further infection, the antibodies that can trigger Fc-mediated effector functions can bind anywhere on the antigen. This lower specificity also means that the immune system does not need prior sensitization to this same antigen; cross-reactive antibodies made for other antigens are often similar enough to bind some portion of a newer antigen. To carry out antibody-mediated immune functions, first, a cross-reactive antibody or one specific to the virus binds to the virus or an infected cell on the variable Fab region of the antibody, then the other end of the antibody, the Fc region, binds to FcRs on immune cells. When several FcRs are bound and cross-linked on the cell surface, signaling cascades trigger Fc effector functions like ADCC. Different FcR types trigger different Fc effector functions; for example, FcγRIII triggers ADCC when IgG antibodies in complex with

the pathogen bind. There are also different IgG subclasses, IgG1, IgG2, IgG3, and IgG4 (with IgG1 being the most abundant) and these subclasses have differing affinities to each FcγR, with IgG1 and IgG3 typically having the highest affinities.

Recently developed recombinant FcR dimers can detect FcR complex formation to mimic the dimerization on immune cell surfaces[73]. Complex formation measured with these dimers and plasma samples has correlated with in vitro cellular assays measuring ADCC and ADCP74, and they are now used for high-throughput analysis in HIV, Influenza, and Malaria[75–78].

ADCC and the agents that trigger it have been correlated to protection in HIV vaccines or show promise in secondary analyses. In the primary analysis of RV144, vaccinees with lower levels of the potential inhibitory HIV-specific IgA antibodies had correlations between protection and ADCC activity[57]. Secondary analyses also showed a specific IgG subclass, IgG3, was correlated with lower infection risk and was more prevalent in RV144 than VAX003 and could drive the more polyfunctional response[52,79]. In RV305, the trial boosted a subset of RV144 participants years later and saw increases in IgG antibodies specific to gp120 that mediated ADCC[59]. In RV306, where four out of five arms of the study received an additional boost after the RV144 regimen, they saw increases in polyfunctionality and gp120 specific antibodies titers after boosting[60]. In HVTN 100, the phase ½ trial testing the RV144 regimen plus a boost in South Africa, there were increases in gp120 specific IgG titers over the RV144 data[61].

1.4 Systems serology combining diverse datasets has highlighted a relationship between ADCC and IgGs in protective vaccine responses

In addition to primary analyses on correlates of protection, the field of systems serology has developed alongside these vaccine trials and has contributed to understanding why RV144 produced efficacious immune responses. Systems serology uses data-driven or "machine-learning" techniques to gain a systems-level understanding of how the immune system functions in both health and disease states. It has been essential in the last few decades where dataset size and complexity have grown considerably, and researchers have needed a method for determining which components are essential to the system of interest and how they are related to one another [68,80]. Techniques include principal component analysis (PCA), decision trees, and Bayesian

networks. However, one of the more powerful techniques in HIV vaccine research has been partial least squares discriminant analysis (PLS-DA) which allows the users to identify unique signatures for each group of interest composed of a multitude of datatypes (e.g., proteins, genes, and cellular activity data) choosing only the most highly associated components for that group. PLS-DA goes beyond traditional statistical methods by identifying components that may not have a statistically significant difference, but when considered in the larger picture of the entire system, may have an important role to play.

Systems serology analysis of RV144 and other trials has further suggested an essential role for ADCC in protection[52,68,81,82]. A 2015 study on data from four HIV vaccine trials, including RV144 and VAX003, was able to identify unique humoral signatures for each vaccine trial that pointed to a direct connection between IgG1 and Fc effector functions (ADCC and ADCP)[83]. This challenged the idea that IgG3, the subclass with the highest affinity to FcRs and the one connected to protection previously, may be the most important for functional responses[79]. Recent animal studies on the administration of broadly neutralizing antibodies for treating HIV-1 infection have suggested the Fc effector functions are even essential here, where the antibodies themselves are already considered broadly neutralizing[84,85].

Although data-driven analysis has expanded our understanding of which humoral components and activities are the most essential for protection from HIV, there are limitations. With this approach, relationships between factors can be inferred, but these are based on statistical correlations and cannot give insight into mechanisms without follow-up experimentation. The observation that several variables change together does not give information about cause-effect relationships. In the case of HIV vaccine follow-up analysis, the data-driven approach used involved grouping participants by vaccine type (i.e., RV144 vs. VAX003, “low risk” vs. “high risk,” or case vs. control), which prevents mechanistic understanding of relationships between personalized IgG and Fc features and their influence on vaccine response.

The personalized IgG and Fc features involved in immune complex formation affect the antigen, IgGs, and FcRs in several ways, making it difficult to predict how to maximize the formation of these complexes intuitively. With highly mutagenic viruses, the antigen itself can be changed

between individuals and, over time, in a single individual. There are multiple IgG subclasses (IgG1, IgG2, IgG3, and IgG4)[86] with differing abundances in the plasma, IgG1 being the highest, followed by IgG2, IgG3, and IgG4, respectively[87]. In addition, each IgG subclass has a unique affinity to each FcR, with IgG1 and IgG3 generally having a higher affinity than IgG2 and IgG4[88]. Different FcR types have different affinity profiles, with the ADCC promoting FcγRIIIa having higher affinity to IgG3 than all other IgG subclasses, whereas in the ADCP promoting FcγRIIa IgG1 has the highest affinity[88]. It is well studied that genetic polymorphisms of FcRs cause differences in affinities to each subclass88, and recent studies have shown that IgG allotypes may also affect affinity to FcRs[89]. IgG1 allotype has also been shown to alter the concentration profile of all vaccine-specific IgG subclasses[90]. Studies have confirmed that differences in IgG subclass concentrations influence FcR activation[52] and that these subclasses decline over time just as vaccine efficacy does[79]. Finally, personalized differences in IgG subclass concentration profiles are highly variable from person to person and over time, alongside genetic and post-translational changes like glycosylation which can also affect binding affinity[68].

Now that data-driven modeling has provided information about key IgG and FcR species involved in cell-mediated functions, mechanistic modeling offers the opportunity to deconvolve the complex set of personalized and genetic factors involved in vaccine protection to elucidate mechanisms to maximize protection in all vaccinees.

1.5 Mechanistic modeling will give new insight into personalized differences in Fc-mediated vaccine responses

Mechanistic or "theory-driven" modeling techniques can use the results of data-driven modeling (only the most critical sets of interconnected components) and any prior knowledge of how they interact with one another and test mechanistic hypotheses of how interventions and interactions may affect the outcome of interest in individual cases. Many techniques fall under theory-driven modeling, such as stochastic agent-based modeling (ABM)[91,92] and deterministic partial differential equation (PDE) modeling[93,94], but one of the most common approaches is ordinary differential equation (ODE) modeling[95–98].

ODE models are constructed using a system of ordinary equations that can quantitatively calculate the abundance of different system components over time, based on known interactions. Unlike PDEs, which account for spatial aspects of the system and become more complicated, ODEs assume a well-mixed system like blood and plasma and primarily utilize concentration and affinity data. For example, models of the dynamics of CD4+ T cell depletion were used to quantify the difference in dynamics of T cell depletion between different HIV strains[99]. A recent study using ODEs tested different models representing different hypothesized mechanisms to explain new dynamics observed in phase I clinical trial testing the administration of broadly neutralizing monoclonal antibodies in HIV infected patients[100].

A small number of ODE-based models of FcR interactions with antibodies have been developed, primarily in cancer treatment settings where the neonatal FcR (FcRn) interacts with therapeutic IgGs[101–106], and to explore IgG multivalency in the context of cancer[107,108]. To date, these approaches have not been applied to understand personalized differences in Fc-mediated immune functions after vaccination.

ODE models are uniquely capable of utilizing personalized concentration data to mechanistically represent a system, allowing for in silico hypothesis testing, saving both time and resources. Using ODEs to represent Fc-mediated immune complex formation allows for multiple levels of complexity in model construction. Model complexity can span the spectrum from representing multivalent in vivo complex formation on cells with multiple FcR types [107,108] to representing a single monoclonal IgG binding in a cell-free assay depending on the scope of the research question. Additionally, the complexity of the model structure can quickly be iterated when model predictions are inaccurate, such as adding a competitive species like IgA or removing a less influential species like IgG2 that could be causing the noise. Given accurate initial concentrations and affinity values, ODE models can quantitatively predict the concentration of Fc-mediated immune complexes in various situations, such as in different individuals, and projected into different genetic backgrounds. System dynamics can be monitored in each individual throughout in silico experiments that capture concentrations of intermediary complexes at intervals impossible in vitro, which can help form new mechanistic hypotheses. Model simulations can predict how altering each concentration and affinity parameter will

quantitatively change complex formation, identifying which are most influential. Finally, in silico experimentation can determine which in vitro or in vivo experiments should be performed; for instance, when IgG1 is identified as influential, model simulations can quickly test the addition of hundreds of different IgG1 concentration boosts and determine which five would be beneficial to test experimentally, saving time and resources.

1.6 Structure of thesis

On the foundation built by data-driven knowledge, vaccine trial outcomes, and mechanistic modeling, I present a dissertation developing a framework for mechanistic ODE modeling of Fc-mediated immune complex formation and demonstrate its potential to understand personalized differences in IgG and Fc receptor features that underly variability in FcR activation after vaccination. The approach will allow us to improve current vaccine interventions rationally.

In the following aims, I have developed, validated, and used a model we specifically developed to represent the high-throughput assays currently being used to predict ADCC activation in personalized vaccine trial samples (**Figure 1.1**). Our goal was to construct a model as approachable by vaccine researchers as possible while representing the complexities that arise with multiple IgG subclasses and personalized and genetic differences in both concentration and affinity (**Figure 1.1**). We aimed to use this model to guide follow-up experimentation, vaccine design, and future data collection alongside vaccine trials towards the goal of providing efficacious and equal vaccine protection in all individual and genetic scenarios. We approached this challenge with the following aims:

Aim 1: Elucidate the effects of personal variability in IgG subclass concentration profiles on FcR complex formation

- Aim 1a: create and validate an ODE model of FcR complex formation
- Aim 1b: use model to evaluate the effect of variation in IgG subclass concentration

Aim 2: Isolate host genetic factors affecting IgG subclass concentration profiles and affinity to FcR to reveal genetic vulnerabilities in FcR activation

Aim 2a: use the model to evaluate the effect of IgG1 allotype (alters IgG subclass concentrations) and FcR polymorphisms (alters the affinity of FcR to all IgG subclasses)
Aim 2b: determine optimal vaccine interventions for different genetic backgrounds

Completion of these aims will be presented in the following format: **Chapter 2** presents published work that describes the model structure and validation (aim 1a), the effects of personalized variation in IgG subclasses (aim 1b), and how IgG1 allotype affects complex formation (aim 2a). The related supplemental materials for this work are presented in **Appendix A**. **Chapter 3** presents recently submitted work that utilized the same framework to describe how genetic factors (IgG1 allotype and FcR polymorphism) affecting IgG subclass concentrations and affinity to FcRs influence FcR complex formation (aim 2a) in addition to predicting the optimal intervention approaches needed for each genetic background (aim 2b).

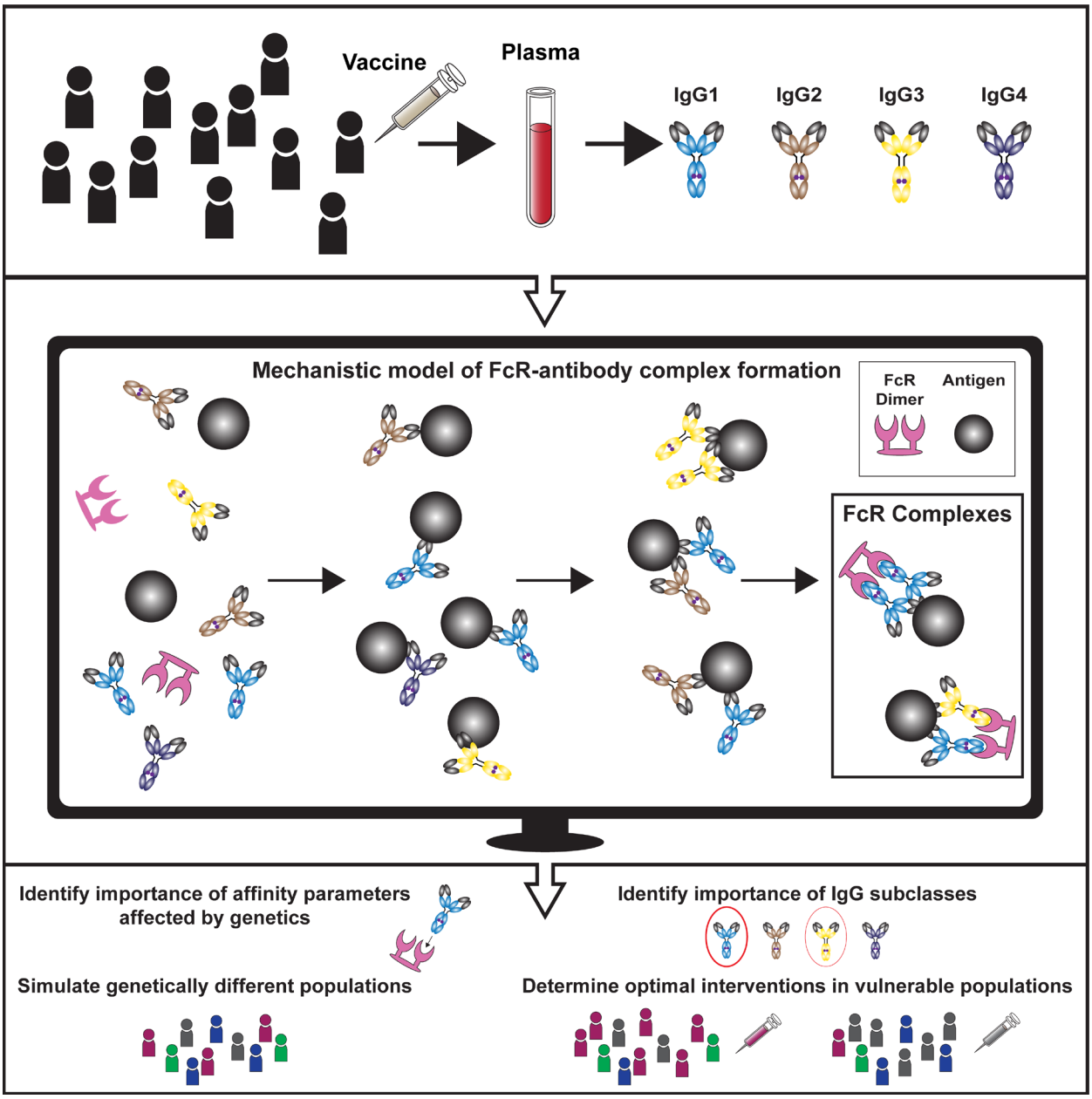

Figure 1-1 Mechanistic modeling approach

Chapter 2 A Systems Approach to Elucidate Personalized Mechanistic Complexities of Antibody-Fc Receptor Activation Post-vaccination

Melissa M. Lemke[1], Milla R. McLean[2], Christina Y. Lee[1], Ester Lopez[2], Emily R. Bozich[1], Supachai Rerks-Ngarm[3], Punnee Pitisuttithum[4], Sorachai Nitayaphan[5], Sven Kratochvil[6], Bruce D. Wines[7,8,9], P. Mark Hogarth[7,8,9], Stephen J. Kent[2,10,11], Amy W. Chung[2,12,*], and Kelly B. Arnold[1,12,13,*]

[1]Department of Biomedical Engineering, University of Michigan, Ann Arbor, MI, USA [2]Department of Microbiology and Immunology, The University of Melbourne, at the Peter Doherty Institute for Infection and Immunity, Melbourne, VIC, Australia [3]Department of Disease Control, Ministry of Public Health, Bangkok, Thailand [4]Vaccine Trial Centre, Faculty of Tropical Medicine, Mahidol University, Bangkok, Thailand [5]Armed Forces Research Institute of Medical Sciences, Bangkok, Thailand [6]The Ragon Institute of Massachusetts General Hospital, Massachusetts Institute of Technology and Harvard University, Cambridge, MA, USA [7]Immune Therapies Group, Burnet Institute, Melbourne, VIC, Australia [8]Department of Immunology and Pathology, Monash University, Melbourne, VIC, Australia [9]Department of Clinical Pathology, The University of Melbourne, Melbourne, VIC, Australia [10]ARC Centre of Excellence in Convergent Bio-Nano Science and Technology, The University of Melbourne, Melbourne, VIC,

Figure 1-1 Mechanistic modeling approach

Australia [11]Melbourne Sexual Health Centre, Alfred Hospital, Monash University Central Clinical School, Carlton, VIC, Australia [12]These authors contributed equally [13]Lead contact
*Correspondence: awchung@unimelb.edu.au (A.W.C.), kbarnold@umich.edu (K.B.A.)

Cell Reports Medicine (2021) 100386. DOI: 10.1016/J.XCRM.2021.100386

2.1 Abstract

Immunoglobulin G (IgG) antibodies that activate Fc-mediated immune functions have been correlated with vaccine efficacy, but it is difficult to unravel the relative roles of multiple IgG and Fc receptor (FcR) features that have the capacity to influence IgG-FcR complex formation but vary on a personalized basis. Here, we develop an ordinary differential-equation model to determine how personalized variability in IgG subclass concentrations and binding affinities influence IgG-FcγRIIIa complex formation and validate it with samples from the HIV RV144 vaccine trial. The model identifies individuals who are sensitive, insensitive, or negatively affected by increases in HIV-specific IgG1, which is validated with the addition of HIV-specific IgG1 monoclonal antibodies to vaccine samples. IgG1 affinity to FcγRIIIa is also prioritized as the most influential parameter for dictating activation broadly across a population. Overall, this work presents a quantitative tool for evaluating personalized differences underlying FcR activation, which is relevant to ongoing efforts to improve vaccine efficacy.

2.2 Introduction

Vaccines are a cornerstone of modern-day global public health interventions, with neutralizing antibody (Ab) titers used as the most common correlate of protection[64,65]. For antigenically variable pathogens (including HIV), induction of long-lasting, broadly neutralizing antibodies via vaccination has been challenging because they quickly escape the highly specific antibody recognition required for neutralization[64–67]. Instead, a number of recent studies have highlighted the importance of cellular Fc effector functions, including Ab-dependent cellular cytotoxicity (ADCC) and Ab-dependent cellular phagocytosis (ADCP), which are activated when the Ab Fc region forms immune complexes with antigens and Fc receptors on innate immune cells[69–72]. The only human HIV vaccine trial to demonstrate significant efficacy to date (the RV144 Thai trial: 60% efficacy at 1 year and 31.2% efficacy at 3.5 years after vaccination) did not induce broadly neutralizing Abs[46,47,57,109]. Instead, follow-up analysis identified non-neutralizing Abs with the capacity to mediate Fc effector functions, including ADCC, increased Ab avidity to HIV envelope protein (env) and tier-1-neutralizing antibodies as correlates of reduced infection risk[57]. These results and others from passive Ab-transfer, macaque studies underscore the importance of

Fc effector functions in vaccine-mediated protection against HIV and other antigenically variable pathogens[84,110]. Since RV144, a number of follow-up HIV vaccine trials have been designed to improve immunogenicity by including additional vaccine boosts, by varied DNA priming, or by changing the vaccine adjuvant, with limited success[58–62,111]. The inability to replicate RV144 results and achieve widespread protection in subsequent trials highlights the need to better understand the quantitative mechanisms that underpin Fc receptor (FcR) activation after vaccination and how those mechanisms may vary across populations of individuals.

The formation of immune complexes that activate Fc effector functions is highly variable in individuals and is determined by personalized Ab and FcR features that are modulated by host genetics and post-translational alterations (Figure A.S1)[68]. The relative concentration of pathogen-specific immunoglobulin G (IgG) Ab subclasses can vary widely among individuals (although generally by rank order IgG1 > IgG2 > IgG3 > IgG4). IgG sub-classes also bind with varying affinities to FcγRs (in general, IgG1 and IgG3 engage all FcγRs with comparatively greater affinity than do IgG2 or IgG4 [Figure 2.1C; Table A.S1]), and additional affinity variation occurs in individuals as a result of genetic and post-translational modifications, such as FcR polymorphisms, IgG allotypes, and IgG glycosylation[89]. Previous studies have confirmed that differences in IgG subclass concentrations influence Fc activation and decline with time after vaccination[52,79]. Analysis of RV144 samples indicated that elevated levels of IgG1 and IgG3 were associated with an improved Fc-effector profile, and depletion of IgG3 resulted in decreased Fc effector functions[52]. Follow-up analysis of RV144 also revealed that a decrease in vaccine efficacy over time (60% at 1 year to 31.5% at 3.5 years after vaccination)[57] paralleled a rapid decrease in HIV-specific IgG3 levels after vaccination (from >80% at 2 weeks after infection[52] to 3% by week 52). To combat that decline in pathogen-specific IgGs over time and to improve Fc effector functions, vaccine ‘‘boosting’’ regimens (repeated vaccination) have been developed. Paradoxically, however, repeated vaccination may have negative effects by skewing subclass profiles toward IgG2 and IgG4, which bind FcRs with weaker affinity and induce weaker Fc effector functions. VAX003 (a predecessor to RV144) vaccine trials demonstrated that repeated vaccine boosting (seven repeated vaccines over 3.5 years) elevated total IgG antibody levels but skewed subclass profiles (elevated IgG2 and IgG4) to less-functional Fc responses[52–55]. Overall, these studies suggest that IgG subclass concentration profiles are critical

for dictating Fc effector complex formation[52], but personalized variability makes it challenging to identify which humoral response components elicit optimal Fc activation, especially in the context of other factors (such as FcR polymorphisms and IgG glycosylation) that have the capacity to influence parallel changes in IgG-FcR binding.

Antigen-specific antibody FcγR immune complex formation can be detected in vaccine samples using recently developed recombinant FcγR dimers, which have been described as a high-throughput and sensitive method that mimics FcγR engagement at the immunological synapse[73]. Formation of these FcγR immune complexes correlates with a range of in vitro cellular Fc effector assays, including ADCC and ADCP, and these complexes are now widely used as surrogate high-throughput assays to assess Fc effector functions against a range of diseases, including HIV, influenza, and malaria[74–78]. In parallel, newly developed methodologies in systems serology research have employed ‘‘data-driven’’ (also called ‘‘machine learning’’) computational approaches to identify unique humoral signatures of IgG and FcR features that characterize vaccine responses[52,68,81–83]. This approach has been valuable for identifying systems of antibody and FcR features that are associated with a vaccine response or cellular function, although one remaining challenge is that they do not provide mechanistic insight into the relationship between personalized differences in IgG and FcR features and vaccine response heterogeneity in populations of individuals. Here, we use an ordinary differential equation (ODE) approach to elucidate IgG and FcγR features that account for personalized differences in IgG-FcγR complex formation and validate a model for HIV target epitopes in human vaccine samples. With this model, we are able to identify mechanisms by which individuals may be differentially sensitive to the RV144 vaccine, and we validate results experimentally with the addition of HIV-specific monoclonal Abs (mAbs) to individual vaccinee samples. Using a personalized sensitivity analysis, we also identify parameters that would best influence complex formation broadly across a population of individuals. Overall, this approach provides a quantitative framework for understanding how personalized differences in IgG and FcR features contribute to variability in IgG-FcR complex formation after vaccination.

2.3 Results

2.3.1 Model predictions of IgG-FcR complex formation validated in an Fc multiplex assay

To gain insight into how IgG and FcR variability in individuals may influence IgG-FcR complex formation, we constructed an ODE model to predict total bound, dimeric antigen-IgG-FcγR complexes formed at steady state (ant:IgG:IgG:FcγR-FcγR) as a function of concentration and

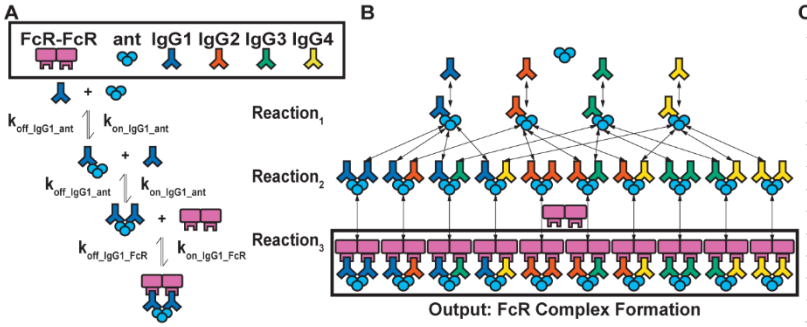

C

Parameter	Baseline Value	Units
K_{eq}-IgGx-env[α]	50,000	mM^{-1}
K_{eq}-IgG1-FcR[β]	2,000	mM^{-1}
K_{eq}-IgG2-FcR[β]	70	mM^{-1}
K_{eq}-IgG3-FcR[β]	9,800	mM^{-1}
K_{eq}-IgG4-FcR[β]	250	mM^{-1}
IgG1 initial concentration[γ]	8.54E-05	mM
IgG2 initial concentration[γ]	1.33E-07	mM
IgG3 initial concentration[γ]	3.07E-06	mM
IgG4 initial concentration[γ]	1.02E-07	mM
env initial concentration[δ]	2.50E-05	mM
FcR initial concentration[δ]	2.00E-05	mM

D

$$Reaction_1 = 2*k_{on\_IgG1\_ant}*[IgG1]*[ant]-k_{off\_IgG1\_ant}*[IgG1\_ant]$$

$$Reaction_2 = k_{on\_IgG1\_ant}*[IgG1]*[IgG1\_ant]-2*k_{off\_IgG1\_ant}*[IgG1\_IgG1\_ant]$$

$$Reaction_3 = k_{on\_IgG1\_FcR}*[FcR]*[IgG1\_IgG1\_ant]-k_{off\_IgG1\_FcR}*[FcR\_IgG1\_IgG1\_ant]$$

Figure 2-2 Model schematic

(A) An example set of reversible reactions describing the sequential binding of IgG1 to antigen (ant) and dimeric FcγR with the respective forward (k_{on}) and reverse (k_{off}) reaction rates.
(B) Ordinary differential equations were used to predict total HIV ant-IgG-FcγR complexes formed as a function of concentration and binding affinity of ant, IgG subclasses, and FcγR. The model assumes a single FcγR type. Reversible reactions are represented by double-ended arrows. Model output was the sum of all dimeric FcγR complexes formed (boxed in black) at steady state.
(C) The baseline parameters for FcγRIIIa-V^{158} complex formation with the following sources: [α]SPR measurement from pooled purified IgG from HIV infected individuals. All IgG subtypes share one affinity value (unpublished data). [β]K_{eq} measured in Bruhns et al.[88]. [γ]The average estimated IgG concentrations from individuals 1–30 in the RV144 data in this manuscript (see STAR Methods for notes on conversion from MFI to mM unit). [δ]Concentrations used in the multiplex experimental protocol.
(D) Equations describing the example reactions in (A). Reactions follow mass-action kinetics and consist of a forward reaction (on rate, k_{on}, multiplied by the concentrations of the substrates) and a reverse reaction (off rate, k_{off}, multiplied by the concentration of the product of the forward reaction). Differential equations for change in each complex over time were generated for each complex. See also Table A.S1 and Figure A.S1.

binding of IgG1, IgG2, IgG3, and IgG4 to antigen and FcγR(Figure 2.1). The model assumed two IgG binding sites per antigen protein to represent the simplest complex that reflects activation through FcγR cross-linking. Total ant:IgG:IgG:FcγR-FcγR complex formation was chosen as the output because antigen-specific IgG cross-linking of FcγR (engagement and clustering of multiple FcγRs) induces the activation of innate immune effector cells to mediate Fc functions and can be compared with steady-state experimental values measured using high-throughput multiplex assays. Importantly, we constructed the model such that it could be applied to any target antigen and FcR, although we chose to focus primarily on the HIV env glycoprotein 120 (gp120) strain A244 (env), one of the proteins used in the RV144 vaccine regimen, and FcγRIIIa, the FcγR upstream of ADCC (a correlate of protection in RV144 trial)[57]. To obtain parameters, we measured median fluorescent intensity (MFI) of antigen-specific IgG1, IgG2,

IgG3, and IgG4 in 105 RV144 vaccinee plasma samples and estimated personal concentrations based on a reference IgG1 concentration (Figure 2.1C)[112]. Although not useful for absolute concentration predictions, these estimated concentrations allowed for predictions of relative complex formation. We approximated baseline affinity parameters for pooled IgG to antigen from surface plasmon resonance (SPR) measurements of HIV-infected patient plasma (Figure 2.1C). Affinity for each antigen-specific IgG subclass to each FcγR was estimated from previously published literature (Figure 2.1C; Table A.S1; the low concentration of antigen-specific IgG subclasses in plasma makes it technically difficult perform SPR on each subclass for each individual)[88]. We used this information to predict relative ant:IgG:IgG:FcγR-FcγR complex formation (nM) in each individual and validated it with matched experimental measurements (MFI) of dimeric, recombinant, soluble (rsFcγR) complex formation measured in multiplex assays (as described above) in a subset of the same individuals (n = 30)[74]. We validated the model for two FcγRIIIa polymorphisms, including higher-affinity FcγRIIIa-V^{158} (Figures 2.2A and A.S2A) and lower-affinity FcγRIIIa-F^{158} (Figure S2B), along with FcγRIIa-H^{131} (Figure A.S2C), finding good agreement between rank-order model-concentration pre-dictions and experimental MFI measurements in a $\log_{10}$-$\log_{10}$ space, in which MFI and concentration are expected to have a linear relationship within the dynamic range (Spearman r = 0.92, root-mean-square error [RMSE] = 246.0; Spearman r = 0.90; Spearman r = 0.89, respectively; all $p < 0.0001$). We also performed validation for one other target antigen: HIV clade B gp120 from the BaL strain with FcγRIIa-H^{131}, FcγRIIIa-F^{158}, and FcγRIIIa-V^{158}, again, finding good agreement between rank-order model predictions and experimental measurements, despite the lower concentrations leaving the linear dynamic range (Spearman r = 0.96, r = 0.95 and r = 0.98, respectively, for HIV clade B gp120 BaL; all $p < 0.0001$; Figures A.S2D–A.S2F). Although model predictions closely mirrored experimental measurements in most individuals, they were moderately less accurate for individuals with higher FcR complex formation. Careful inspection, most visibly for FcγRIIIa-F^{158}, revealed that these individuals (especially vaccinees 4, 12, 18, and 23; Figures 2.2A and A.S2) were unique in that all had IgG1 concentrations greater than 1 SD above the group average. We speculate that minor deviations in this group may be due to the fact that our baseline model used average binding affinity parameters (for env and FcγRIIIa) that do not accurately reflect personalized differences that may arise from glycosylation or Ab Fab epitope recognition, which we predict would have a greater influence on individuals with high

IgG1 (discussed in greater detail below). These differences may also arise from differences in units of model output and experimental measurements (concentration versus median fluorescent intensity [MFI], respectively).

2.3.2 Sensitivity analysis highlights the importance of IgG1 and IgG3 for HIV env activation of FcγRIIIa

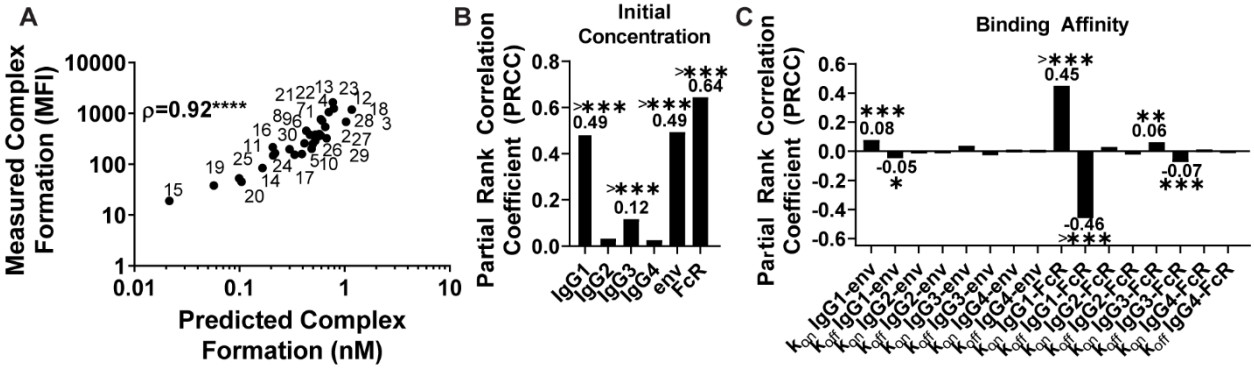

Figure 2-3 Model validation and global sensitivity analysis for HIV env and RV144 samples

(A) Model predictions for dimeric FcγRIIIa-V^{158} complex formation were compared with rsFcγRIIIa-V^{158} multiplex experimental measurements for 30 RV144 vaccinee samples (labeled 1–30) (Spearman correlation coefficient of 0.92, $p < 0.0001$).
(B and C) A global uncertainty and sensitivity analysis[133] of initial concentration (B) and binding parameters (C), in which partial rank-correlation coefficient (PRCC) indicates output sensitivity to parameters. k_{on} indicates forward reaction rates, and k_{off} indicates reverse reaction rates. $*p < 0.05$, $**p < 0.01$, $***p < 0.001$, $^{>}***p < 0.0001$.
See also Figures A.S2, A.S3, and A.S4.

Focusing on HIV env gp120 strain A244 (env), the main protein antigen used in RV144, and FcγRIIIa, the main FcR involved in natural killer (NK) cell-mediated ADCC, we next performed a global uncertainty and sensitivity analysis[113] to identify parameters that are key drivers in activating the formation of the env-IgG-FcγRIIIa complex. In this analysis, complex formation (output) was calculated for 2,000 unique sets of parameter values (i.e., IgG1–4 concentrations and binding affinities to env and FcγRIIIa, respectively), sampled from uniform-probability density functions tailored to each parameter (Figure 2.1C). Notably, partial rank-correlation coefficients (PRCCs) calculated for each parameter (initial concentrations and affinities) suggested that IgG1 and IgG3 were the only globally significant subclasses. For these parameters, higher PRCC values indicated greater influence on complex formation. IgG1 and IgG3 parameters were important in terms of both concentration (PRCC = 0.79 and 0.12, respectively) and affinities to FcR (k_{on} PRCC = 0.45 and 0.06, respectively) and HIV (IgG1 k_{on} PRCC = 0.08), with IgG1 considerably more sensitive than IgG3 parameters (Figures 2.2B and

2.2C). This was unsurprising given that both have a high affinity to FcγRIIIa and greater relative average plasma concentration compared with other subclasses (Figure 2.1C). The importance of IgG1 and IgG3 parameters were also observed for the lower-affinity FcγRIIIa polymorphism (FcγRIIIa-F^{158})(Figure A.S3). The sensitivity analysis also illustrated that IgG1 and IgG3 affinity to FcRs was more influential than IgG1 and IgG3 affinity to the HIV env, emphasizing the possible greater importance of genetic and post-translation modifications that influence Ab Fc region affinity (such as glycosylation and FcR polymorphisms) over modifications that influence Fab affinity to the target. Although this analysis was focused on monomeric gp120 because of its relevance to RV144, the fact that IgG1 affinity to env was not a critical parameter in the model suggests that strain-related differences in affinity would not influence results. Interestingly, FcR complex formation was also significantly sensitive to env and FcR concentrations, which has implications for variability in FcR complex formation in tissue compartments with different levels of FcR expression and virus dissemination. To start with the simplest possible model, IgG binding cooperativity was not initially included in the model. To determine whether that could influence results, a second model framework was created in which a cooperativity constant (k_c) was included for every binding interaction of a second IgG[114]. A global sensitivity analysis for each FcR (kc was varied from 0.01 to 100) indicated that the cooperativity constant was not a significant parameter in any of the models and, so, was not included in the remaining analysis (Figure A.S4).

2.3.3 Model reveals personalized differences in the benefit of increasing IgG1

Because IgG1 and IgG3 concentration were both identified as sensitive parameters in the global sensitivity analysis and correlated with enhanced Fc functions in the RV144 trial, we used the model to further explore the landscape of complex formation as IgG1 and IgG3 concentrations were altered together over 2,500 physiologically relevant combinations to predict complex formation (Figure 2.3A).

This analysis predicted a sensitive range of IgG1 concentration between 18 and 252 nM, in which small changes in HIV-specific IgG1 would increase complex formation, but insensitivity above that range. The model additionally suggested that increases in IgG3 concentration could lead to even greater complex formation starting at 4.6 nM, with a steeper slope to indicate more sensitivity to smaller increases in IgG3 and a much higher limit. The IgG3 occurred at IgG3

levels of 589 nM, 192X the median IgG3 concentration of the vaccinees (Figure A.S5A). Unexpectedly, this analysis illustrated how high IgG1 (greater than 252 nM) may negatively affect complex formation if IgG3 is also high (greater than 21.6 nM). Inspection revealed that this occurred because of a lower IgG1 binding affinity for FcγRIIIa compared with IgG3; therefore, at high concentrations, IgG1 can outcompete IgG3 for the env and reduce the overall affinity of immune complexes to FcγRIIIa. This effect is also seen in the lower affinity polymorphism FcγRIIIa-F^{158} (Figure A.S5B). Results from the global sensitivity analyses for FcγRIIa-H^{131} and FcγRIIa-R^{131} suggested that IgG1 parameters were even more dominant because of an even lower binding affinity of IgG3 for FcγRIIa compared with FcγRIIIa (Figure A.S3). Using experimentally measured values for env A244-specific IgG1 and IgG3

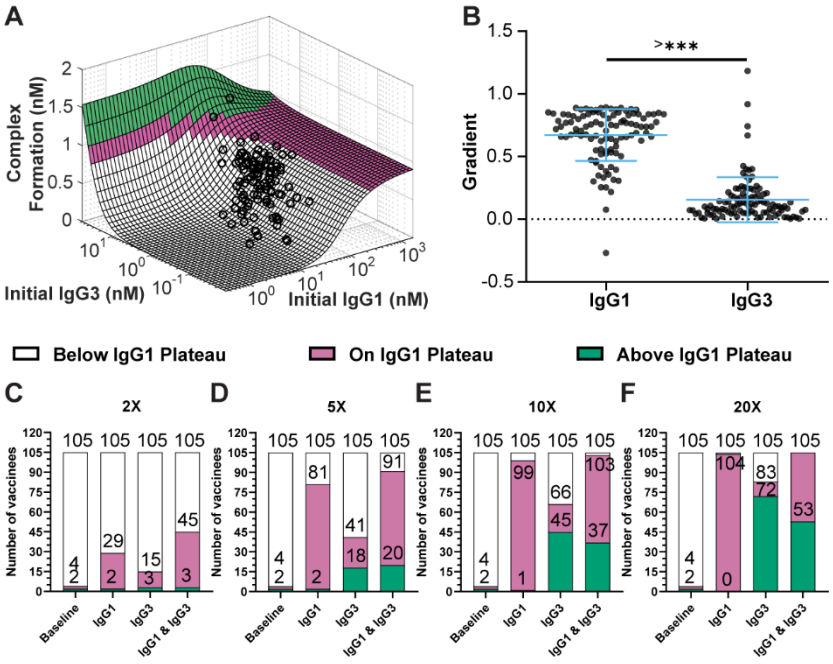

Figure 2-4 Combined changes in IgG subclass concentrations identifies an optimal range of antigen-specific IgG1 and IgG3

(A) Model predictions for env:IgG:IgG:FcγRIIIa:FcγRIIIa complex formation at steady state (z axis) for 2,500 simulations over a range (0.004×–20×) of the IgG1 and IgG3 baseline initial concentration combinations (x and y axis). Grid colors represent complex formation levels, which were determined based on the IgG1 plateau: below the IgG1 plateau (<0.77 nM, white), on the IgG1 plateau (0.77–0.98 nM; pink), and above the IgG1 plateau (>0.98 nM, green). RV144 vaccinee samples (n = 105) were plotted (black circles) at their corresponding individual env-specific IgG1 and IgG3 concentrations.
(B) Gradients in the direction of IgG1 and IgG3 were calculated for each individual as a measure of the immediate sensitivity of each vaccinee to changes in IgG1 or IgG3 concentration. A two-tailed Wilcoxon matched-pairs signed-rank test indicated the IgG1 gradient was significantly greater than that of IgG3; $p < 0.0001$.

(C–F) Complex formation level achieved (below IgG1 plateau, white; on IgG1 plateau, pink; above IgG1 plateau, green) at baseline and under the following conditions: fold change of either IgG1, IgG3, or both at either 2× (C), 5× (D), 10× (E), or 20× (F) the individual baseline concentrations. The data labels on the stacked bar graph indicate the total number of vaccinees that achieved that respective activation level and all those below it.

See also Figure A.S5.

concentration in 105 RV144 participants, we plotted each individual on the generated predictive surface (Figure 2.3A) and found that unique combinations of IgG1 and/or IgG3 concentrations would be required to boost complex formation for each individual. A comparison of the gradient (slope) calculated from the surface for each vaccinee in their immediate IgG1 and IgG3 directions indicated that significantly more vaccinees fell in the IgG1-sensitive region (i.e., increasing IgG1 would result in increased complex formation) than in the IgG3-sensitive region (Wilcoxon matched-pairs signed-rank test; $p < 0.0001$; Figure 2.3B). Visual inspection of the surface also suggested that some individuals were predicted to be sensitive to both IgG1 and IgG3 (Figure 2.3A) and that a few were predicted to have reduced complex formation with increases in IgG1 levels also seen with a single negative IgG1 gradient (Figure 2.3B).

To illustrate this concept more concretely, we used the model to simulate a theoretical vaccine boosting regimen that increased HIV-specific IgG1 or IgG3 individually or simultaneously by 2X, 5X, 10X, and 20X in each individual. We categorized the complex formation achieved in relation to the complex formation on the IgG1 plateau by tallying the number of individuals that achieved a complex formation ‘‘below IgG1 plateau’’ (<0.77 nM), ‘‘on IgG1 plateau’’ (0.77–0.98 nM; on IgG1 plateau +10%), or ‘‘above IgG1 plateau’’ (>0.98 nM) in each case (Figures 2.3C–2.3F). Results illustrated how complex formation on the IgG1 plateau (pink bars; 0.77–0.98 nM) could be achieved in approximately one-quarter of individuals (27/105) with 2X IgG1 (Figure 2.3C) and in most (98/105) with 10X IgG1 (Figure 2.3E). Notably, however, complex formation above the IgG1 plateau (green bars; 0.98 nM) would require high IgG3 without an increase in IgG1. To reach complex formation above the IgG1 plateau, most individuals (72/105) would require at least 20X IgG3 (Figure 2.3F). Importantly, these IgG3 additions must occur without the addition of IgG1, which significantly decreased the proportion of complex formation above the IgG1 plateau in comparison with IgG3 alone in the 20X cases (binomial test; $p = 0.0001$; Figure 2.3F). The simulations also illustrated how large additions (20X) of IgG1 and IgG3 together could prevent complex formation above the IgG1 plateau because of competition between IgG1 and IgG3 to form complexes as described above. Intriguingly, two individuals in our population already had the capacity to induce complex formation above the IgG1 plateau at baseline; however, simulated boosting with IgG1 alone reduced complex formation on the IgG1 plateau in those individuals (Figures 2.3E and 2.3F). Although there were a limited number of IgG3-high individuals in the RV144 cohort evaluated in this study (n = 105), it is possible that

more exist across the entire RV144 study (more than 16,000 participants), as well as in other related trials that employed boosting, including RV305 and RV306[60]. Overall, these results suggest that vaccine interventions aimed at increasing HIV-specific IgG1 are expected to increase complex formation in most individuals, but reach a limit, and that different individuals are predicted to be sensitive to IgG1 based on proximity to that limit. Furthermore, they suggest that high concentrations of IgG1 may reduce complex formation in individuals with high levels of IgG3.

2.3.4 Experimental validation of IgG1 sensitivity predictions

To validate the concept of differential IgG1 sensitivity experimentally, we used the model to select a subset of individuals predicted to be insensitive or sensitive to IgG1 concentration and added a monoclonal IgG1 Ab to serum samples from those individuals. Because the multiplex assay requires high-affinity antibodies to ensure binding to the pathogen, we selected an HIV-specific IgG1 monoclonal antibody, PGT121, reported to bind with high avidity to clade B HIV-env proteins[84,115,116]; however, PGT121 binds comparatively weakly to A244[117]. We, therefore,

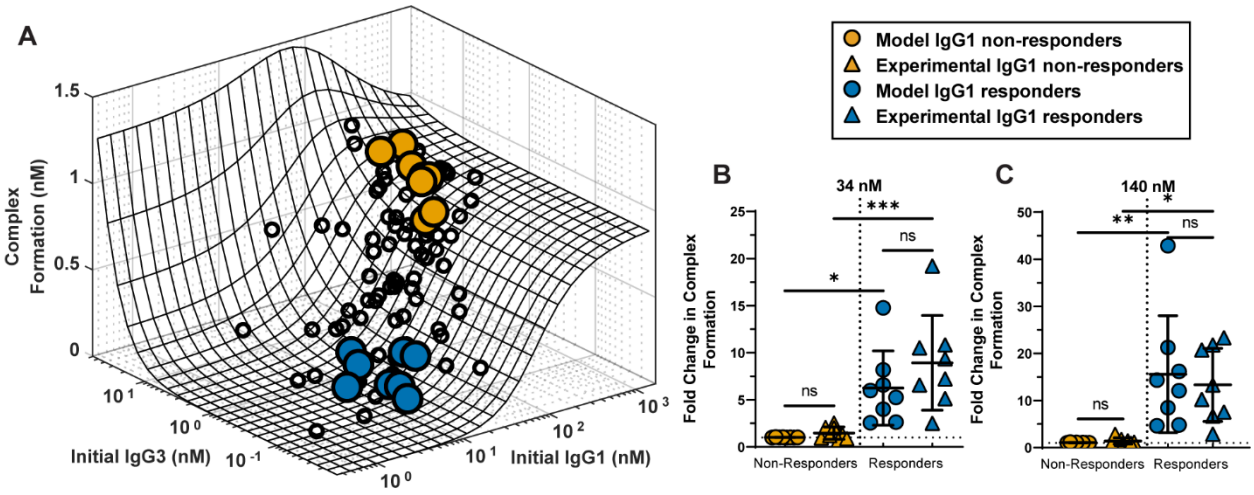

Figure 2-5 Experimental validation of IgG1 sensitivity

(A) Measured gp120 BaL-specific initial IgG1 and IgG3 concentrations were used to predict FcγRIIIa-V^{158} complex formation at steady state (z axis) for RV144 vaccinee samples (n = 105; black circles). Individuals were selected based on predicted IgG1 sensitivity: "responders" (blue circles; vaccinees 9, 15, 18, 19, 24, 26, 27, and 30) and "non-responders" (orange circles; vaccinee 1, 3, 4, 12, 13, 16, 22, and 29).
(B and C) Model predictions (circle) and experimental measurements (triangle) of fold change in complex formation for IgG1 responders (blue) and non-responders (orange) with the addition of either 34 (B) or 140 (C) nM monoclonal PGT121 IgG1. $*p < 0.05$, $**p < 0.01$, $***p < 0.001$, $^{>}***p < 0.0001$, ns indicates p value ≥ 0.05 by ordinary one-way ANOVA.
See also Figure A.S5.

measured clade B HIV BaL gp120-specific IgG subclass concentrations in each individual and plotted them on the generated IgG1 and IgG3 surface as described above (Figure 2.4A).

We chose a group of individuals that the model predicted to be sensitive to increases in BaL IgG1 (we termed them ‘‘IgG1 responders’’; blue; vaccinees 9, 15, 18, 19, 24, 26, 27, and 30) and a group that was predicted to not be sensitive to IgG1 (we termed them ‘‘IgG1 non-responders’’; orange; vaccinees 1, 3, 4, 12, 13, 16, 22, and 29; Figure 2.4A) and added an HIV-specific IgG1 monoclonal Ab to each (34 and 140 nM) before measuring changes in IgG-FcγRIIIa complex formation with multiplex assays described above. Overall, model predictions were not significantly different than experimental measurements for both responders and non-responders at both concentrations (one-way ANOVA with multiple comparisons; non-responders: 34 nM, $p > 0.9922$; 140 nM, $p > 0.9996$; responders: 34 nM, $p = 0.3581$; 140 nM, $p = 0.9258$), and IgG1 responders demonstrated a significantly higher fold change in complex formation experimentally (5-fold and 7-fold) than non-responders did (1.3-fold and 1.3-fold) after addition of 34 and 140 nM IgG1 (one-way ANOVA with multiple comparisons; $p = 0.0004$ and $p = 0.0150$, respectively; Figure 2.4B). Model predictions were also significantly correlated with experimental measurements for responders and non-responders (Spearman; 34 nM addition: $r = 0.80$, $p = 0.0003$; 140 nM addition: $r = 0.84$, $p = 0.0001$; Figures A.S5C and A.S5D).

2.3.5 IgG1 allotype may significantly influence IgG-FcR complex formation

We next used the model to assess whether IgG concentration differences arising from genetic background could have significantly reduced FcγR-IgG complex formation in HVTN702 vaccinees compared with that of RV144. Recent work indicates IgG1 allotype can influence vaccine-specific IgG subclass distribution in individuals, with G1m1,3 generally having greater IgG1 and IgG3 but less IgG4 than G1m-1,3 and G1m1[90]. These allotypes have been linked to ethnicity[118], with G1m1,3 allotype likely more prevalent in individuals of Asian ethnicity[119], and G1m-1,3 and G1m1 allotypes likely more prevalent in white individuals and in those of Black African ethnicity[118]. One key question is whether IgG1 allotype-linked changes in IgG subclass concentrations could be sufficient to significantly reduce IgG-FcR complex formation in HVTN 702 vaccinees compared with RV144. We used IgG subclass distributions previously measured in HIV phase I vaccinees with known different allotypes[90] to alter IgG1–4 concentrations in each RV144 vaccinee according to the other allotypes by calculating a conversion factor (Figure 2.5A).

Thus, we were able to ‘‘project’’ RV144 data used in this study (likely high prevalence of

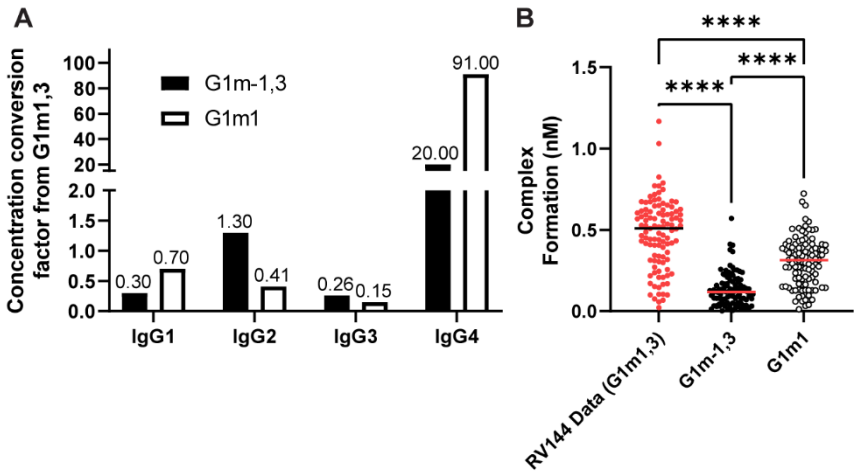

Figure 2-6 IgG1 concentration differences resulting from Gm allotype are predicted to significantly alter FcR complex formation

(A) Conversion factors for each initial IgG concentration from G1m1,3 to indicated allotypes. Projections were simulated by multiplying each vaccinee's initial IgG concentrations by the respective conversion factors and performing the simulations according to the baseline protocol.
(B) Model predicted complex formation for FcγRIIIa-V^{158} in G1m-1,3 (n = 105; black circles) and G1m1 (n = 105; white circles) compared with the original data, assumed to be G1m1,3 (n = 105; red circles) ∗p < 0.05, ∗∗p < 0.01, ∗∗∗p < 0.001, >∗∗∗p < 0.0001, using the Friedman test with Dunn's multiple comparisons test.

G1m1,3[119]) onto the G1m-1,3 and G1m1 allotypes expected to be prevalent in the HVTN 702 trial performed in South Africa[118] (Figure 2.5B). Overall, the model predicted that there would be a significant reduction in IgG-FcR complex formation in G1m1 and G1m-1,3 allotypes, likely

because of reductions in IgG1 for G1m1 and G1m-1,3 in comparison with G1m1,3 (rather than changes in IgG3 and IgG4). For this reason, the model suggests higher boosts of IgG1 concentration may be more important in the South African population of the HVTN 702 trial than it would be in the Thai population of the RV144 trial. Overall, results illustrate how this approach can be used as a hypothesis-testing tool to isolate and evaluate factors that may contribute to failed vaccine trials.

2.3.6 IgG1 binding affinity for FcR is important for increasing FcγRIIIa complex formation broadly across a population

After observing the importance of varying individual sensitivities to two parameters (IgG1 and IgG3 concentration), we performed a personalized single-parameter sensitivity analysis for each individual in our study, predicting complex formation after altering each parameter over 0.004X to 20X baseline values for that person. A sensitivity metric (change in complex formation/change in the input parameter) was calculated for each parameter and used to illustrate the resulting personalized, single-parameter sensitivities (Figure 2.6A).

We then evaluated complex formation ‘‘below IgG1 plateau’’ (<0.77 nM), ‘‘on IgG1 plateau’’

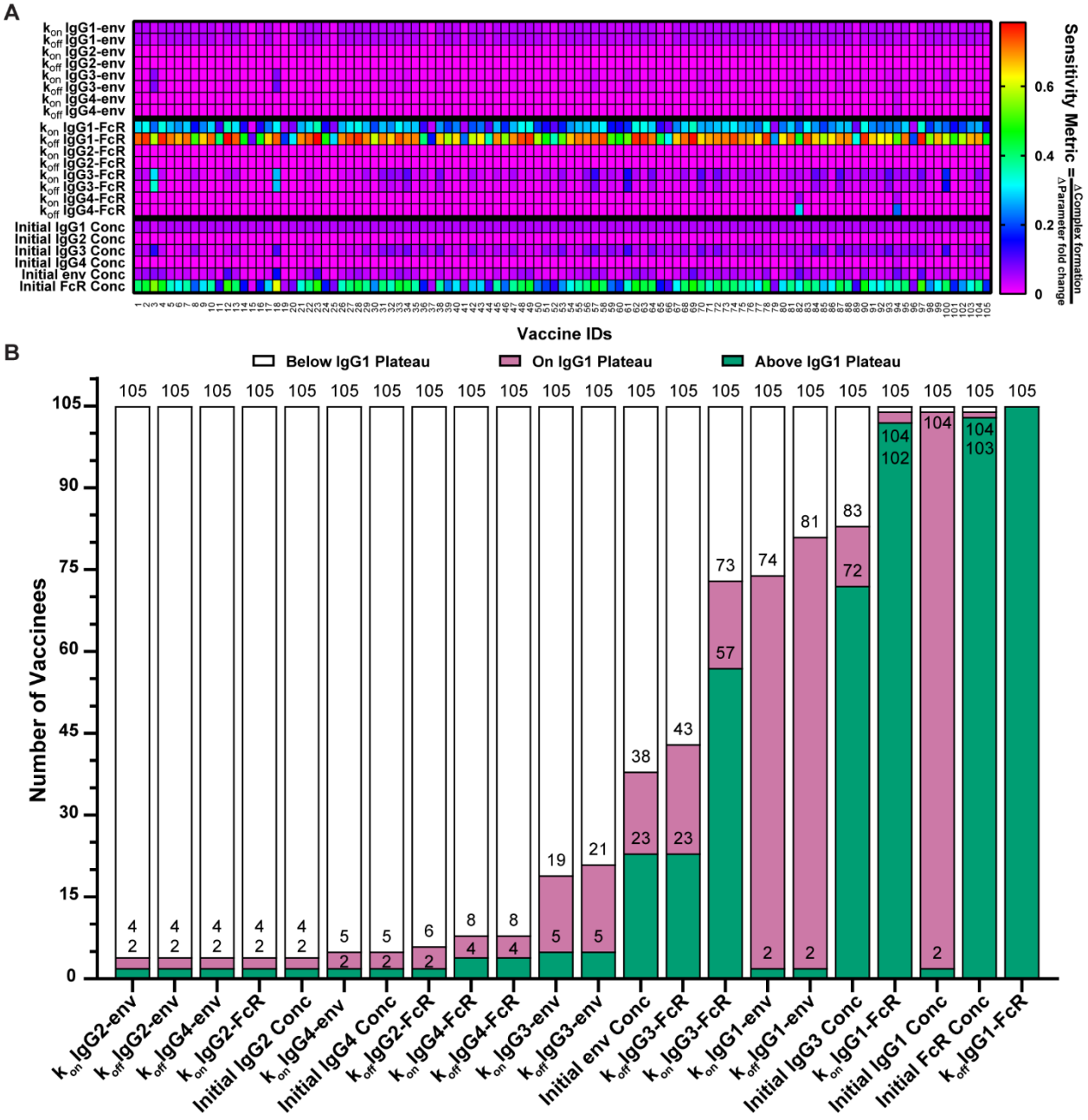

Figure 2-7 Personalized, single-parameter sensitivity analysis illustrates universal sensitivity of IgG1 affinity for FcγR

(A) For each vaccinee (x axis, labeled 1–105), parameters (y axis) were altered individually 0.004×–20× the baseline, and a sensitivity metric was calculated by dividing the change in complex formation by the change in the parameter multiplier (color bar).

(B) The number of vaccinees at each activation level (below IgG1 plateau, white: < 0.77 nM below the IgG1 plateau; on IgG1 plateau, pink: 0.77 – 0.98 nM, on IgG1 plateau +10%; or above IgG1 plateau, green: >0.98 nM, >10% above plateau) for each parameter perturbation, based on the maximum complex formation level achieved over the seven simulations from 0.004× to 20× for each parameter. The data labels on the stacked bar graph indicate the total number of vaccinees that have achieved that respective complex formation level and all those below it.

See also Figure A.S6.

(0.77–0.98 nM; on IgG1 plateau +10%), or ‘‘above IgG1 plateau’’ (>0.98 nM), as described above. We observed the same variability in individual sensitivity to IgG1 and IgG3 concentration parameters, consistent with the variability in baseline IgG1 and IgG3 concentrations seen in our previous analysis (Figure 2.3A). Specifically, most individuals were sensitive to IgG1 concentration, but sensitivity plateaued in accordance with the IgG1 plateau observed in Figure 2.3A because 103/105 patients were limited to complex formation on or below the IgG plateau at any level of IgG1 concentration 0.004X–20X (Figure 2.6B). Likewise, we saw variability in IgG3-related parameters that reflects the small number of individuals within the IgG3-sensitive region on Figure 2.3A, with 72 reaching complex formation above the IgG1 plateau, 11 on the IgG1 plateau, and 22 below the IgG1 plateau for some IgG3 concentrations of 0.004X–20X (Figure 2.6B). All but two individuals (vaccinees 82 and 94, who both had very high IgG4 levels) were not sensitive to changes in IgG2 and IgG4 parameters, with only 4–8 vaccinees reaching complex formation on or above the IgG1 plateau with alterations in these parameters, reinforcing the deleterious effect of high IgG4 concentrations seen in the VAX003 trial. Perhaps the most interesting outcome of the personalized, single-parameter sensitivity analyses was that most all individuals were extremely sensitive to (1) IgG1 Fc affinity to FcR (105/105 reached complex formation above the IgG1 plateau with a 0.004X change in the k_{off}; Figure 2.6B); and (2) FcR concentration (103/105; Figure 2.6B). Of note, IgG1 Fc affinity and FcR concentration remain the most broadly sensitive parameters in personalized, single-parameter sensitivity analyses of FcγRIIIa-F^{158}, FcγRIIa-H^{131}, and FcγRIIa-R^{131}, with less IgG3 sensitivity seen in FcγRIIa, as expected (Figure A.S6). Overall, there was a significantly higher proportion of complex formation above the IgG1 plateau with changes in k_{on} and k_{off} IgG1-FcR than with changes in IgG1 concentration (binomial test; $p < 0.0001$). These results place a high priority on physiological or therapeutic alterations that could influence IgG1 affinity for FcR, such as glycosylation, and has important implications for individuals with different FcγRIIIa polymorphisms (which alters affinity of the FcR for all IgGs). In terms of glycosylation, model results predict significant differences are expected to arise from IgG1 Fc glycosylation in the RV144 vaccinees we evaluated, but not from Fab glycosylation or from Fc glycosylation of other IgG (2–4) subclasses (Figure A.S7A). Model predictions also suggest that significant differences would be expected to arise from IgG1 binding-affinity alterations because of FcγRIIIa polymorphisms in this population of RV144 vaccinees (Figures A.S7B and A.S7C).

2.3.7 The model reveals synergistic effects of combined changes in IgG1 concentration and IgG1 FcγRIIIa binding affinity

Given the variability in individual sensitivity to IgG1 concentration, we next hypothesized that IgG and FcR modifications that influence IgG1 affinity for FcγRIIIa (including FcR polymorphism and glycosylation) have the potential to have synergistic effects when changed in combination with IgG1 concentration. This would mean that IgG1 Fc glycosylation and FcR polymorphism would have differential effects on FcγR activation across individuals, depending on an individual's levels of HIV-specific IgG1. To test that idea across a range of perturbations, we increased IgG1 concentration and FcγRIIIa binding affinity separately and in combination by 2X, 5X, and 10X to reflect therapeutically relevant alterations that could be achieved by glycoengineering (Figure 2.7A).

We selected these perturbations based on potential concentration changes and previously reported affinity changes related to glycosylation of the IgG1 Fc region[120–123] (Table A.S2). Interestingly, this analysis illustrated how alterations in affinity of IgG1 to FcγRIIIa may be most effective for increasing FcγRIIIa complex formation broadly across vaccinated individuals. For example, although a 2X increase in IgG1 concentration results in complex formation at the IgG1 plateau in 26% (27/105) of individuals, a 2X increase in FcγRIIIa binding affinity would be predicted to result in a complex formation above the IgG1 plateau in 40% of individuals (42/105) (Figure 2.7B). Compellingly, although a 5X increase in concentration results in complex formation on the IgG1 plateau in most (75%; 79/105) individuals, a 5X increase in binding affinity would result in complex formation above the IgG1 plateau in most (82%; 86/105) individuals (affinity change results in significantly more complex formation above the IgG1 plateau by a binomial test; $p < 0.0001$; Figure 2.7B). model, the respective median increases are predicted to be 0.33 nM and 1.4 nM, for a sum total change of 1.7 nM. However, tuning them simultaneously in the model by 5X results in a 2.7 nM increase in complex formation, a 57% increase over what would be expected from simple summation. The model predicted that combined changes were significant compared to additive individual changes across all conditions evaluated (Wilcoxon matched-pairs signed-rank test; all $p < 0.0001$; Figures 2.7C–2.7E). This result suggests that synergistic effects may arise from combinatorial increases in both IgG1

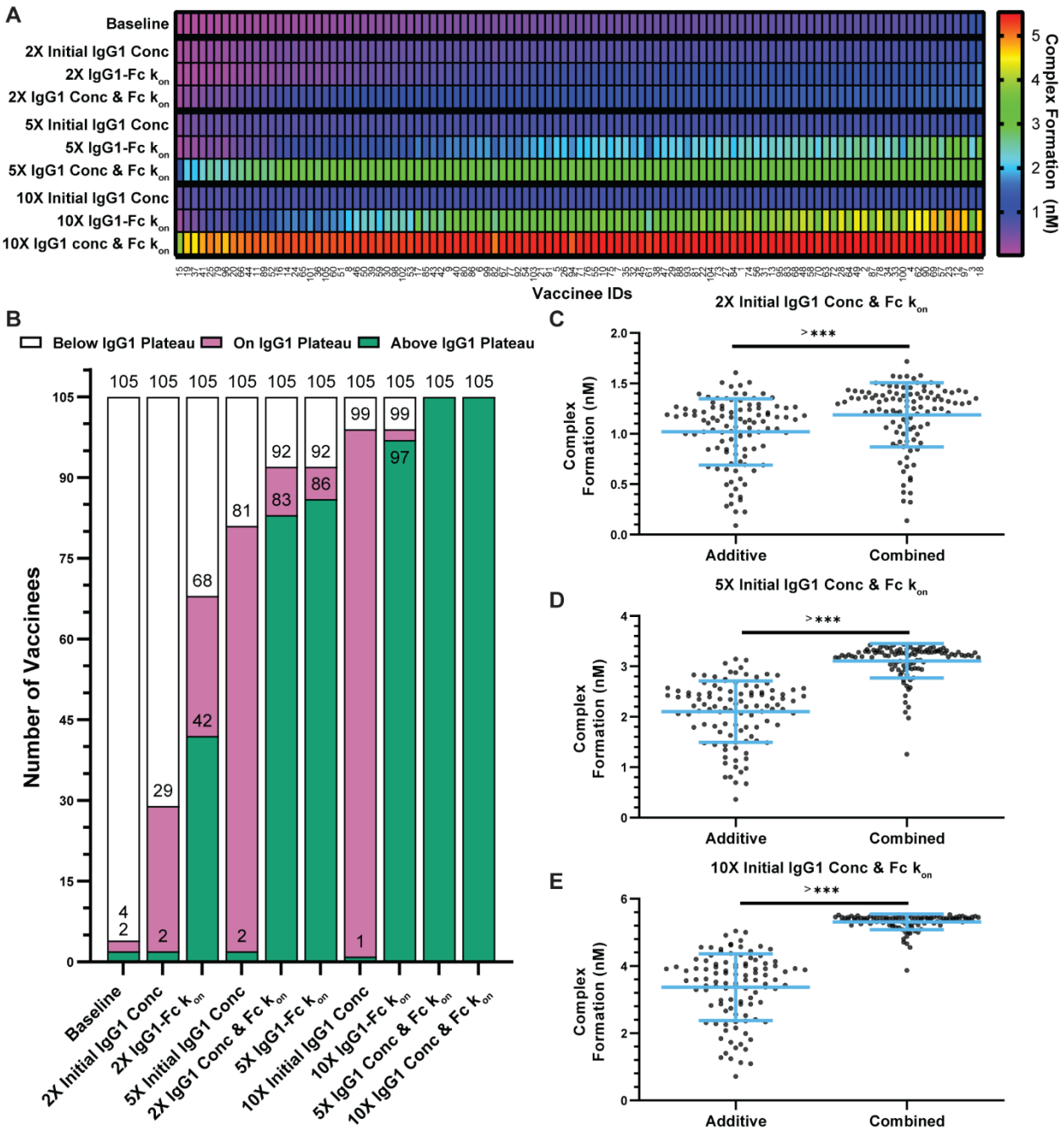

Figure 2-8 Combined changes in IgG1 concentration and IgG1 Fc binding result in synergistic changes in complex formation

(A) Predicted complex formation for each vaccinee at baseline and when IgG1 concentration and IgG1 binding affinity (k_{on}) are increased separately or together. Color bar indicates complex formation.
(B) The number of vaccinees at each complex formation level (below IgG1 plateau, white; on IgG1 plateau, pink; above IgG1 plateau, green) for each condition in (A).

(C–E) Complex formation resulting from (1) simple addition of complex formation predicted from separate initial IgG1 concentration and IgG1-FcγR affinity parameter perturbations ("Additive") at 2× (C), 5× (D), or 10× (E); or (2) simultaneous perturbations of IgG1 concentration and IgG1-FcγR affinity within the model ("Combined"). Comparison made with a two-tailed Wilcoxon matched-pairs signed rank test with $\alpha = 0.05$. $^{>}$***$p < 0.0001$.

concentration and IgG1 FcR affinity that would not be apparent from studying each feature in

isolation.

2.4 Discussion

Here, we present a quantitative approach for understanding how personalized variation in IgG and FcγR features may contribute to variability in cellular FcR activation after vaccination. Our results have important implications in the context of failed HIV vaccine trials that were modeled upon RV144. It is possible that larger numbers of boosts and alternative adjuvants used in other trials may have had a limited effect on IgG-FcγRIIIa complex formation because of a plateau in the benefit of increasing IgG1. Furthermore, the model suggests that elevated IgG1 induced with boosting may even inhibit Fc responses in some individuals that have high IgG3. It is also possible that IgG subclass-distribution differences linked to genetic background (IgG1 allotype) have the potential to significantly reduce immune complex formation in follow-up RV144 trials in which G1m1,3 allotypes are less prevalent than G1m-1,3 and G1m1 (such as HVTN702). Given measurements of IgG1, IgG2, IgG3, and IgG4 in plasma samples from other vaccine trials, the analysis presented here could be usefully extended to directly address these questions. In contrast to highly variable individual responses to IgG subclass concentrations, model results highlighted the global importance of IgG1 affinity for FcγRIIIa and suggest that this may be the most effective way to increase FcγRIIIa activation broadly across a population. This is especially interesting in the context of a number of reported physiologically and therapeutically relevant perturbations to the IgG1 Fc region that could influence binding affinity, including FcR polymorphisms and glycosylation[124,125]. Results here suggest that vaccine adjuvants able to modulate IgG1 Fc glycosylation may be the most effective way to improve FcγRIIIa complex formation in many vaccinees. For example, a 2X increase in IgG1-FcR k_{on} would boost 65% of vaccinee samples into at least complex formation on the plateau, whereas a 2X increase in IgG1 concentration alone would promote complex formation on the plateau in only 28% of vaccinees. Furthermore, the model predicted that a 5X increase in IgG1-FcR k_{on} would result in complex formation above the IgG1 plateau in 82% of the individuals we evaluated, which was not achievable with similar changes in IgG1 and IgG3 concentrations. Importantly, model predictions prioritize the importance of IgG1 Fc glycosylation across a multitude of other potential glycosylation modifications, including those to IgG2, IgG3, and IgG4 Fc regions as well as those that mediate Fab binding in all IgG subclasses. Previous studies have demonstrated

that different vaccine strategies induce varied antigen-specific antibody glycosylation[126]; however, specific adjuvant-mediated modulation of Fc-glycosylation is not yet possible. Model results may help guide the focus for future experimental measurements of glycosylation in vaccine samples.

The approach presented here adds a complementary dimension to previous systems serology research, which has been based on data-driven computational approaches[52,68,82,83,127–130]. Although data-driven algorithms have been valuable for identifying signatures of antibodies and FcR features associated with vaccines and/or cellular functions, it has been challenging to gain insight into mechanisms that underpin heterogeneity across populations of individuals[68]. Our previous systems-serology analysis of the data from HIV vaccine trials (including RV144 and VAX003)
identified important statistical associations between IgG1, IgG3, and Fc-effector functions in the RV144 trial but was not able to define mechanisms responsible for heterogeneity in Fc effector functions across individuals[52,83]. The mechanistic model presented here builds on that by illustrating how individuals may be differentially sensitive to vaccine regimens that increase IgG1 concentration and identifies a mechanism by which some individuals may be negatively affected by an increase in IgG1. It also highlights the importance of IgG1 affinity for FcγRIIIa as a critical parameter for increasing FcγRIIIa activation and ADCC broadly across populations of individuals. Altogether, these results complement information obtained from previous data-driven analyses.

This model is a simple reconstruction of key events understood to be involved in FcγRIIIa activation upstream of ADCC and represents a first step toward the quantitative understanding of intercellular IgG-FcR signaling. Our current model only considers FcγRIIIa, a single FcγR type believed to be upstream of ADCC, and a single HIV epitope (env) that was central to RV144 vaccination. Although it provides insight into concepts of personalized mechanisms that may limit FcγRIIIa complex formation after RV144 vaccination, predicting vaccine efficacy and the full quantitative mechanisms underlying responses to treatment in humans will be more complex. Future iterations of this work could include multiple epitopes to assess competition or a range of

other infectious diseases, including SARS-CoV-2[130], Mycobacterium tuberculosis, and Ebola, or even to enhance monoclonal antibody therapeutics[69].

Overall, the results of this study resonate with existing literature from HIV vaccine trials and also provide insights for maximizing FcγRIIIa complex formation after vaccination across patient populations. Especially surprising were quantitative insights that predicted limitations in vaccine platforms that induce large increases in HIV-specific IgG1, contrasted with a seemingly unlimited benefit of increasing IgG1 FcγRIIIa binding affinity. Computational methods may be valuable for accelerating and guiding future vaccine development because these methods can predict which component(s) of an Ab (Fab or Fc) have the greatest contribution to Fc effector functions and may save time and cost in experimental assays. Importantly, this approach could be useful for projecting vaccine trial results from one genetic background to another, providing information on the role of genetic parameters, independent of other variations in IgG and FcR features that occur across populations. Overall, we believe that this approach could help guide the development of future vaccine strategies against antigenically variable pathogens and understand personalized mechanisms that underpin FcR activation.

2.4.1 Limitations of the study

In this study, model predictions were validated with cell-free multiplex assays, which were necessary to overcome challenges associated with low sample volume and to provide a direct comparison between model predictions and experimental measurements. Future work involving cellular assays represents a critical next step. This will require consideration of FcγR cell-surface concentrations and activation thresholds associated with cellular function, which have not yet been accessible with the rsFcγR dimer-binding assays (complex formation is measured in MFI units). Additionally, linking vaccine efficacy to levels of FcγR complex formation would require the use of case-control vaccine-failure samples, which were not available for use in this study but could be evaluated in the future.

2.5 STAR Methods

2.5.1 Key Resources Table

Table 2-1 Key Resources Table

REAGENT or RESOURCE	SOURCE	IDENTIFIER
Antibodies		
Human HIV-specific IgG1 mAb PGT121	Center for Antibody Development and Production, Scripts Research Institute	N/A
Polyclonal Anti-Human Immunodeficiency Virus Immune Globulin, Pooled Inactivated Human Sera (HIVIG)	NIH AIDS Reagents program	#3957
Biological samples		
RV144 phase III clinical trial plasma samples	U.S Military HIV Research Program (MHRP)[58,74]	N/A
Chemicals, peptides, and recombinant proteins		
HIV-1 Clade AE A244 gp120	NIH AIDS reagents	#12569
HIV-1 Clade B BAL gp120	NIH AIDS reagents	#4961
Influenza Hemagglutinin (HA) protein H3/Switzerland/2013	Sinobiological	11085-V08H
Dimeric rsFcγR	Hogarth lab, Burnet Institute[73,74]	N/A
SULFO-NHS-LC-BIOTIN NO-WEIGH 10 x 1mg	Thermo Fisher Scientific	A39257
Bio-plex Pro Magnetic COOH Beads XX (XX refers to bead region)	Bio-rad	MC100XX-01
Streptavidin, R-Phycoerythrin Conjugate (SAPE)	Life technologies	S866
Deposited data		
De-identified personal RV144 IgG subtype concentration data (estimated from MFI measurements)	This paper; Figshare	10.6084/m9.figshare.14810397
Data within Figures 2.2-2.7, A.S3-A.S11	This paper; Figshare	10.6084/m9.figshare.13229162
Software and algorithms		
Source code for simulations and analysis	This paper; Figshare and Github	10.6084/m9.figshare.13229177
Other		
Collection of deposited data and code from this paper	This paper; Figshare	10.6084/m9.figshare.c.5474580

2.5.2 Resource Availability

Lead contact

Further information and requests for resources and reagents should be directed to and will be fulfilled by the lead contact, Kelly Arnold (kbarnold@umich.edu).

Materials availability

This study did not generate new unique reagents.

Data and code availability

De-identified individual RV144 IgG subtype concentration data (estimated from MFI measurements) and all data within figures have been deposited at Figshare and are publicly available as of the date of publication. DOIs are listed in the Key resources table. All original MATLAB code for running personal simulations, surface simulations, and sensitivity analyses has been deposited at GitHub and linked through Figshare and is publicly available as of the date of publication. DOIs are listed in the Key resources table.
Any additional information required to re-analyze the data reported in this paper is available from the lead contact upon request.

2.5.3 Experimental Model and Subject Details

RV144 samples

RV144 phase III clinical trial plasma samples[58] were provided by the U.S Military HIV Research Program (MHRP). Samples from week 26 (2 weeks post-vaccination) RV144 vaccine recipients (n = 30; n = 75 from two separate shipments) were evaluated using data from a previously published study[74]. All relevant human research ethics committees approved all experimental studies. All plasma samples were provided de-identified of demographics including gender and age.

2.5.4 Method Details

Experimental methods

HIV-specific multiplex IgG subclass, rsFcγR dimer-binding assay

HIV-specific IgG subclass and recombinant soluble FcγR (rsFcγR) dimer binding multiplex data were used from a previously published RV144 study[74]. Extracted multiplex data included previously published IgG1, IgG2, IgG3, IgG4, rsFcγRIIa-H^{131}, rsFcγRIIIa-V^{158}, rsFcγRIIIa-F^{158} dimer data from the customized multiplex or ELISA binding assays using HIV-1 Clade AE A244 gp120 (NIH AIDS reagents catalog#12569), HIV-1 Clade B BAL gp120 (NIH AIDS reagents catalog #4961) recombinant protein antigens and Influenza Hemagglutinin (HA) protein (H3/Switzerland/2013, Sinobiological) as a positive control antigen, as nearly all individuals have previously been exposed to Influenza A virus.

These dimeric rsFcγR assays have been applied to several HIV and other infectious disease studies, which have demonstrated that they correlate with and hence are predictive of in vitro cell-based ADCC and ADCP assays[73–76,78]. All multiplex data was reported as an arbitrary Median Fluorescence Intensity (MFI).

For responder and non-responder IgG1 validation assays, multiplex assays were repeated as previously described[74] with and without the addition of 5mg or 20mg (ie 34 and 140 nM) of human HIV-specific IgG1 mAb PGT121 (purchased from the Center for Antibody Development and Production, Scripts Research Institute).

Surface plasmon resonance

SPR was conducted as previously described[131]. Briefly biotinylated gp120 BAL (NIH AIDS Reagents) was immobilized onto a SA sensor chip at approximately 300, 500, and 800 response units. A blank flow cell with no immobilized ligand was used as a reference flow cell. Injections of 60 ml of purified HIV-IgG (NIH AIDS Reagents program) at 1:3 dilutions ranging from 0.5 to 0.006 mg/ml were passed across flow cells at a flow rate of 20mg/ml, with subsequent 360s dissociation time to determine IgG disassociation. Regeneration after each injection used two pulses of 10 mM glycine HCl, pH 2.5. SPR measurements were conducted in HBS-EP buffer (0.01M HEPES (pH 7.4), 0.15M NaCl, 3mM EDTA, 0.005% [vol/vol]). Kinetic data were calculated using the BIA evaluation program, with data being fitted to the simplest 1:1 Langmuir binding model.

Computational methods

MFI conversion to mM

MFI measurements were converted to concentration measurements using a conversion factor based on a reference IgG1 concentration of 10,000 ng/mL[112]. For multiplex readings, when a standard is available there is a log-linear relationship between MFI and concentration when measurements are within the machine's dynamic range[132]. Conversion formulas were based on this typical relationship. We assumed that MFI measurements were in the dynamic range and that the average IgG1 concentration was 10,000 ng/mL. The conversion factor found for IgG1 was then applied to the remaining species within that given assay. This method was only used for IgG subclass concentrations and not complex formation first because the reference concentration is from a similar vaccine trial and is not measured directly from RV144 vaccinees. Furthermore, MFI of IgG subclasses and MFI of FcR complex formation were measured in different experimental assays, using different fluorescent detector reagents (ie each reagent has different relative fluorescence per molecule) such that absolute quantitative comparisons across assays are extremely difficult. Given these uncertainties, we are not comfortable converting our experimental FcR complex measurements to nM, implying a direct prediction of concentration.

$$MFI_n = MFI\ of\ species\ n\ for\ vaccinee\ 1-105$$
$$mw_n = molecular\ weight\ of\ species\ n\ in\ kDa$$
$$ref = reference\ concentration = 10{,}000\,\frac{ng}{mL}$$
$$cf = conversion\ factor$$
$$ngml = concentration\ in\ ng/mL$$
$$cf = \frac{log_{10}(ref)}{mean(log_{10}(MFI_{IgG1}))}$$
$$ngml_n = 10^{(log_{10}(MFI_n)*cf)}$$
$$mM_n = \frac{ngml_n}{mw_n * 10^6}$$

ODE model

A system of ODE equations was created to describe the env-IgG-FcγR system in Figure 2.1B. We assumed no degradation or production of species over the short time span of the model.

Initial concentrations of lgG1, lgG2, lgG3, lgG4 were set for each individual using measurements made in sera samples from each vaccinee (see below). The average of these personal values for vaccinees 1-30 were used as the baseline measurements for initial IgG concentrations in the global sensitivity analysis. The initial concentrations of env (~25 nM) and rsFcγR dimer (~20 nM) were set based on multiplex experimental conditions described previously and annotated below (Figure 2.1C)[74]. The initial concentration of each complex was set to zero. Binding parameters for lgG1, lgG2, lgG3, lgG4, and FcγR dimers were set based on literature values[88] while env binding parameters were determined via SPR measurements as described below (see Figure 2.1C and Table A.S1). We obtained K_As for each IgG subclass binding to FcγRIIIA-V^{158} from the literature[88]. We converted these K_As to k_{on}s by estimating a universal k_{off} from pooled RV144 serum samples (0.01 s-1). We used MATLAB's ode113 solver function to predict the concentration of each complex over 100000 s, with an absolute error tolerance of 1e-50, relative tolerance of 1e-10. We assumed sequential IgG antibody binding to env prior to engagement of any env-IgG-IgG complex with any FcγR dimer. We assumed no cooperativity in IgG binding env (affinity values are independent of the presence of another IgG on the same envelope protein). For antigen-IgG complexes containing two of the same IgG subclass we used literature values for the reported value of that subclass[88]. For complexes containing two different IgG subclasses, we averaged the two individual IgG subclass affinities. All parameters used (and sources) are reported in Figure 2.1C and Table A.S1.

Sensitivity analysis

We performed a global uncertainty and sensitivity analysis[133] using population averages for baseline concentration parameters (Figures 2.2B, 2.2C, A.S3, and A.S4), as well as a personalized single-parameter sensitivity analysis, using personalized concentration parameters as baseline (Figures 2.6A and A.S6). In the global sensitivity analysis algorithm provided by the Kirschner lab at the University of Michigan (Figures 2.2B, 2.2C, A.S3, and A.S4), we assigned uniform probability density functions (pdfs) to each parameter (initial concentrations and affinities) with a minimum 0.004X of baseline and a max 20X of baseline for all parameters except k_c (0.01X-100X and base-line = 1)[133]. These pdfs were sampled using Latin hypercube sampling (LHS) to create random combinations of parameter values. The model was evaluated under each of the 2,000 sets of random parameter combinations, allowing for a multidimensional exploration of the system. Partial rank correlation coefficient (PRCC) calculated within the

algorithm determined the correlation between each input variable's variance throughout the multidimensional analysis and the output variable, giving a sensitivity measure for each parameter and a statistical significance of its effect on complex formation.

Combinatorial IgG1 and IgG3 concentration parameter alterations (Figures 2.3 and A.S5)
2,500 simulations were run with differing combinations of initial IgG1 and IgG3 concentrations. All combinations of 50 values were uniformly spaced on a logarithmic scale between 0.004X-20X baseline concentration for Figures 2.3A and A.S5B and 0.004X-500X for Figure A.S5A for both IgG1 and IgG3 and were simulated with FcγRIIIa-V^{158} affinity parameters for Figures 2.3A and A.S5A, and for both polymorphisms in FcγRIIa and FcγRIIIa in Figure A.S5B. Results were plotted as a grid surface. We predicted individual complex formation (n = 105) based on IgG subclass 1-4 concentrations. Individuals were plotted as circles at their specific IgG1 and IgG3 initial concentrations with their individually predicted complex formation concentration. Complex formation below the IgG1 plateau (< 0.77 nM, white), on the IgG1 plateau (0.77– 0.98 nM, pink), and above the IgG1 plateau (> 0.98 nM, green) categories were defined based on the IgG1 plateau on the grid surface, with complex formation on the IgG1 plateau going from the plateau minimum to 10% higher than the plateau's maximum value. The grid was colored based on the minimum threshold value achieved within each square. Simulations of IgG1, IgG3, or simultaneous fold changes were performed at 2X, 5X, 10X, and 20X of personal baselines. Vaccinees were binned into complex formation below, on, or above the IgG1 plateau under each of these conditions based on the previously mentioned thresholds. IgG1 and IgG3 gradients were calculated for each surface grid intersection (n = 2,500) using MATLAB's built-in gradient function, which calculated the numerical gradient based on the complex formation data (z-axis) and the uniform logarithmically spaced increments of IgG1 and IgG3 concentration (x and y-axis). Each vaccinee's gradient (n = 105) was approximated by using the gradient value at the nearest grid intersection corresponding to their personalized IgG1 and IgG3 concentrations.

IgG1 sensitivity validation (Figure 2.4)
We simulated the addition of either 34 or 140 nM IgG1 to each of the 30 vaccinees we had baseline complex formation measurements from to predict 8 IgG1 responders (highest fold change in complex formation from baseline) and 8 non-responders (lowest foldchange in complex formation from baseline after IgG1 addition). In order to experimentally validate our

model and predictions, HIV-specific monoclonal PGT121 IgG1 was added in the specified amounts to each plasma sample prior to being assessed for FcγRIIIa dimer binding via multiplex assay. Due to the large quantities of monoclonal Ab required for this assay and the need to use a monoclonal Ab with described ability to bind FcγRIIIa, we used PGT121 IgG1, which binds with high avidity to Clade B HIV envelope proteins, but binds comparatively weakly to A244 strains[84,115–117]. Thus we performed these simulations using HIV Clade B gp120 BAL-specific IgG1-4 concentrations. Complex formation for each responder and non-responder with each addition were captured by the model and measured in the multiplex assay and then converted into concentration using the same methods as IgG conversion.

Allotype simulations (Figure 2.5)

We projected complex formation into differently allotyped populations by first calculating a conversion factor under the assumption that our original dataset is entirely G1m1,3. We used time-matched (26 weeks; n = 6) human IgG subtype concentration data from a Phase I study on a candidate vaccine containing HIV-1 clade C CN54 gp140 envelope protein[112]. In collaboration with the authors, we grouped vaccinees by allotype (G1m-1,3 n = 3; G1m1,3 n = 1; G1m1 n = 2) and took the mean of each IgG subtype for each allotype. We calculated conversion factors for each IgG by dividing the given allotype's mean concentration by G1m1,3s mean concentration as follows:

$$cf_{G1mj}^{IgGi} = conversion\ factor\ for\ IgGi\ to\ allotype\ G1mj$$

$$m_{G1mj}^{IgGi} = mean\ concentration\ of\ IgGi\ in\ allotype\ G1mj$$

$$cf_{G1mj}^{IgGi} = m_{G1mj}^{IgGi} / m_{G1m1,3}^{IgGi}$$

To run the simulations to project the RV144 data available to us into G1m-1,3 and G1m1 populations, we converted each IgG initial concentration for each vaccinee based on the respective conversion factor as follows:

$$IgGi_{G1mj}^{x} = Initial\ IgGi\ concentration\ for\ vaccinee\ x\ in\ allotype\ G1mj$$

$$IgGi_{G1mj}^{x} = cf_{G1mj}^{IgGi} * IgGi_{G1m1,3}^{x}$$

With the converted IgG initial concentrations, the simulations were performed as described in the ODE model section above.

Personalized single-parameter sensitivity analysis (Figures 2.6 and A.S6)

We altered each parameter (k_{on} and k_{off} for each reaction and initial species concentrations) one at a time at three values above and below baseline (0.004X, 0.02X, 0.1X, 1X, 2.5X, 5X, and 20X) and calculated the predicted complex formation as total env-IgG-FcγR complexes at steady state. The sensitivity metric for each parameter was defined based on the following equation:

$$sm_{i,j} = \text{ sensitivity metric to parameter i for vaccinnee j}$$

$$\overline{fc} = fold\ change\ vector = [0.004\ 0.02\ 0.1\ 1\ 2.5\ 5\ 20]$$

$$\overline{com_{i,j}} = [complex\ formation_{0.004X\_i,j} \cdots complex\ formation_{20X\_i,j}]$$

$$sm_{i,j} = \frac{\max(\overline{com_{i,j}}) - \min(\overline{com_{i,j}})}{\max(\overline{fc}) - min(\overline{fc})} = \frac{\max(\overline{com_{i,j}}) - \min(\overline{com_{i,j}})}{20 - 0.004}$$

We summarized the personal sensitivity simulation by binning vaccinees into low medium or high activation based on the maximum complex formation they achieve for each parameter when altered 0.004X-20X from baseline.

Individual and combinatorial IgG1 concentration and Fc affinity simulations (Figure 2.7)

We simulated alterations (2X, 5X, 10X, or 20X from baseline) in either IgG1 concentration, IgG1 k_{on} to FcγRIIIa-V^{158}, or both simultaneously. Each vaccinee's complex formation was captured for under each condition and plotted on a heatmap. These results were summarized by binning vaccinees into complex formation below, on, or above the IgG1 plateau based on the previously mentioned thresholds for each condition. The combinatorial simulation results were compared to the additive result, based on the following formula for each alteration to each individual: additive complex formation = baseline + ΔIgG1 concentration alone + ΔIgG1-FcγR k_{on} alone.

Glycosylation simulations

We obtained data on fold change in IgG1-FcγR affinity with each glycosylation type from the published literature[120]. We applied the maximum fold change in affinity (31X) seen in Dekkers et al. for FcγRIIIa-V^{158} to each IgG subtype's Fc (k_{on} IgGx-FcR) and Fab (k_{on} IgGx-env) region individually to compare change in complex formation with the same change in affinity (Figure A.S7A).

FcγR polymorphism simulations

We obtained FcγR polymorphism and class specific affinity parameters from the literature, calculated values listed in Table A.S1[88]. The affinity values were reported in K_A, and we converted each K_A to a k_{on} using a constant estimated k_{off} of 0.01 s-1. We ran a simulation for each vaccinee at each set of FcγR parameters and then compared each polymorphism with a two-tailed Wilcoxon matched-pairs signed-rank test performed in GraphPad Prism with $\alpha = 0.05$.

Software

ODE modeling, sensitivity analyses, and 3-D plots were completed using MATLAB 2019a (MathWorks, Natick, MA). Visualization of the remaining plots, and statistics were completed using GraphPad Prism version 8.0.0. Custom MATLAB code is available, as stated in the Key resources table, to run the simulations necessary to generate the data (steady-state complex formation concentrations) used in this analysis. Additionally, this code will replicate Figures 2.2A–2.2C, 2.3A, 2.3B, 2.4A, and 2.6A. All other figures can be replicated using the data generated by these simulations or by making small alterations to code as indicated in comments.

Quantification AND Statistical Analysis

Figures 2.2, A.S3, and A.S4: To evaluate model validation (Figure 2.2A), a two-tailed Spearman correlation was performed in GraphPad Prism on the measured MFI and predicted nM complex formation values with $\alpha = 0.05$. The global sensitivity analysis (Figures 2.2B, 2.2C, A.S3, and A.S4) and partial rank correlation coefficient (PRCC) calculation method, which has been previously published[133], uses Latin hyper-cube sampling (LHS) to randomize input parameters and calculates PRCC for each parameter by calculating the linear correlation between the parameter input and complex formation output while discounting the linear effects of all other parameter inputs. The significance of each PRCC value is tested by comparing its T value, which accounts for the number of other parameters and number of samples, to a critical t-value giving a p-value used to determine if the PRCC is significantly different from zero. Statistical details are included in the figure legends.

Figure 2.3: The gradients were compared using a two-tailed Wilcoxon matched-pairs signed-rank test performed in GraphPad Prism with $\alpha = 0.05$. To compare 10X and 20X IgG3 additions, we used a binomial test performed in Graphpad prism on the proportion of high versus the

combination of medium and low activating individuals with $\alpha = 0.05$. We used the 10X IgG3 addition proportions as the expected values (45 above the IgG1 plateau, 60 on or below the IgG1 plateau) and the 20X proportions as the observed values. To compare IgG1 & IgG3 additions to IgG3 alone additions, we used a binomial test performed in Graphpad prism on the proportion of individuals with complex formation above the IgG1 plateau versus the combination of individuals with complex formation on or below the IgG1 plateau with $\alpha = 0.05$. We used the IgG3 alone addition proportions as the expected values for each respective addition level and the IgG1 & IgG3 proportions as the observed values for each respective addition level. Statistical details are included in the figure legends.

Figure 2.4: IgG1 addition model and experimental measurements within each addition level (34nM or 140nM) were compared using an ordinary one-way ANOVA performed in GraphPad Prism with multiple comparisons and the Tukey test with a single pooled variance and no matching or pairing ($\alpha = 0.05$). Only the results between model and experimental results within the same condition or responders and non-responders within the same condition are reported in the figure. Statistical details are included in the figure legends.

Figure 2.5: Complex formation for each Gm allotype was compared using a Friedman's test with Dunn's multiple comparison test in GraphPad Prism ($\alpha = 0.05$). Statistical details are included in the figure legends.

Figure 2.6: To compare proportions of complex formation above the IgG1 plateau, we used a binomial test performed in Graphpad prism on the proportion of complex formation above the IgG1 plateau versus the combination of individuals with complex formation on or below the IgG1 plateau with $\alpha = 0.05$. To compare proportions of individuals with complex formation on the IgG1 plateau, we used a binomial test performed in Graphpad prism on the proportion of complex formation on the IgG1 plateau versus the combination of individuals with complex formation above and below the IgG1 plateau with $\alpha = 0.05$. We used the IgG1 concentration proportions as the expected values when comparing to k_{off} IgG1-FcR, and IgG3 concentration proportions as the expected values when comparing to IgG1 concentration proportions. Statistical details are included in the figure legends.

Figure 2.7: The additive and combination complex formations for each fold change (2X, 5X, 10X) were compared using a two-tailed Wilcoxon matched-pairs signed-rank test performed in GraphPad Prism with $\alpha = 0.05$. To compare proportions of complex formation above the IgG1 plateau, we used a binomial test performed in Graphpad prism on the proportion of complex formation above the IgG1 plateau versus the combination of individuals with complex formation on or below the IgG1 plateau with $\alpha = 0.05$. To compare proportions of complex formation on the IgG1 plateau, we used a binomial test performed in Graphpad prism on the proportion of complex formation on the IgG1 plateau versus the combination of individuals with complex formation above and below the IgG1 plateau with $\alpha = 0.05$. We used the affinity alone alteration proportions as the expected values and the concentration alone alteration proportions as the observed values. Statistical details are included in the figure legends.
Figure A.S2: To further evaluate model validation (Figure A.S2A), we calculated a log-log least-squares fit of Measured MFIs versus Predicted concentration in GraphPad Prism and captured the RMSE. To evaluate model validation (Figures A.S2B–A.S2F), a two-tailed Spearman correlation was performed in GraphPad Prism on the measured MFI and predicted nM complex formation values from each dataset with $\alpha = 0.05$. Statistical details are included in the figure legends.

Figure A.S5: To evaluate model validation after IgG1 additions (Figure A.S5), a two-tailed Spearman correlation was performed in GraphPad Prism on predicted versus measured fold change in complex formation with $\alpha = 0.05$. Statistical details are included in the figure legends.

Figure A.S7: Change in complex formation with glycosylation of Fc or Fab regions of IgG1-4 were compared using an ordinary one-way ANOVA performed in GraphPad Prism with multiple comparisons and the Tukey test with a single pooled variance and no matching or pairing ($\alpha = 0.05$). The complex formation in different FcR polymorphisms was compared using a two-tailed Wilcoxon matched-pairs signed-rank test performed in GraphPad Prism with $\alpha = 0.05$. Statistical details are included in the figure legends.

Chapter 3 A Quantitative Approach to Unravel the Role of Host Genetics in IgG-FcγR Complex Formation after Vaccination

Melissa M. Lemke[1], Robert Theisen[1], Emily R. Bozich[1], Milla R. McLean[2], Christina Y. Lee[1], Ester Lopez[2], Supachai Rerks-Ngarm[3], Punnee Pitisuttithum[4], Sorachai Nitayaphan[5], Sven Kratochvil[6], Bruce D. Wines[7,8,9], P. Mark Hogarth[7,8,9], Stephen J. Kent[2,10,11], Amy W. Chung[2†*], Kelly B. Arnold[1†*]

[1]Department of Biomedical Engineering, University of Michigan, Ann Arbor, MI, USA [2]Department of Microbiology and Immunology, The University of Melbourne, at the Peter Doherty Institute for Infection and Immunity, Victoria, Australia [3]Department of Disease Control, Ministry of Public Health, Bangkok, Thailand [4]Vaccine Trial Centre, Faculty of Tropical Medicine, Mahidol University, Bangkok, Thailand [5]Armed Forces Research Institute of Medical Sciences, Bangkok, Thailand [6]The Ragon Institute of Massachusetts General Hospital, Massachusetts Institute of Technology and Harvard University, Cambridge, MA, USA [7]Immune Therapies Group, Burnet Institute, Melbourne, VIC, Australia [8]Department of Immunology and Pathology, Monash University, Melbourne, VIC, Australia [9]Department of Clinical Pathology, The University of Melbourne, Melbourne, VIC, Australia [10]ARC Centre of Excellence in Convergent Bio-Nano Science and Technology, The University of Melbourne, Victoria, Australia [11]Melbourne Sexual Health Centre, Alfred Hospital, Monash University Central Clinical School, Victoria, Australia [†]These authors have contributed equally to this work and share senior authorship

*** Correspondence:** Kelly B. Arnold (kbarnold@umich.edu) and Amy W. Chung (awchung@unimelb.edu.au)

Keywords: systems serology, Fc receptor, IgG1 allotype, Fc receptor polymorphism, ODE model, HIV, RV144, ADCC

Frontiers in Immunology. In revision.

3.1 Abstract

Fc-mediated immune functions have been correlated with protection in the RV144 HIV vaccine trial and are important for immunity to a range of pathogens. IgG antibodies (Abs) that form complexes with Fc receptors (FcRs) on innate immune cells can activate Fc-mediated immune functions. Genetic variation in both IgGs and FcRs have the capacity to alter IgG-FcR complex formation via changes in binding affinity and concentration. A growing challenge lies in unraveling the importance of multiple variations, especially in the context of vaccine trials that are conducted in homogenous genetic populations. Here we use an ordinary differential equation model to quantitatively assess how IgG1 allotypes and FcγR polymorphisms influence IgG-FcγRIIIa complex formation in vaccine-relevant settings. Using data from the RV144 HIV vaccine trial, we map the landscape of IgG-FcγRIIIa complex formation predicted post-vaccination for three different IgG1 allotypes and two different FcγRIIIa polymorphisms. Overall, the model illustrates how specific vaccine interventions could be applied to maximize IgG-FcγRIIIa complex formation in different genetic backgrounds. Individuals with the G1m1 and G1m1,3 allotypes were predicted to be more responsive to vaccine adjuvant strategies that increase antibody FcγRIIIa affinity (e.g. glycosylation modifications), compared to the G1m-1,3 allotype which was predicted to be more responsive to vaccine boosting regimens that increase IgG1 antibody titers (concentration). Finally, simulations in mixed-allotype populations suggest that the benefit of boosting IgG1 concentration versus IgG1 affinity may be dependent upon the presence of the G1m-1,3 allotype. Overall this work provides a quantitative tool for rationally improving Fc-mediated functions after vaccination that may be important for assessing vaccine trial results in the context of under-represented genetic populations.

3.2 Introduction

Antibodies (**Abs**) are a vital component of the protective immune response elicited by vaccination. Immunoglobulin G (**IgG**) Abs that activate Fc effector functions are important for protection against a number of pathogens[69,71,130,134,135] and have been correlated with protection in HIV vaccine trials[57,83]. Antigen bound IgG immune complexes can trigger Fc effector functions by the crosslinking of IgG Fc portions with Fc receptors on the surface of innate immune cells. Fc functional capacity is directly related to the number of complexes formed,

which is regulated by numerous factors including IgG subclass concentrations, availability of FcRs and their respective binding properties[68]. These properties vary in individuals and several studies have demonstrated that they are influenced by genetic factors including IgG1 allotypes and FcR polymorphisms[88,90,136].

Currently, four human IgG1allotypes (G1m1, G1m2, G1m3, G1m17) have been identified[86]. These allotypic determinants are inherited in a Mendelian pattern, i.e. sets of G1m haplotypes are inherited. G1m3 and G1m17 allotypes are mutually exclusive and refer to different amino acid changes at the same position[137]. G1m17 allotypes are almost always linked with G1m1 (written together as G1m1,17 but hereafter referred to as G1m1 in this text), whereas G1m3 can exist with or without G1m1 (e.g. G1m1,3 or G1m-1,3 respectively). Interestingly, common allotypes are shared within ethnic or genetic populations. Africans have an enriched prevalence of G1m1,17 allotypes, Caucasians have enriched G1m1,17 and G1m-1,3 allotypes while Asians have enriched G1m1,17 and G1m1,3 allotypes [118,119]. Recent research suggests that IgG1 allotypic variation is linked with IgG subclass concentrations, potentially due to allotype-linked variation in expression and degradation[136]. Importantly these allotype-linked differences in IgG subclass concentrations are also observed in an antigen-specific manner upon vaccination. For example a recent phase I HIV vaccine trial[112] observed that G1m1 vaccinees (G1m1 & G1m1,3) reported to have higher HIV-specific IgG1:IgG2 ratios compared to the G1m-1,3 allotype, mainly driven by elevated HIV-specific IgG1 titres in G1m1 individuals[90].

In parallel, a range of FcγR polymorphisms have been identified in humans, some of which have greater Fc binding affinity and hence are associated with enhanced Fc functional capacity[88,138–140]. Individuals carrying the high affinity FcγRIIa H^{131} polymorphism, most commonly associated with enhanced ADCP, have positive outcomes in both cancer [141] and infectious diseases, including HIV [142,143]. The FcγRIIIa V^{158} polymorphism, with higher affinity than FcγRIIIa F^{158}, has been associated with enhanced ADCC functionality and linked to better outcomes within the mAb cancer field[144,145]. Conversely, this same polymorphism has been associated with HIV disease progression[146] and the lack of protection in the HIV VAX004 vaccine trial [125]. Though FcR polymorphisms clearly dictate affinity for IgG subclasses, their

overall role in FcγR activation is more ambiguous, especially in the context of variability in IgG subclass concentrations.

To date, few studies have explored the relative roles of IgG1 allotypes and FcR polymorphisms in FcR activation after vaccination, as their distributions are not controlled in vaccine trials. In addition, it is difficult to unravel the parallel influences of both subclass concentrations and binding affinities that arise from differences in IgG1 allotype and FcγR polymorphism combinations. Recently, we computationally assessed the mechanistic underpinnings of IgG-FcγR complex formation after vaccination and demonstrated that synergistic relationships can occur between antibody parameters that regulate FcγR activation, that would not be apparent from studying each in isolation [147] multiple immunogenetic changes may also have synergistic influences upon FcγR activation, which are greater than those that would be expected from simply summing changes evaluated in isolation. These are often too complex to be captured experimentally when parameters are examined individually.

Here we use data from the HIV RV144 vaccine trial and a mechanistic computational model to assess the relative roles of IgG1 allotypes and FcγR polymorphisms in IgG-FcγRIIIa immune complex formation after HIV vaccination. We demonstrate how genetic background may influence an individual's Fc functional response upon vaccination and suggest specific interventions that would most effectively improve IgG-FcγRIIIa immune complex formation in each allotype/polymorphism combination.

3.3 Materials and Methods

We applied an ordinary differential equation (ODE) model as previously published and validated with RV144 plasma samples[147]. The model predicts IgG-FcγR dimer complex formation (ant:IgG:IgG:FcγR:FcγR) at steady state as a function of IgG subclass, antigen, and FcR dimer concentrations. In the model, two IgG antibodies bind each antigen before forming a complex with dimeric FcR. We obtained parameters for the model from literature and with measurements made previously[147] where median fluorescent intensity (MFI) of HIV env glycoprotein 120 (gp120) strain A244 (env) specific IgG1, IgG2, IgG3, and IgG4 was measured in the plasma of 105 RV144 vaccinees[74]. We converted MFI measurements into a relative concentration

measurement based on a reference concentration[112] of HIV-specific IgG in a similar vaccine trial. The concentrations predicted throughout by the model are thus not to be used as absolute measures, but as relative measures.

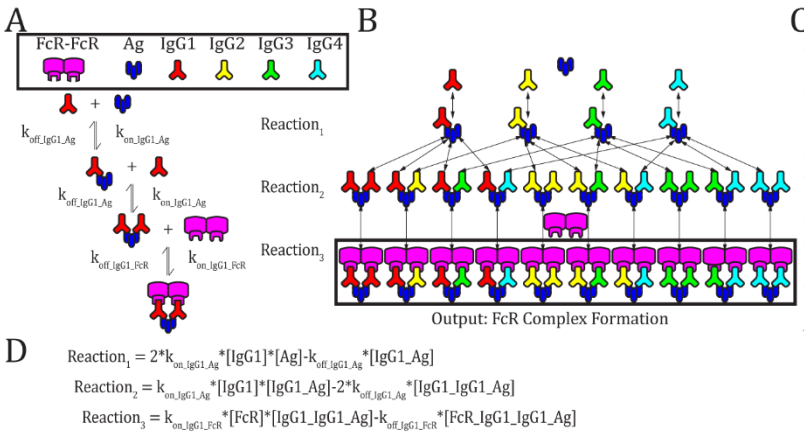

Parameter	Baseline Value	Units
K_{eq}-IgGx -env [α]	5,000	$\times 10^{5} nM^{-1}$
K_{eq}-IgG1 -FcR [β]	200	$\times 10^{5} nM^{-1}$
K_{eq}-IgG2 -FcR [β]	7	$\times 10^{5} nM^{-1}$
K_{eq}-IgG3 -FcR [β]	980	$\times 10^{5} nM^{-1}$
K_{eq}-IgG4 -FcR [β]	25	$\times 10^{5} nM^{-1}$
IgG1 initial concentration [γ]	85.4	nM
IgG2 initial concentration [γ]	0.133	nM
IgG3 initial concentration [γ]	3.07	nM
IgG4 initial concentration [γ]	0.102	nM
env initial concentration [δ]	25	nM
FcR initial concentration [δ]	20	nM

Figure 3-1 Model schematic

(A) An example set of reversible reactions describing the sequential binding of IgG1 to antigen (Ag) and dimeric FcγR with the respective forward (k_{on}) and reverse (k_{off}) reaction rates. (B) Ordinary differential equations were used to predict total HIV ant-IgG-FcγR complexes formed as a function of concentration and binding affinity of ant, IgG subclasses, and FcγR. The model assumes a single FcγR type. Reversible reactions are represented by double ended arrows. Model output was the sum of all dimeric FcγR complexes formed (boxed in black) at steady state. (C) The baseline parameters for FcγRIIIA-V[158] complex formation with the following sources: [α]SPR measurement from pooled purified IgG from HIV infected individuals. All IgG subtypes share one affinity value (unpublished data). [β]K_{eq} measured in Bruhns et al[88] . [γ]The average estimated IgG concentrations from individuals 1-30 in the RV144 data in this manuscript (see methods for notes on conversion from MFI to mM unit). [δ]Concentrations used in multiplex experimental protocol. (D) Equations describing the example reactions in panel A. Reactions follow mass action kinetics and consist of a forward reaction (on rate, k_{on}, multiplied by the concentrations of substrates) and a reverse reaction (off rate, k_{off}, multiplied by the concentration of the product of the forward reaction). Differential equations for change in each complex over time were generated for each complex.

3.3.1 Evaluating combined IgG1 concentration and affinity parameter changes

In order to evaluate the relative and combined roles of IgG1 allotype (i.e. IgG subclass changes) and FcR affinity (i.e. FcR polymorphisms), IgG1 affinity for FcγRIIIA-V[158] or IgG1 concentration were held constant at its baseline value (listed in the parameter table in **Figure 3.1C)**, while the other parameter was varied over 50 values spanning 1.7-256 nM or 2e-6-8e-4 $nm^{-1}s^{-1}$. Model outputs from all simulations were subtracted by the baseline complex formation to calculate the difference in complex formation for each condition. We simulated 2,500 different combinations of IgG1 concentration and IgG1 affinity for FcγRIIIA-V[158] spanning 1.7-256 nM or 2e-6-8e-4 $nm^{-1}s^{-1}$ respectively while holding all other model parameters at baseline. We then subtracted each of these values by the model output with both IgG1 affinity and

concentration at baseline. To identify regions where synergy between IgG1 concentration and IgG1 affinity for FcγR occurred, we used element-wise subtraction of the additive simulations (parameters were altered in isolation and added together) from simulations where parameters altered together in the model. The range of possible IgG1 concentration values was calculated by multiplying the maximum and minimum calculated IgG1 concentrations in the RV144 plasma samples[147] by each allotype conversion factor and taking the minimum and maximum results across all possible allotypes[143]. Maximum and minimum IgG1 affinity values were selected as the highest and lowest affinity glycosylation forms of IgG1 across all FcgRIIIA polymorphisms [148].

3.3.2 Evaluating Boosting of IgG1 concentrations in individuals with different FcγRIIIa polymorphisms

In order to model how changes in IgG subclass concentrations (that may occur upon vaccine boosting) can influence IgG-FcγR complex formation in individuals with different FcγRIIIa polymorphism, we used the model to predict complex formation for each polymorphism by altering initial IgG1 and IgG3 concentrations from 0.004X to 20X baseline (post-vaccination measurements) in 2,500 different combinations. Affinity values for each FcγRIIIa polymorphism to each IgG subclass were used from previously published literature[88]. We used IgG1 and IgG3 titers measured in RV144 vaccinees post-vaccination and after a simulated 170% IgG1 boost. This boosting value was chosen by using the highest fold change in HIV-specific Ab titers recorded in the RV306 follow up trial from 26 weeks (our initial post-vaccination timepoint) and after boosting in group 4b with AIDSVAX B/E and ALVAC-HIV at 18.5 months[60]. A Wilcoxon matched pairs signed rank test was used to evaluate the difference in predicted complex formation for each individual across the two polymorphisms, both before and after boosting. All parameters besides initial IgG1 and IgG3 remained at their baseline value listed in the parameter table (**Figure 3.1C)** for all the above-described simulations. Specific IgG1 and IgG3 values were chosen using MATLAB's log spacing function, logspace(), to give 50 values between 0.004X and 20X baseline.

3.3.3 Simulating IgG1 allotypes and glycosylation

Baseline IgG subclass initial concentrations from all 105 RV144 vaccinees were assumed to be the G1m1,3[119] IgG1 allotype. These were then converted into G1m1 and G1m1,3 for simulations based on conversion factors for initial IgG1, IgG2, IgG3 and IgG4 concentration as previously published[147] estimated using allotyped human plasma samples from previous a Phase I HIV vaccine trial[112]. To predict affinity changes resulting from glycosylation, we estimated those that would be expected from afucosylation of IgG1 by taking the highest fold change for affinity of IgG1 to FcγRIIIa-V[158] (31X; $62*10^{-3}$ $nM^{-1}s^{-1}$) reported in the literature[148]. This high affinity glycosylation (afuscosylation with hyper-galactosylation and bisection) was compared to a baseline affinity ($2*10^{-3}$ $nM^{-1}s^{-1}$).

In order to evaluate affinity changes resulting from glycosylation, projected upon all vaccinees for each of the three allotypes, the IgG-FcR immune complex formation was simulated at baseline, and the difference between each individual's complex formation at baseline and with glycosylation for each allotyped population and compared them with a Friedman test with Dunn's multiple comparisons in GraphPad Prism.

Allotype projections were performed as previously published[147], by first calculating the conversion factor. Under the assumption that the original RV144 data was G1m1,3[119], the conversion factor was calculated to generate the corresponding IgG subclass concentrations for the G1m-1,3 and G1m1 allotypes. To calculate this value, we found the mean concentration for each IgG within each allotype from human plasma samples analyzed in Kratochvil et al.[112]. Then, these values were divided by the corresponding mean IgG concentration for samples with the G1m1,3 allotype.

$$cf_{G1mj}^{IgGi} = conversion\ factor\ for\ IgGi\ to\ allotype\ G1mj$$

$$m_{G1mj}^{IgGi} = mean\ concentration\ of\ IgGi\ in\ allotype\ G1mj$$

$$cf_{G1mj}^{IgGi} = m_{G1mj}^{IgGi} / m_{G1m1,3}^{IgGi}$$

Each vaccinee's initial IgG concentrations and baseline initial IgG concentrations were converted using the respective conversion factors as follows:

$$IgGi_{G1mj}^{x} = Initial\ IgGi\ concentration\ for\ vaccinee\ x\ in\ allotype\ G1mj$$

$$IgGi_{G1mj}^{x} = cf_{G1mj}^{IgGi} * IgGi_{G1m1,3}^{x}$$

3.3.4 Determining preferred boosting method in IgG1 allotypes

Simulations as above, projecting all 105 RV144 vaccinees as the three IgG1 allotypes and two FcRIIIA polymorphisms (FcγRIIIa-V^{158} and FcγRIIIa-F^{158}) were calculated, providing predictions for six different genetic combinations (**Figure 3.5A**). In each of these six genotypes we then simulated a boost in either IgG1 initial concentration or k_{on} IgG1-FcR (ie IgG1 affinity to FcR) by 10%, 25%, 50%, 75%, 100%, 250%, 500%, 750%, or 1000% above their personal baseline. The six genotypes were compared at baseline using a Friedman test with Dunn's multiple comparisons in GraphPad Prism 9.

To modify the original parameter to include the boost, a new concentration or affinity was calculated using the following formula, where the original parameter is specific to the individual and genotype:

$$New\ parameter = original\ parameter + (original\ parameter * boost)$$

3.3.5 Evaluating mixed allotype populations

To determine the importance of affinity and concentration-based interventions within 10 mixed allotype populations, simulations were run as described above projecting all 105 RV144 vaccinees into different allotypes. Within this analysis, 10 mixed allotype populations were simulated with varying proportions of individuals assigned to each allotype. Each allotype is represented in each population at 100%, 66%, 33%, 17%, or 0% (see **Figure 3.6** for specific breakdowns). Each vaccinee (n = 105) was randomly assigned an allotype to fulfill the population breakdown. In populations where vaccinees couldn't be evenly split into the population's allotypes, remaining vaccinees were again randomly assigned an allotype (i.e. 70 vaccinees assigned to G1m1, 18 assigned to G1m1,3 and 17 to G1m-1,3 in Population F). We performed this randomized vaccinee allotype assignment 25 times for each population to create a more robust and representative population n = 2,625 for each population. All simulations were run with FcγRIIIa-V^{158} affinity values.

3.4 Results

3.4.1 Synergism between IgG1 concentration and IgG1 affinity

Genetic background has the potential to influence both IgG1 concentration (via IgG1 allotypes) and IgG1 binding affinity for FcR (via FcR polymorphisms). In order to better understand the relationship between these two parameters and how they influence FcγRIIIa activation, we applied an ODE model to predict Antigen-IgG-FcR immune complex formation as both parameters were altered simultaneously over a physiological range of 2500 unique parameter

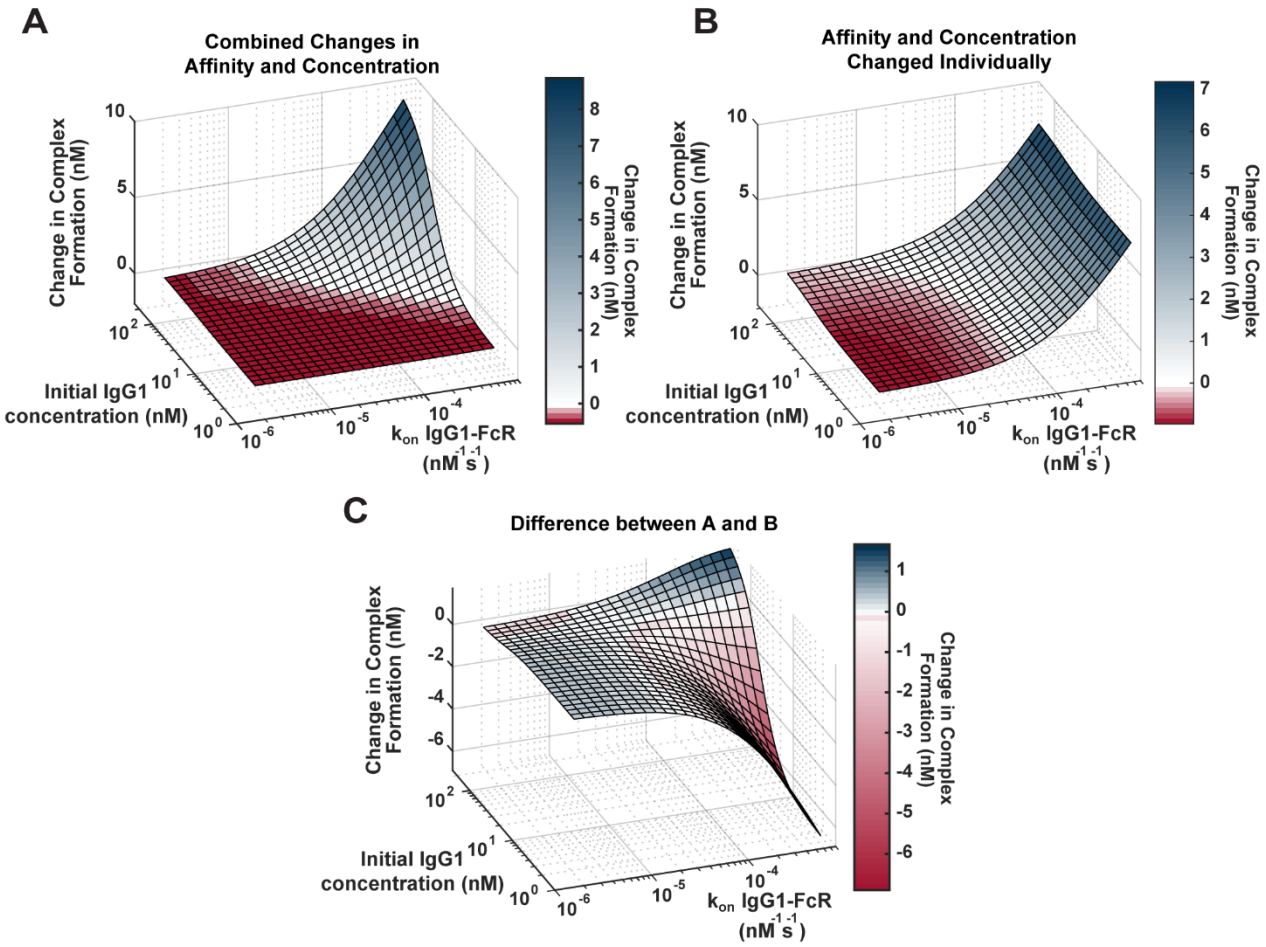

Figure 3-2 Landscape illustrating the relationships between IgG1 concentration and IgG1- FcγR affinity across the physiological landscape of parameters (2500 unique parameter combinations)

(A) Model predictions for the change in complex formation from baseline when IgG1 initial concentration (x axis) and k_{on} IgG1-FcγR (y axis) were altered individually and the resulting change in complex formation is added together (z axis). Color indicates predicted change in complex formation from baseline. (B) Model predictions for the change in complex formation from baseline when both parameters are altered simultaneously in the model. Color indicates predicted change in complex formation from baseline. (C) The difference between (A) and (B), illustrating parameter combinations where synergy occurs. Blue indicates positive synergy, where the combined parameter changes (B) result in greater complex formation compared to was predicted by separate changes added together (A), white indicates no synergy, and red indicates anergy; where the combined parameter changes (B) result in lower complex formation compared to was predicted by separate changes added together (A).

changes are much greater than what would be expected from adding separate changes, whereas the negative regions (red) represent parameter combinations where actual changes would be much less than what would be expected from adding individual changes. This landscape indicates the potential for synergistic complex formation (blue) when both concentration and affinity are high (102-230 nM, and 2.9e-5-7e-4 $nM^{-1}s^{-1}$). Interestingly it also illustrates the potential to overestimate complex formation when IgG1 affinity is high, but IgG1 concentration is low (1.7-102 nM, and 2.9e-5-7e-4 $nM^{-1}s^{-1}$). Altogether these results have important implications for how genetic background (which has the capacity to alter both IgG1 concentration and IgG1 affinity for FcγR) may influence FcγR activation after vaccination and may allow for more rational design of vaccine interventions.

3.4.2 FcR polymorphism influences FcγR activation after boosting

One interesting result of the previous simulations in Figure 2 was that there is a limit in the effects of increasing IgG1 concentration alone, and at higher IgG1 concentrations, IgG1 affinity determines the limit. This result has implications for vaccine boosting in individuals with different FcR polymorphisms. We hypothesized that the effect of boosting (large changes in IgG1 concentration) would be limited in individuals with the low affinity FcγRIIIa-F^{158} polymorphism, whereas it would be much higher in individuals with the higher affinity FcγRIIIa-V^{158} polymorphism. Therefore we hypothesized that the differences in immune complex formation between the two polymorphisms would become even greater after boosting (compared to first vaccination).

To test this idea, we ran simulations for the high and low affinity FcγRIIIa polymorphisms by changing the affinity for all IgGs to FcγRIIIa according to published values[88](FcγRIIIa-V^{158} light pink, and FcγRIIIa-F^{158} dark pink, respectively; **Figure 3.3A**) at 2,500 different initial IgG1 and IgG3 concentration combinations with all other parameters maintained using baseline values

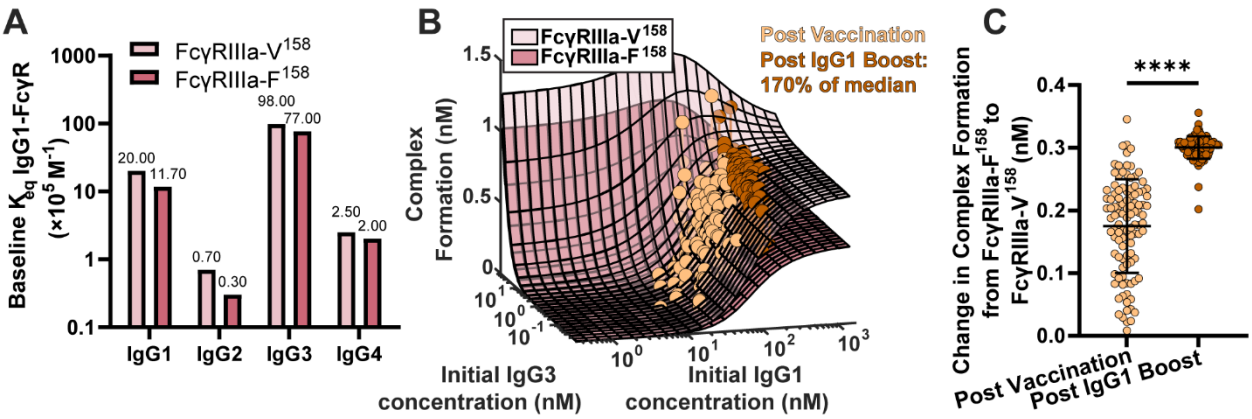

Figure 3-3 FcγR polymorphisms have a greater influence on complex formation after IgG1 boosting.

(A) Baseline K_{eq} of each IgG subtype to the high affinity FcγRIIIa-V^{158} polymorphism (light pink) and the low affinity FcγRIIIa-F^{158} polymorphism (dark pink) as reported by Bruhns et. al [88]. (B) Complex formation (z axis) predicted by the model for 2500 combinations of initial IgG1 and IgG3 concentration (x and y axes) for FcγRIIIa-V^{158} (light pink) and FcγRIIIa-F^{158} (dark pink). Each dot represents an RV144 plasma sample (n=105) with respective initial IgG1 and IgG3 concentrations plotted post-vaccination (baseline-light orange), and after a simulated 170% (145 nm) boost of IgG1 (dark orange). The simulated boost magnitude was estimated based on the highest fold change seen in RV306 between 26 weeks and peak HIV specific IgG titre (2.64X in arm 4b) [60]. (C) The difference in complex formation predicted between the FcγRIIIa-F^{158} and FcγRIIIa-V^{158} polymorphisms post-vaccination (light orange) and post-IgG1 boost (dark orange; Wilcoxon matched-pairs signed rank test; **** p-value < 0.0001).

(FcγRIIIa-V^{158} light pink, and FcγRIIIa-F^{158} dark pink; **Figure 3.3B**). IgG1 and IgG3 have previously been identified as the significant IgG subtypes of importance[147] due to IgG1's high initial concentration and IgG3's high affinity to FcR (**Figure 3.1C and 3.3A**). The resulting profile of both polymorphism surfaces revealed that changes in IgG1 concentration were predicted to increase complex formation up to a certain point, illustrated by a plateau around 300 nM, after which no additional changes in complex formation would be predicted regardless of IgG1 increases. Comparing results for the two polymorphisms (light pink vs. dark pink surface) revealed that the biggest differences between polymorphisms occur in the plateaus regions, when IgG1 concentration is high; specifically, the FcγRIIIa-V^{158} polymorphism plateau is 66% higher than the FcγRIIIa-F^{158} plateau.

Based on individual IgG1 and IgG3 initial concentrations measured in the RV144 plasma samples (n=105) we plotted each individual on both surfaces at baseline (light orange), and after a simulated boost[60] in IgG1 concentration (dark orange; **Figure 3.3B**). After first vaccination, many vaccinees were predicted to be in an IgG1 sensitive region, regardless of FcR

polymorphism. However, an increase in antigen-specific IgG1 (similar to the boost applied in RV306) moves many vaccinees from the IgG1 sensitive region (30-300 nM) onto or nearing the plateau region, where complex formation is highly dependent on FcR polymorphism. Indeed, the difference in complex formation between the polymorphisms after boosting was significantly greater than it was at baseline (after first vaccination) (Wilcoxon matched-pair rank test, $p < 0.0001$; **Figure 3.3C**).

3.4.3 The G1m-1,3 IgG1 allotype is not predicted to be sensitive to IgG1 Fc glycosylation modifications

Model results in Figure 3.2 revealed the potential for unexpected interactions between IgG1 concentration and IgG1 affinity. In a setting with low IgG1 concentration, there is the potential that large increases in IgG1 affinity to FcγR will have little to no effect on IgG-FcγR complex formation. Conversely, at high IgG1 concentrations, results revealed the potential for non-linear increases in complex formation. Based on these observations, we used the model to assess how IgG1 concentration differences in IgG1 allotypes may influence sensitivity to FcR affinity modifications (e.g. glycosylation).

Previous studies suggest that IgG1 allotype alters all four IgG subclass concentrations, hence we used these measurements to estimate the median IgG1, IgG2, IgG3 and IgG4 concentrations for each allotype (**Figure 3.4A**) [112]. As the G1m1,3 allotype is expected to be prevalent in the original RV144 (Thai) population, we assumed all original RV144 vaccinees (n=105) were of the G1m1,3 (**Figure 3.4A,** white bar) allotype [119] which is expected to have higher IgG1 and IgG3 concentrations, compared to G1m1 (gray bar) and G1m-1,3 (black bar) which have higher IgG4. Using results in Figure 2, we plotted each IgG1 allotype on the surface based on expected

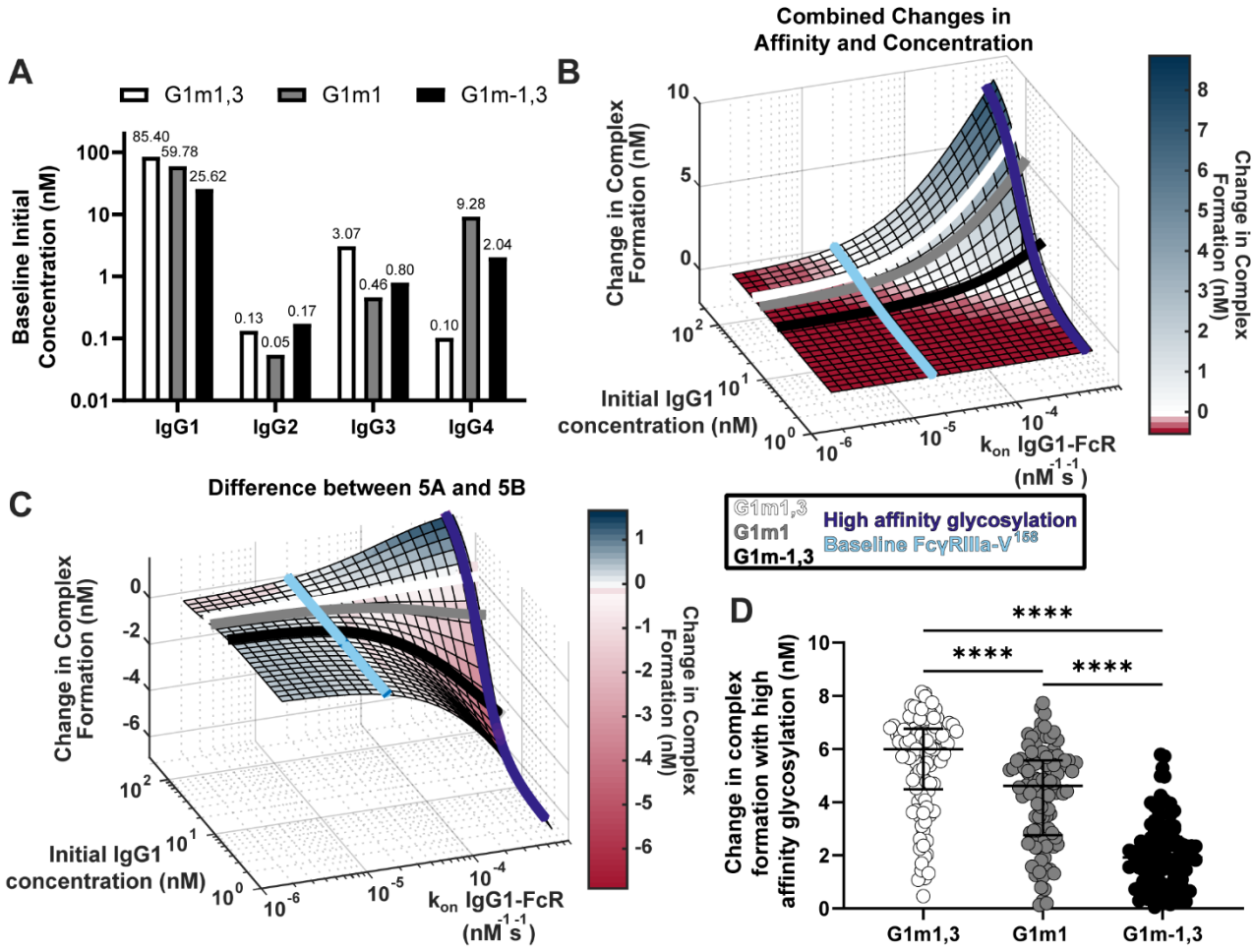

Figure 3-4 Glycosylation differentially impacts IgG1 allotypes.

(A) Expected IgG1, IgG2, IgG3, and IgG4 concentrations for G1m1,3 (white), G1m1 (gray), and G1m-1,3 (black) allotypes based on previously published work [112,147]. (B) Model predictions for complex formation as IgG1 concentration and k_{on} IgG1- FcγR are altered over physiological ranges (Figure 3.2B). Lines indicate IgG1 concentrations for three different IgG1 allotypes (G1m1,3 (white), G1m1 (gray), G1m-1,3 (black)), and the affinity change expected from an afucosylation glycosylation modification (purple) compared to baseline (light blue). (C) The difference (Figure 3.2C) between the combined parameter change surface (Figure 3.2A) and the additive surface (Figure 3.2B). Lines indicate IgG1 concentrations for three different IgG1 allotypes (G1m1,3 (white), G1m1 (gray), G1m-1,3 (black)), and the affinity change expected from an afucosylation glycosylation modification (dark blue) compared to baseline FcgRIIIaV158 (light blue).(D) Change in complex formation from baseline affinity to an afucosylated affinity in each allotype, G1m1,3 (white), G1m1 (gray), and G1m-1,3 (black) (Friedman test with Dunn's multiple comparisons test; **** p-value < 0.001).

median IgG1 concentration (**Figure 3.4B-C**). Using this same principle, we also added lines showing where the baseline affinity measurement is for FcγRIIIa-V^{158} (light blue, 2e-5 $nM^{-1}s^{-1}$) as well as potential maximal increases in affinity similar to what would be expected with an IgG1 Fc afucosylation modification (purple, 62e-5 $nM^{-1}s^{-1}$) based on values in the published literature [148]. Results indicate that G1m1,3 and G1m1 allotypes are expected to follow similar trajectories, where increases in affinity would considerably increase complex formation after ~3e-5 $nM^{-1}s^{-1}$ reaching complex formation levels of 6.5 nM and 5.2 nM respectively. Conversely for the G1m-1,3 allotype (lower IgG1 concentration) the model illustrates how similar glycosylation modification would result in much lower complex formation (only ~1.8 nM complex formation after a high affinity glycosylation modification (**Figure 3.4B**)).

Plotting the same lines representing IgG1 allotypes and FcRs onto a second surface illustrating the differences between combined changes in concentration and affinity and the individually changed analysis, we see that at baseline FcγRIIIa-V^{158} affinity values (Figure 3.4C, light blue) the predicted combined effects of IgG concentration changes are not much different between an individual and additive method. In contrast, after afucosylation, the additive method would overestimate complex formation in G1m-1,3 by 4.3 nM, while it is only slightly different in G1m1 (1.1 nM) and G1m1,3 (0.08 nM) (**Figure 3.4C**). Using the same conversion factors as above, we projected every RV144 vaccinee from G1m1,3 into G1m1 and G1m-1,3, and simulated each individual's complex formation after RV144 first vaccination and with the afucosylation change in affinity. Unsurprisingly, the change in complex formation with afucosylation was significantly different in each allotype following the trend of median IgG1 concentration (Median change in complex formation: G1m1,3, 6.0 nM; G1m1 4.6 nM; G1m-1,3 1.9 nM; Friedman test with Dunn's multiple comparisons, all $p<0.0001$) (**Figure 3.4D**).

3.4.4 IgG1 allotype determines whether vaccine boosts that increase IgG1 concentration vs. boost that increase IgG1 affinity would be more effective for improving FcR activation

Our model results suggest that the effect of changes in IgG1 concentration varies depending on a given IgG1 affinity to FcR. One intriguing implication of this result is that individuals with different IgG1 allotypes (different baseline IgG1 concentration) could be differentially sensitive Click or tap here to enter text.

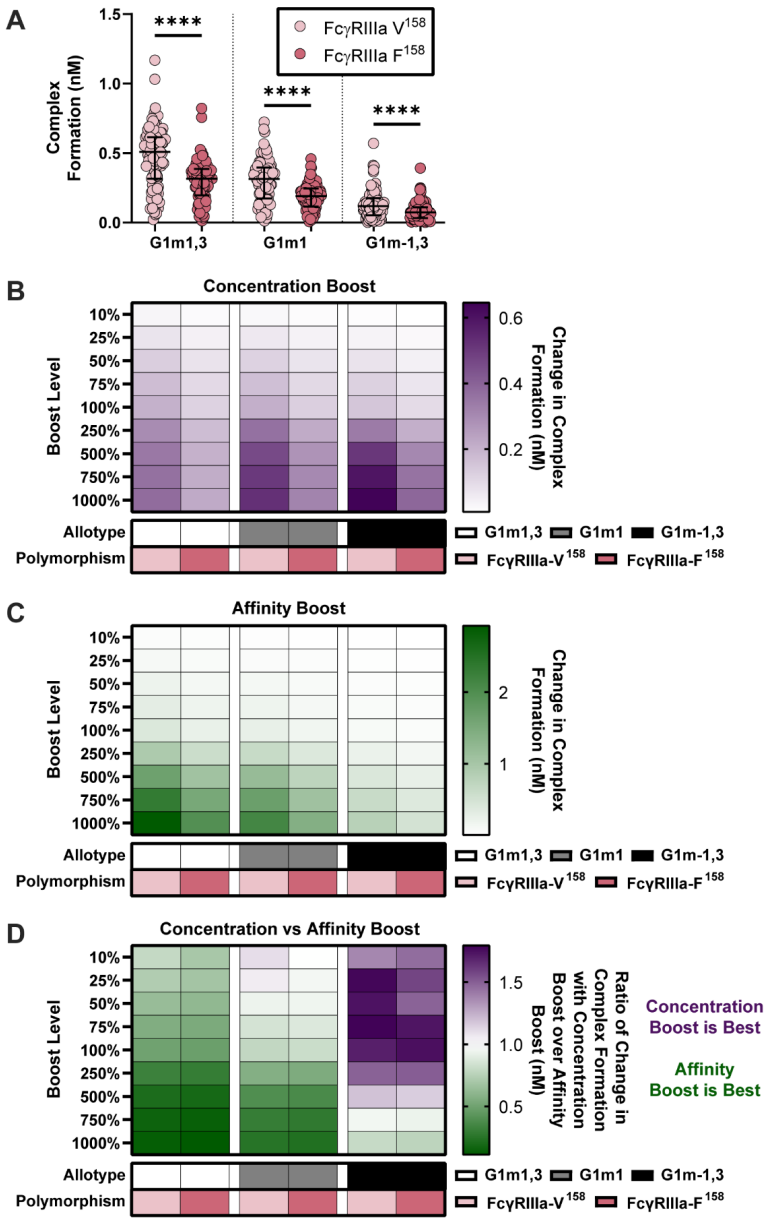

Figure 3-5 IgG1 allotype determines whether boosting IgG1 concentration or boosting IgG1 affinity (k_{on} IgG1- FcγR) would be most effective for increasing complex formation.

(A) Model predictions for complex formation of RV144 vaccinees (n=105) in two FcγRIIIa polymorphisms, FcγRIIIa-V^{158} (light pink) and FcγRIIIa-F^{158} (dark pink), and three IgG1 allotypes, G1m1,3 (original RV144 data), G1m1 and G1m-1,3. Polymorphisms were simulated by altering the binding affinities of each IgG subtype to FcγR as previously published[88] and indicated in Figure 3.3A. Allotypes are simulated by multiplying each vaccinee's IgG1, IgG2, IgG3 and IgG4 initial concentration by its respective conversion factor as previously published [147] and indicated in Figure 4A (Friedman test with Dunn's multiple comparisons test comparing the two polymorphisms within each allotype; **** p-value < 0.001). (B) Simulated IgG1 concentration boosting in each allotype (G1m1,3, white; G1m1, gray; G1m-1,3 black) and polymorphism (FcγRIIIa-V^{158}, light pink; FcγRIIIa-F^{158}, dark pink) combination. Boosts were calculated by multiplying the individual's baseline initial IgG1 concentration value by the boost levels and then this was added on top of each individual's baseline. Color indicates median change in complex formation for each genetic background. (C) Simulated boosting of k_{on} IgG1- FcγR in each allotype (G1m1,3, white; G1m1, gray; G1m-1,3 black) and polymorphism (FcγRIIIa-V^{158}, light pink; FcγRIIIa-F^{158}, dark pink) combination. Boosts were calculated by multiplying the individual's baseline k_{on} IgG1-FcγR value by the boost levels and then this was added on top of each individual's baseline. Color indicates median change in complex formation for each genetic background and boost as indicated. (D) The ratio of median change in complex formation with a boost in IgG1 concentration over median change in complex formation with a boost in k_{on} IgG1-FcγR (affinity) at each boosting level. This ratio shows which type of boost is most effective for increasing complex formation (IgG1 concentration, purple; k_{on} IgG1-FcγR, green) and when both are equally beneficial (white).

affinity via glycosylation. To explore this idea quantitatively, we simulated 6 different genotypes (FcγRIIIa-F^{158} and FcγRIIIa-V^{158} polymorphisms in the G1m1,3, G1m1 and G1m-1,3 allotypes). As expected we found significant differences in complex formation across all 6 genotypes (**Figure 3.5A**).

We then simulated nine different boosts, 10%-1000% above values after first vaccination for either IgG1 concentration (**Figure 3.5B**) or IgG1 affinity (**Figure 3.5C**) in all vaccinees. We used the median change in complex formation for each genetic background and boosting level to create heatmaps that illustrate the expected resulting change in complex formation. Intriguingly, results illustrated how concentration boosting (increasing antibody titers) has a larger effect on the allotypes with lower initial IgG1 concentration (**Figure 3.5B**) and that affinity boosts have a larger effect on the allotypes with higher initial IgG1 concentration (**Figure 3.5C**).

In order to definitively show which type of boosting is optimal for each boosting level and genetic background, we calculated the ratio of change in complex formation with a boost in IgG1 concentration over change in complex formation with a boost in IgG1 affinity to FcγRIIIa (**Figure 3.5D**). The resulting heat maps illustrates how concentration boosting is predicted to be more beneficial than affinity boosting for the G1m-1,3 allotype until 750% (purple). The lower starting concentration of IgG1 in G1m-1,3 (median IgG1 25.62 nM) prevents affinity changes from improving complex formation until it reaches at least 1e-4 $nM^{-1}s^{-1}$. Conversely, model results indicated that the G1m1,3 and G1m1 allotypes (with higher starting IgG1 concentrations) would be most responsive to changes in affinity (**Figure 3.5D**). Overall, these results suggest specific vaccine interventions that may be differentially effective for inducing improved Fc effector functions for individuals with different IgG1 allotypes.

3.4.5 Amount of G1m-1,3 allotype in a population determines whether boosting IgG1 antibody titers will be effective

Given that the model predicts that IgG1 allotype drives the preferred boosting type and that many populations worldwide have different allotype distributions, we next simulated boosting in mixed allotype populations. These populations were simulated by randomly assigning vaccinees to an

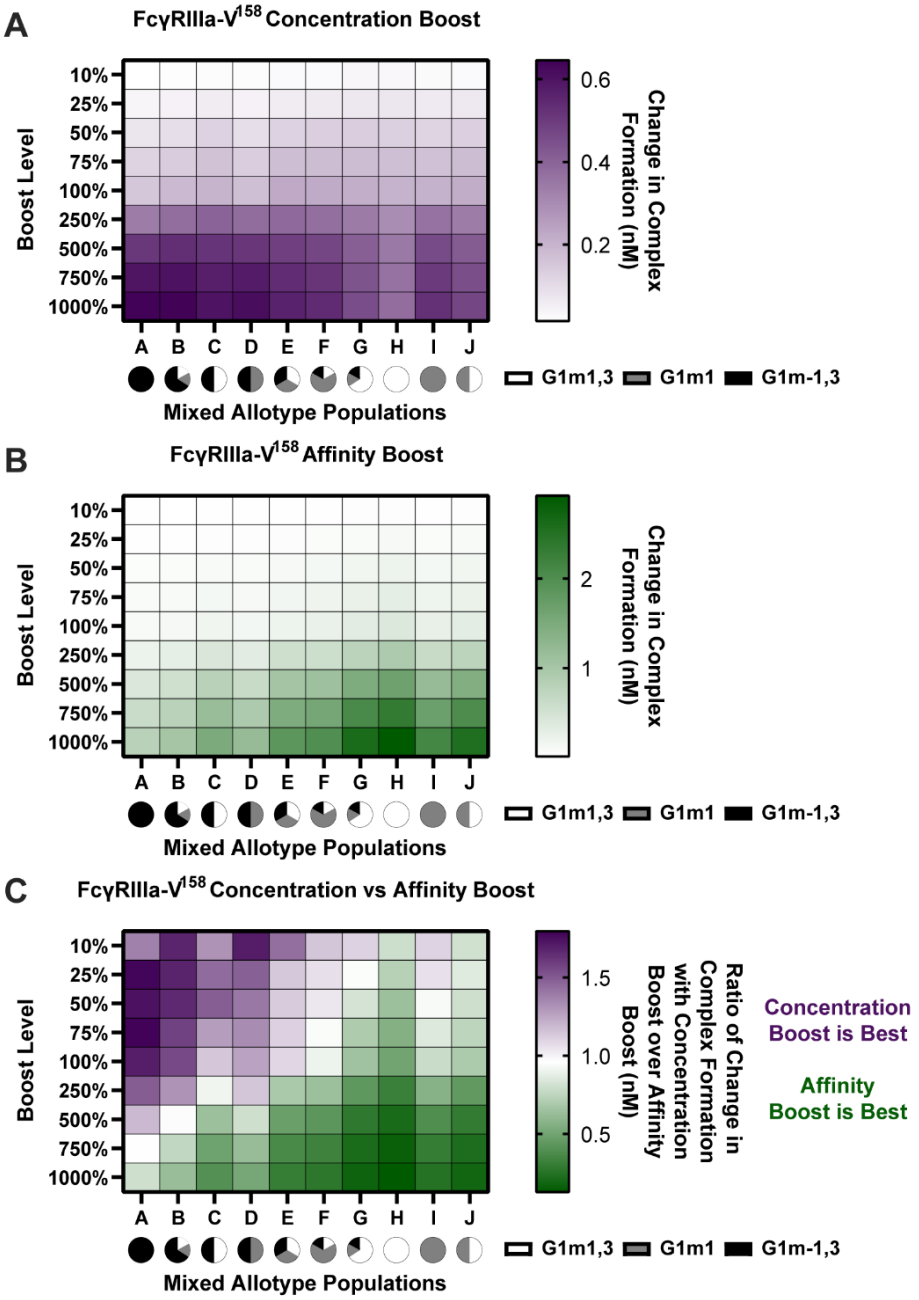

Figure 3-6 In mixed allotype populations, the benefit of boosting IgG1 concentration vs. IgG1 affinity is dependent on the presence of the G1m-1,3 allotype.

(A) Boosting of initial IgG1 concentration in mixed allotype populations (G1m1,3, white; G1m1, gray; G1m-1,3 black) for FcγRIIIa-V^{158}. Color indicates predicted change in complex formation(B) Boosting of k_{on} IgG1- FcγR in mixed allotype populations (G1m1,3, white; G1m1, gray; G1m-1,3 black). Color indicates predicted change in complex formation (C) The ratio of median change in complex formation with a boost in IgG1 over median change in complex formation with a boost in k_{on} IgG1-FcγR at each boosting level. This ratio indicates which type of boost is predicted to be most effective for increasing complex formation (IgG1 concentration, purple; k_{on} IgG1-FcγR, green).

allotype based on the given ratio of allotypes for the indicated population (Populations A-J; **Figure 3.6**). Each individual was then projected into their assigned allotype. To be robust in these assignments, this was repeated 25 times for each population and the data was pooled (n = 2,625 for each population).

We performed both IgG1 concentration and IgG1 affinity boosting as described above (**Figure 3.6**). Overall, we found that the populations with majority G1m-1,3 (populations A-D) benefit more from concentration boosts, and populations higher in G1m1,3 benefit more from FcR affinity boosts (populations G, H, and J) (**Figure 3.6A-B**). Interestingly, population C, which was 50% G1m1,3, and 50% G1m-1,3, only gained minimal benefits from affinity boosts compared to populations G, H and J, (**Figure 3.6B**). When we evaluated the ratio of change in complex formation from a concentration boost over change with an affinity boost, we found IgG1 concentration boosting to be beneficial for almost all populations at the lowest boosting level (10-25%), but only remained beneficial at higher boosting levels in populations with a higher prevalence of G1m-1,3 allotypes (**Figure 3.6C**). Notably the level at which affinity boosting becomes more beneficial than concentration boosting seems to closely follow the level of G1m-1,3 within the population. Altogether this suggests specific guidelines for rational vaccine design to improve FcγRIIIa activation in future trials with mixed allotype populations.

3.5 Discussion

Here we identify specific mechanisms by which heterogeneity in FcγR activation after vaccination may be linked to IgG1 allotypes and FcγR polymorphisms. Importantly, we found that vaccine boosting regimens which increase IgG1 antibody titers may have limited utility in some allotypes (G1m1,3 and G1m1) and may be more effective in others (G1m-1,3). Instead, for G1m1,3 and G1m1 allotypes, vaccine boosting strategies that modulate IgG1 affinity to FcγR (e.g. via adjuvants that modify glycosylation) may be required to improve FcγR activation. The model also illustrates how the influence of FcγRIIIa affinity from different FcR polymorphisms is predicted to have limited influence upon FcR activation until higher IgG1 antibody titers are reached, such as those expected after vaccine boosting. These differences arise from synergistic relationships between IgG1 concentration and affinity for FcγR that could not have been predicted without a computational model.

The computational model also demonstrates how concurrent changes in antigen specific IgG1 antibody titers and IgG1 affinity for FcγR may have more (synergistic), or less (anergistic) of an effect on FcγR activation than previously appreciated. These results suggest that focusing vaccine design on either concentration or affinity alone may not have the expected result. The model identified specific values for IgG1 affinity to FcγR (~10^{-4} $nM^{-1}s^{-1}$ at baseline IgG1 concentration), that would need to be reached before changes IgG1 concentration will have a great effect (**Figure 3.2**). This can be visualized in **Figure 3.2C** where predictions of the additive effects of changes in affinity and concentration in isolation were often overestimated than the actual effects when both were changed in combination.

Perhaps one of the most important outcomes reported here is the potential for differential sensitivity of IgG1 allotypes to boosting regimens that increase antibody titers vs. vaccine adjuvants that may influence glycosylation profiles (i.e. FcR affinity). The model predicts that 2 of the 3 allotypes we evaluated would not be sensitive to boosting regimens that increased IgG1 concentration. This has implications for RV144 and associated follow-up trials, where different allotype distributions would be expected depending on geographic location. Though IgG1 allotype was not measured directly in RV144, the Thai population would likely have a greater prevalence of the G1m1,3 allotype compared to other trials conducted in South Africa, which have previously been reported to have greater prevalence of G1m1 and G1m-1,3[118]. Model results suggest that while an initial vaccination would be most effective in G1m1,3 (due to high baseline IgG1 titers), boosting regimens to increase IgG1 concentration may not improve Fc-mediated functions. Indeed RV305[60] and RV306[58] conducted in Thai populations did increase HIV-negative specific IgG titers, but to our knowledge the resulting changes in FcγR activation have not yet been evaluated. While the model suggests that FcγR polymorphism is not essential in determining which boosting type and boosting level will be most beneficial (**Figure 3.6**), it would still make an impact in individuals with relatively high HIV specific IgG1 titers (G1m1,3 and G1m1).

A key limitation is the study is the evaluation of only one FcγR type (FcγRIIIa) and one epitope, though we would expect similar results for different FcγRs and epitopes[147]. The model could be

easily expanded to explore additional FcRs and to examine multiple FcRs simultaneously. Furthermore, this study is based only upon assumed IgG1 allotypic distributions. Future experimental vaccine studies using will be needed to be conducted using samples with known allotype and FcR polymorphisms to confirm this study.

Overall, thus study illustrates several different scenarios where host genetics is predicted to influence Fc effector responses upon vaccine boosting and that different vaccine boosting regimens are likely to have varied benefits depending on host genotypes. Given that Fc effector functions have been demonstrated to be important for the control and protection of numerous other infectious diseases including COVID-19 and influenza where different vaccine boosting regimens are currently being administered[78,130,149,150], future studies that explore the influence of antibody allotypes and FcR polymorphism upon these vaccine boosting strategies are also warranted.

3.6 Conflict of Interest

The authors declare that the research was conducted in the absence of any commercial or financial relationships that could be construed as a potential conflict of interest.

3.7 Author Contributions

M.M.L. designed the study, performed computational analysis, created figures, and wrote the manuscript.
R.T. and E.R.B, performed computational analysis and edited the manuscript.
M.R.M. and E.L. performed experimental measurements and edited the manuscript
S.K. provided information used to calculate conversion factors for IgG1 allotypes and edited the manuscript.
S.R.N, P.P. and S.N. conducted the RV144 Vaccine trial.
B.D.W. and P.M.H. provided rsFcγR dimers and edited the manuscript.
S.J.K arranged institutional ethics and edited the manuscript.
A.W.C. designed the study, wrote the manuscript, and oversaw experimental analysis.
K.B.A. designed the study, wrote the manuscript, and oversaw computational analysis.

3.8 Funding

This work was supported by the Australia National Health & Medical Research Center (NHMRC) (APP1125164 to A.W.C.) and the American Foundation for AIDS Research (amfAR) Mathilde Krim Fellowship (109499-61-RKVA) to A.W.C, and by start-up funds from the University of Michigan to K.B.A. S.J.K and A.W.C are supported by NHMRC fellowships.

3.9 Acknowledgments

The data necessary to calculate allotype conversion was generously shared by Robin J. Shattock and Paul F. McKay (Imperial College London). The authors would like to thank participants in the RV144 trial.

3.10 Data Availability Statement

The code written for this study can be found on GitHub at https://github.com/melissalemke/FcR-ODE-Genetics.git.

3.11 Ethics Statement

All relevant human research ethics committees approved all experimental studies. All plasma samples were provided de-identified of demographics including gender and age.

Chapter 4 Draft Notes on Unpublished Work

4.1 HIV-specific Antibody Fc Receptor Interactions

4.1.1 Introduction

Using the previously published model[147] we have performed simulations related to antibody decay that occurs post-vaccination, as well as further investigation of allotype's effect on the optimal type of boosting.

4.1.2 Methods

See chapter 3, the same model, parameters, and methods were used. The antibody decay simulations were performed by uniformly reducing all IgG subtypes by 0-100% in increments of 10% and taking the median at each point for each genetic background.

4.1.3 Results

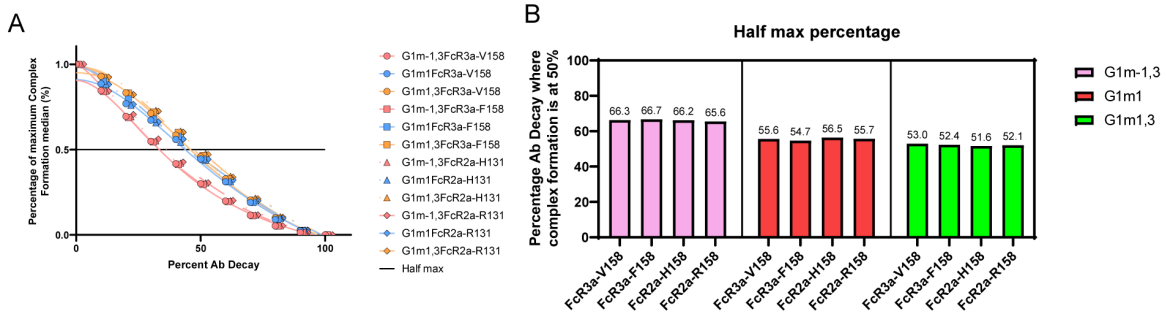

Figure 4-1 Antibody decay after vaccination reduces complex formation sooner for those with G1m-1,3 allotype.

(A) Percent of maximum median complex formation for each genetic population with simulated antibody decay. (B) Percentage of antibody decay where percentage of maximum complex formation is halved for each genetic population.

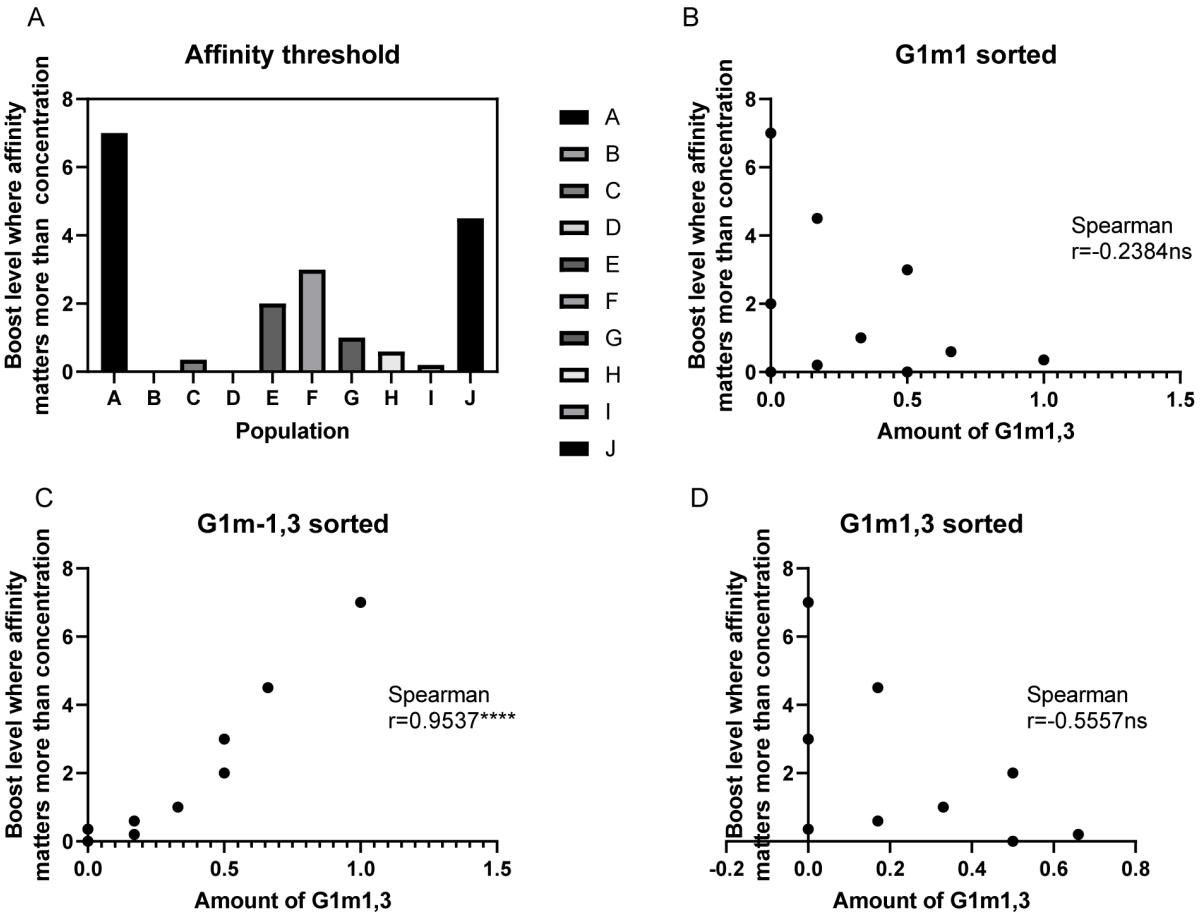

Figure 4-2 Amount of G1m-1,3 allotype in a population determines when an affinity boost is more influential than a concentration boost.

(A) The boosting level at which a boost in affinity of IgG1 to FcR becomes more beneficial than boost in IgG1 concentrations in simulated mixed allotype populations. See figure 3-2 for the source data and methods (note: the populatin labels had been rearranged). (B-D) Correlations of boost level where affinity is more beneficial than concentration and amount of G1m1 (B), G1m-1,3 (C), and G1m1,3 (D) in the population.

4.1.4 Limitations

We do not have access to specific data on antibody decay for our RV144 samples so we had to assume uniform decay in all IgG subtypes. Additionally, as stated in chapter 3, we do not have specific allotype data on the RV144 cohort so our allotype projections are based IgG subtype distributions in a small cohort for a different HIV vaccine trial[112].

4.1.5 Future Directions

We plan to use these methods on datasets with known allotypes and potentially multiple timepoints to track HIV-specific antibody decay.

4.2 Non-HIV-specific and HIV-specific Antibody Fc Receptor Interactions

4.2.1 Introduction

To investigate the effects of non-HIV specific IgG antibodies on the system, we introduced a non-specific IgG (IgGn) that can only bind to the FcRs. This represents all other IgG antibodies in the plasma and is several orders of magnitude higher in concentration, leading to competition for FcRs. We hypothesized that complex formation in an individual will be significantly effected by their non-specific IgG concentration, not just their individual HIV-specific IgG profile.

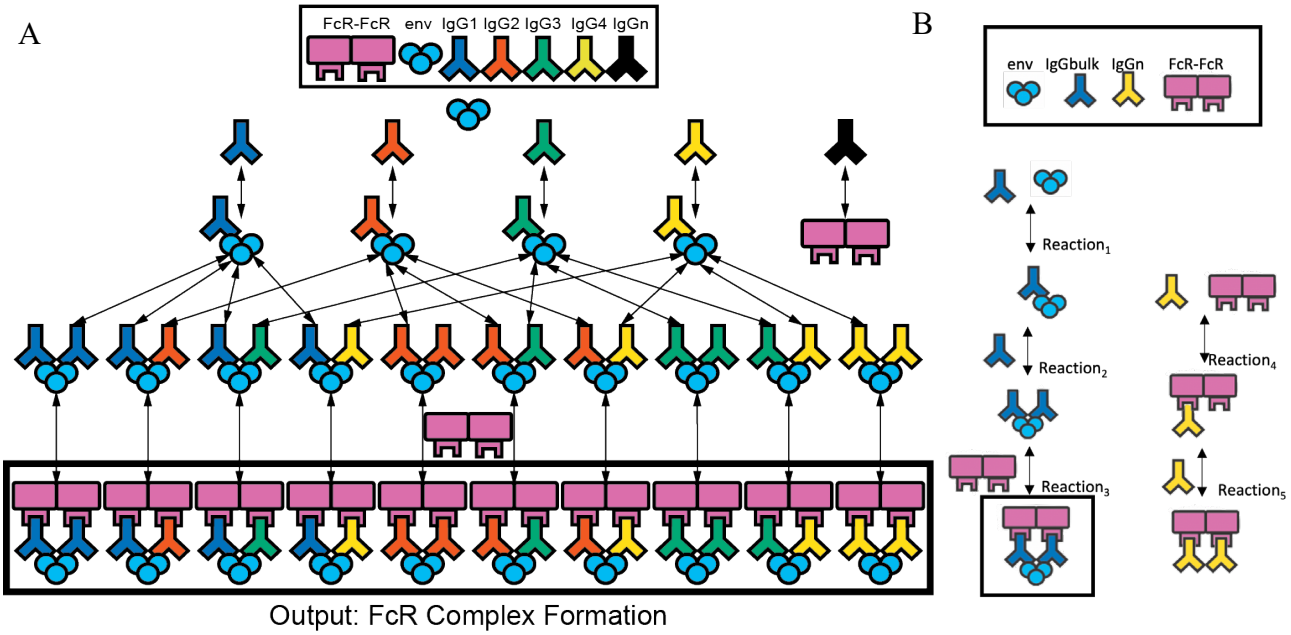

Figure 4-3 Model Schematic

Ordinary differential equations were used to predict total HIV ant-IgG-FcγR complexes formed as a function of concentration and binding affinity of ant, IgG subclasses, and FcγR. The model assumes a single FcγR type. Reversible reactions are represented by double-ended arrows. Model output was the sum of all dimeric FcγR complexes formed (boxed in black) at steady state. Non-HIV-specific antibodies are labeled IgGn (A) Model with all four IgG subtypes. (B) A simplified model where bulk HIV-specific IgG (IgGbulk) is the only HIV-specific antibody.

4.2.2 Methods

Based on the previous model used in chapters 2 and 3, we have added a non-specific IgG (IgGn) that binds to FcR only. Additionally we have a smaller model where there is only one HIV-specific IgG (IgGbulk) reperesenting the bulk HIV-specific IgG measurement. This smaller model can also be created by setting IgG2, IgG3 and IgG4 to zero in the larger model and using IgG1 as IgGbulk.

We have used two sets of experimental data when analyzing this model. The first is an HIV+ cohort of HIV progressors and viral controllers. For this dataset we have personalized bulk IgG, IgG subtype amounts, and complex formation measued in MFI. IgG concentrations were calculataed using previous methods with a reference concentration from HIV+ individuals

(108,000 ng/mL)[151]. The second dataset is from pooled plasma samples from HIV – and HIV + humans, with and without the addition of a monoclocal HIV IgG (PGT121), and with and without washing away all non-specific antibodies.

Table 4-1 Affinity parameters

Affinities	IgG1	IgG2	IgG3	IgG4	IgG_n
Kon IgG-env ($nM^{-1}s^{-1}$)	10				
Koff IgG-env (s^{-1})	$2*10^{-4}$				
Kon IgG-FcR ($nM^{-1}s^{-1}$)	20	0.7	98	2.5	Weighted avg of affinities based on individual IgG subtype concentrations
Koff IgG-FcR (s^{-1})	$1*10^{-2}$				

Table 4-2 Concentration parameters

Conc (nM)	IgG1	IgGn	Env	FcR
Progressors	653	83,800	25	26
Viral Controllers	807	72,600		

4.2.3 Results

Initial experimental results show that the presence of IgGn does indeed interfere with complex formation for all epitopes except A244 (**Figure 4-4**). For the HIV+ samples with and without PGT121 (orange and purple) without IgGn, increasing plasma sample concentrations increased complex formation. This is expected since IgGn is removed so the plasma samples only contain

FcR complex forming antibodies. When HIV+ with PTG121 group is observed with IgGn still remaining in the plasma sample, we see the higher the sample concentration, the lower the complex formation. This is due to the higher levels of IgGn in the plasma sample relative to the constant PGT121 concentration.

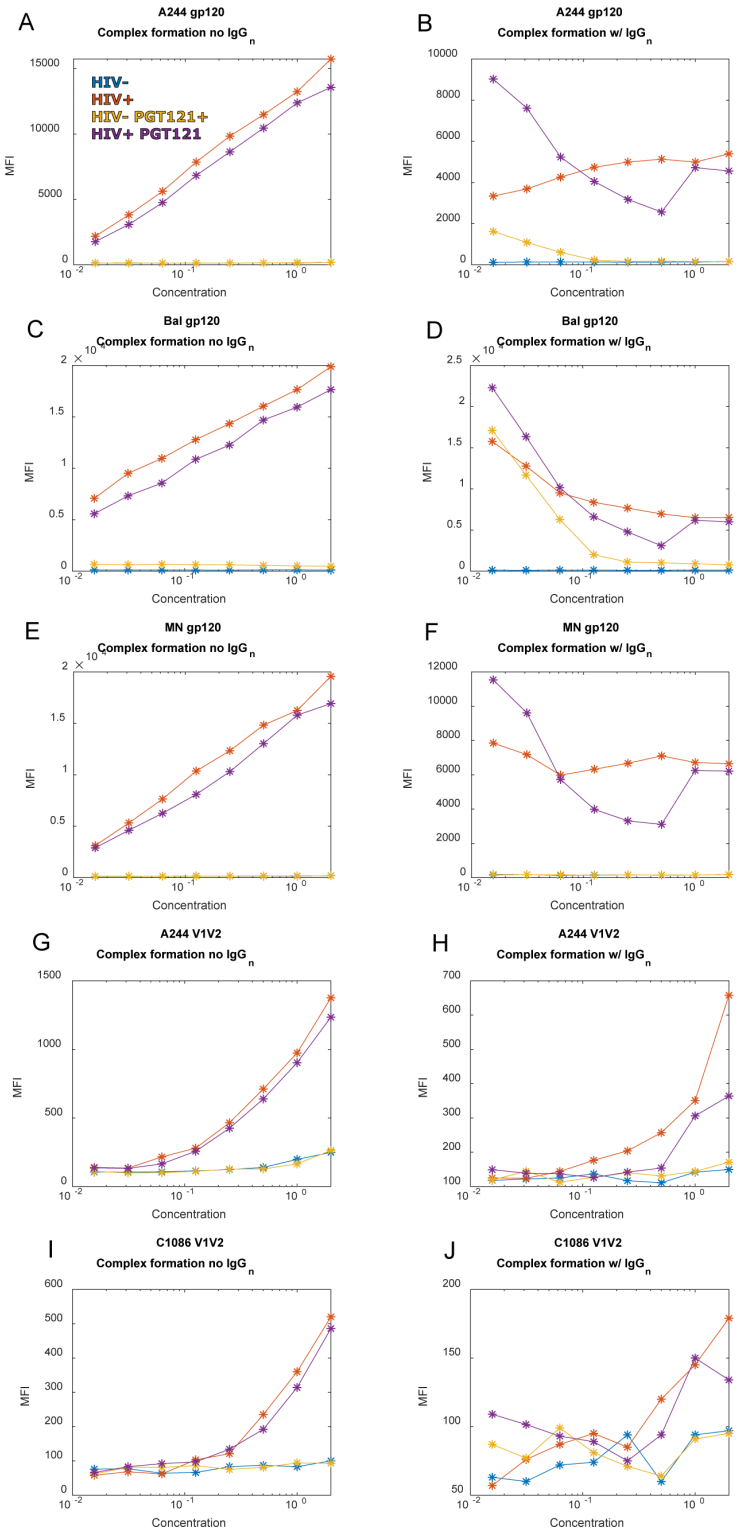

Figure 4-4 The presence of non-specific IgG interferes with complex formation in multiple epitopes

Experimentally measured complex formation in pooled samples from HIV- individuals (blue), HIV+ (orange), HIV- with added PGT121 (yellow), and HIV+ with added PGT121 (purple). The concentration of the pooled samples is varied on the x axis but the concentration of PGT121 is kept constant. The panels on the left show experimental results when the non-specific IgG (IgG_n) has been washed away, and the panels on the right are from the same experimental protocol where IgGn remains. Panel titles show all HIV epitopes tested.

When the model was used to mimic these experiments, most of the general trends matched, but the model is underestimating HIV+ samples and overestimating HIV- with PGT121 samples (**Figure 4-5**).

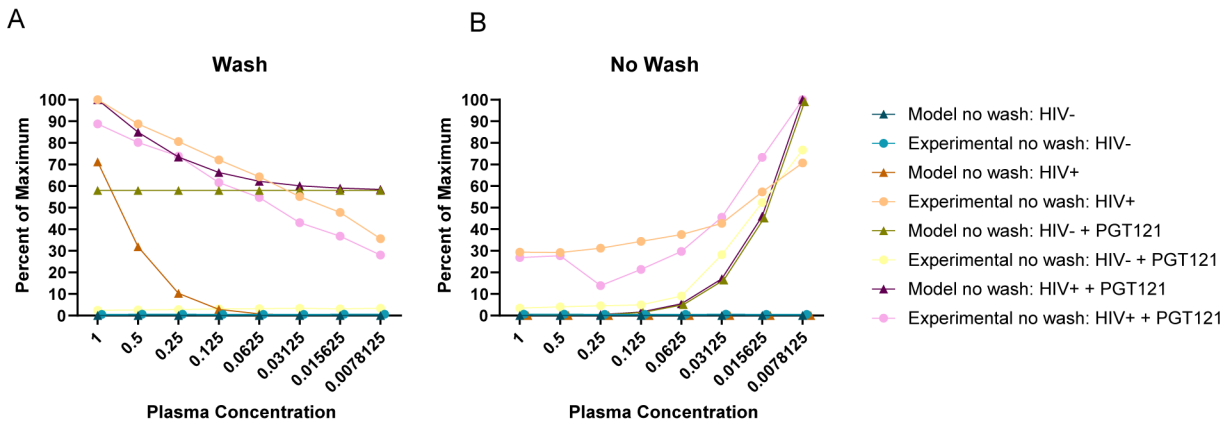

Figure 4-5 Model predicted percent of maximum complex formation compared to experimental

(A) Percent of maximum complex formation without IgGn in both model and experimental conditions for A244 as seen in figure 4-4. (B) Percent of maximum complex formation with IgGn in both model and experimental conditions for A244 as seen in figure 4-4.

When predicting complex formation with and without IgGn on a personalized basis, we saw much larger differences between the two in the model predictions than we did in the experiemetal measurements (**Figure 4-6**).

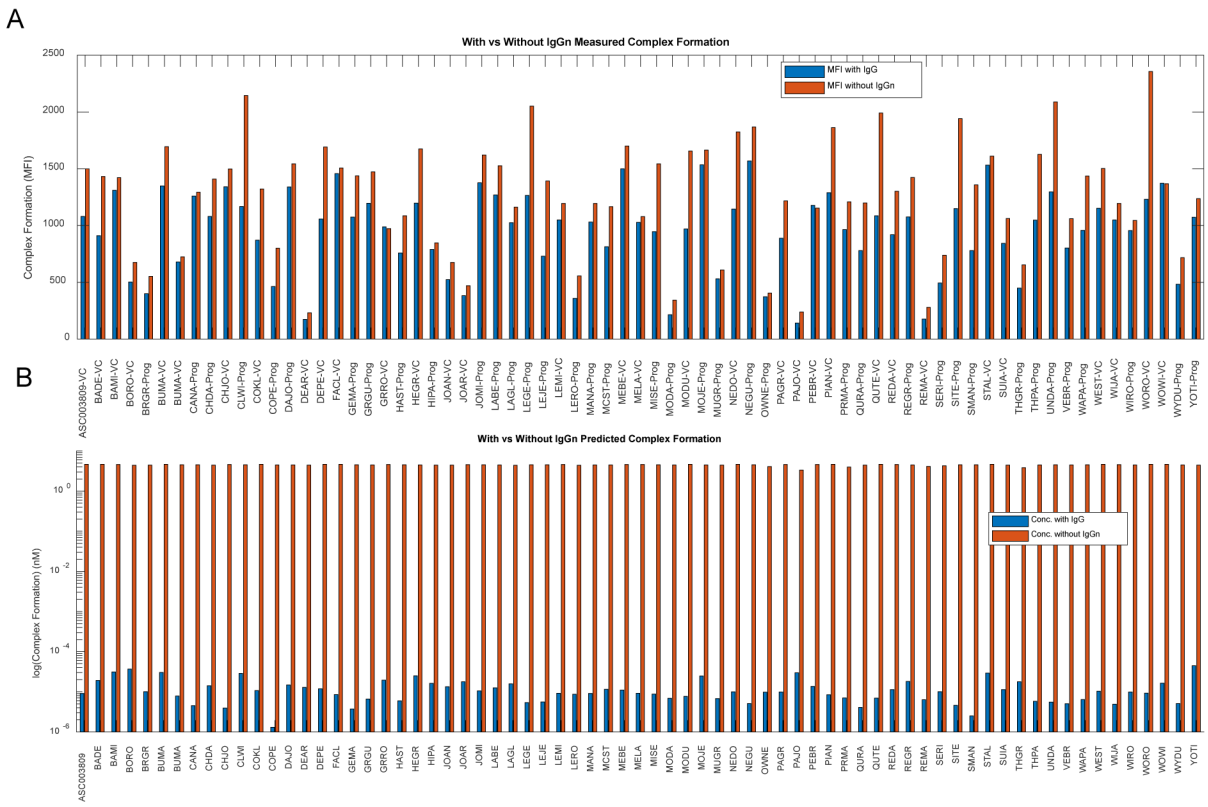

Figure 4-6 Measured and predicted complex formation with and without IgGn

(A) Measured complex formation in the viral controllers (VCs) and progressors (Prog) with (blue) and without (orange) IgGn. (B) Predicted complex formation.

4.2.4 Limitations

The model under-estimates HIV+ samples, perhaps because it is underestimating HIV specific IgG concentrations or affinity. The model over-estimates HIV- +PGT121 with wash (without IgGn) perhaps because the PGT121 is washed out/low efficacy.

The small difference in complex formation with and without IgGn in the personalized data measured experimentally may be due to using older beads that have degraded.

4.2.5 Future Directions

We will investigate the differences in the model and experimental results in figure 4-5 by studying the code and perhaps rerunning the experiment.

4.3 SARS-CoV-2-specific Antibody Fc Receptor Interactions

4.3.1 Introduction

We can use the same model as in chapters 2 & 3 to look at other antigens like SARS-CoV-2 to look at personalized FcR complex formation.

4.3.2 Methods

Personalized RBD-specific IgG subtype concentrations data were pre-processed by removing the assay background and then setting all values below zero to the lowest non-zero value for that detector. Concentrations were determined by converting measured MFIs using a reference concentration (18.5 ug/mL) from a human study of serum SARS-CoV-2 specific IgG levels in COVID-19 convalescent subjects[152] using the previously published methods[147].

Affinity values for RBD to antibodies are the median of literature values [153–160].

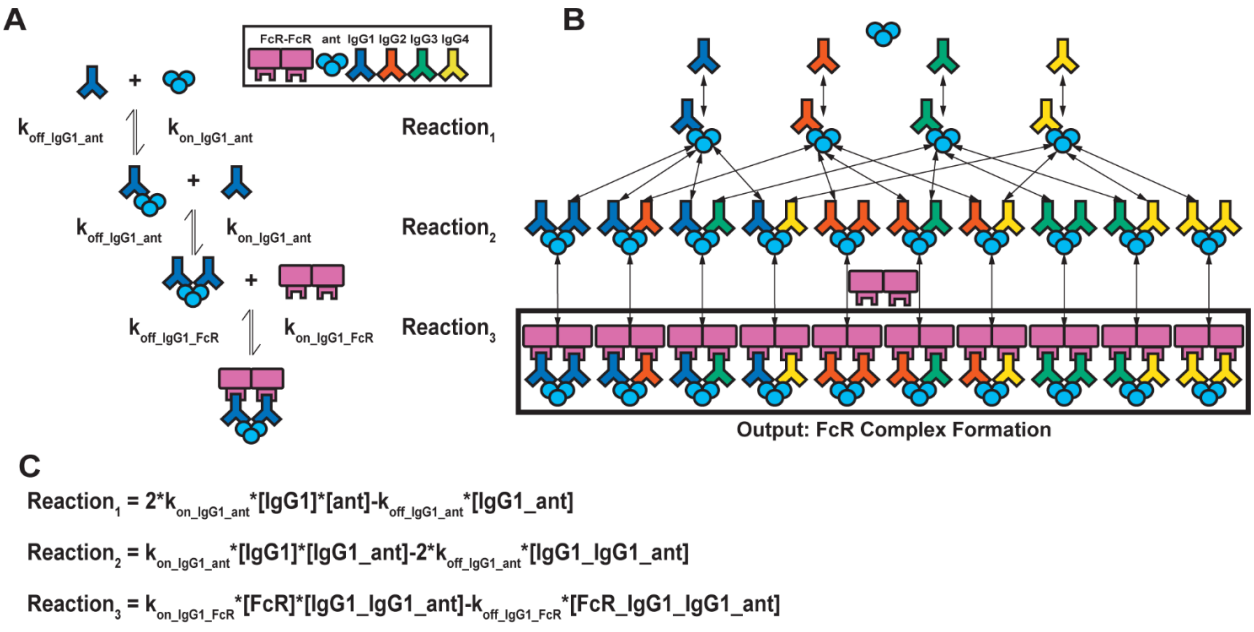

Figure 4-7 Model schematic

(A) An example set of reversible reactions describing the sequential binding of IgG1 to antigen (ant) and dimeric FcγR with the respective forward (k_{on}) and reverse (k_{off}) reaction rates.
(B) Ordinary differential equations were used to predict total HIV ant-IgG-FcγR complexes formed as a function of concentration and binding affinity of ant, IgG subclasses, and FcγR. The model assumes a single FcγR type. Reversible reactions are

represented by double-ended arrows. Model output was the sum of all dimeric FcγR complexes formed (boxed in black) at steady state.
(C) Equations describing the example reactions in (A). Reactions follow mass-action kinetics and consist of a forward reaction (on rate, k_{on}, multiplied by the concentrations of the substrates) and a reverse reaction (off rate, k_{off}, multiplied by the concentration of the product of the forward reaction). Differential equations for change in each complex over time were generated for each complex.

Table 4-3 Parameters

Parameters	IgG1	IgG2	IgG3	IgG4
k_{on} – RBD ($M^{-1}s^{-1}$)	$5.07*10^5$ [153–160]			
k_{off} – RBD (s^{-1})	$3.38*10^{-3}$ [153–160]			
K_D – RBD (nM)	4.51 [153–160]			
k_{on} – FcRs ($M^{-1}s^{-1}$)	Same as previously published model[88,147]			
k_{off} – FcRs (s^{-1})				
Median Concentration – COVID + Samples in Healthy vs COVID cohort (nM)	67.8	0.49	2.32	0.05
Median Concentration – DRASTIC (nM)	105.6	4.77	2.32	1.33

Table 4-4 Sensitivity ranges for parameters

Ranges used in sensitivities and seen in literature	Affinities	Concentrations Healthy vs COVID cohort	Concentrations DRASTIC
Low	0.001X	0.001X	$6.5*10^{-5}$X
High	10X	50X	150X

4.3.3 Results

The model accurately predicts the rank order of complex formation in five different FcRs (**Figure 4-8**). A global sensitivity analysis shows that IgG1 related parameters are significantly important along with IgG3 parameters, and that FcR affinities matter much more than affinitites to the antigen (**Figure 4-9**). Additionally IgG1vsIgG3 landscapes for all FcRs were unable to separate the data based on gender, hospital location, NIH severitiy score, or oxygen intervention (**Figure 4-10**). This led us to test the input data to see if there were differences between the groups to begin with for several different SARS antigens in terms of initial IgG concentrations (**Figure 4-11**) or final measured complex formation (**Figure 4-12**) and there were very few.

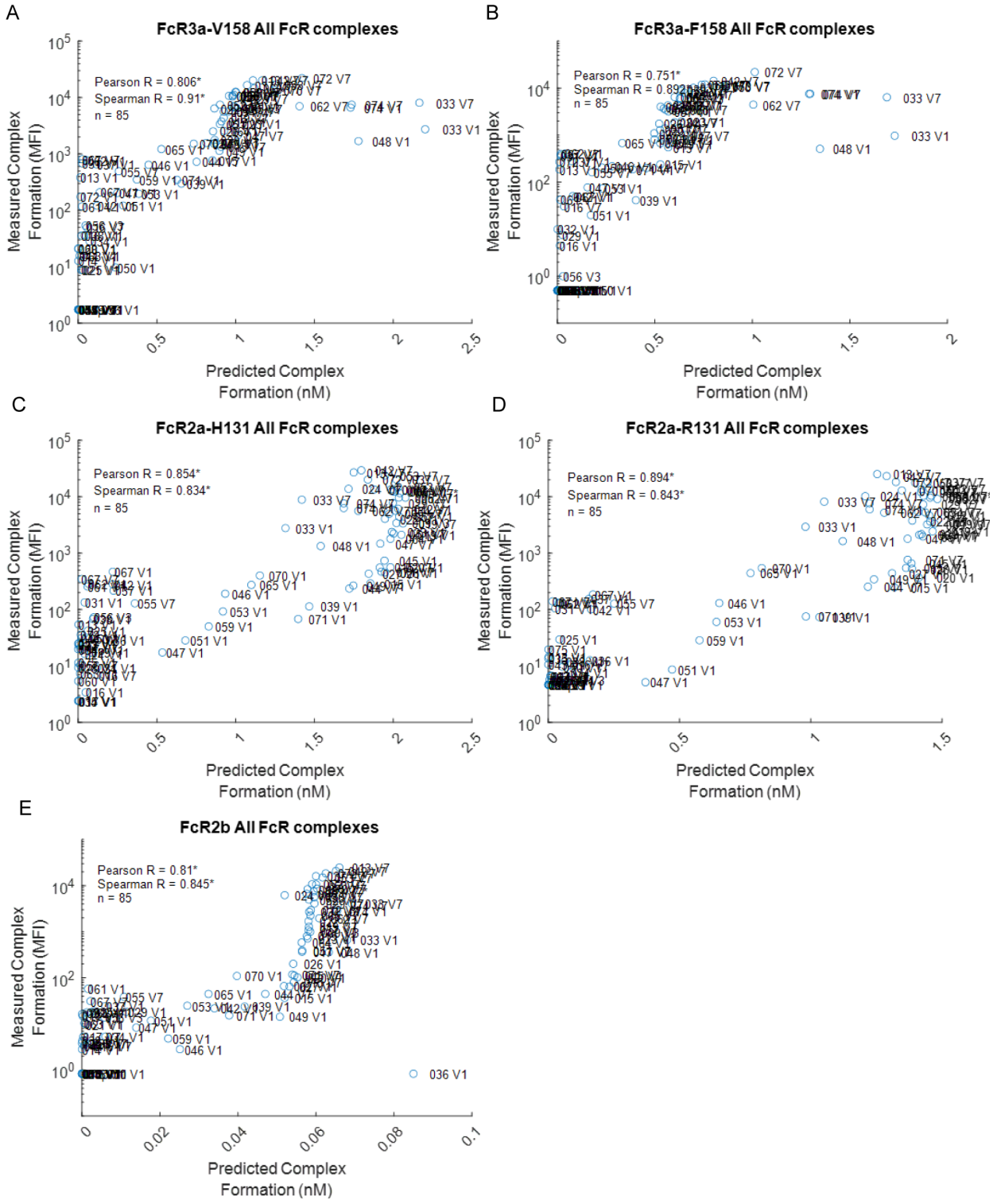

Figure 4-8 SARS-CoV-2 initial FcR validations using the DRASTIC cohort

Measured complex formation compared to predicted complex formation for five different FcRs.

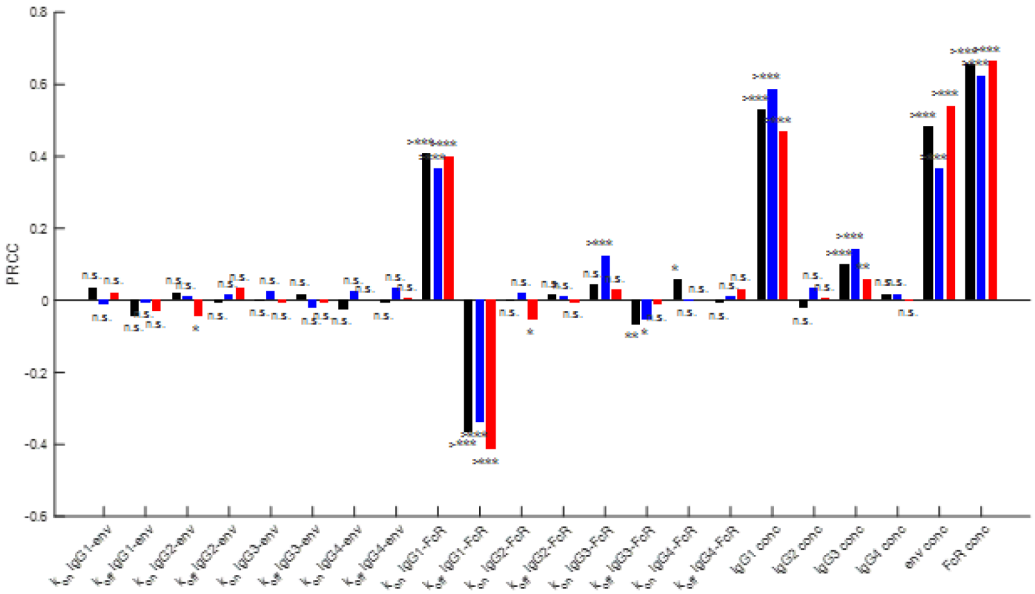

Figure 4-10 Global sensitivity

Global sensitivity analysis results for the overall median of the DRASTIC cohort (black), as well as the median of the ICU patients (blue), and the ward patients (red).

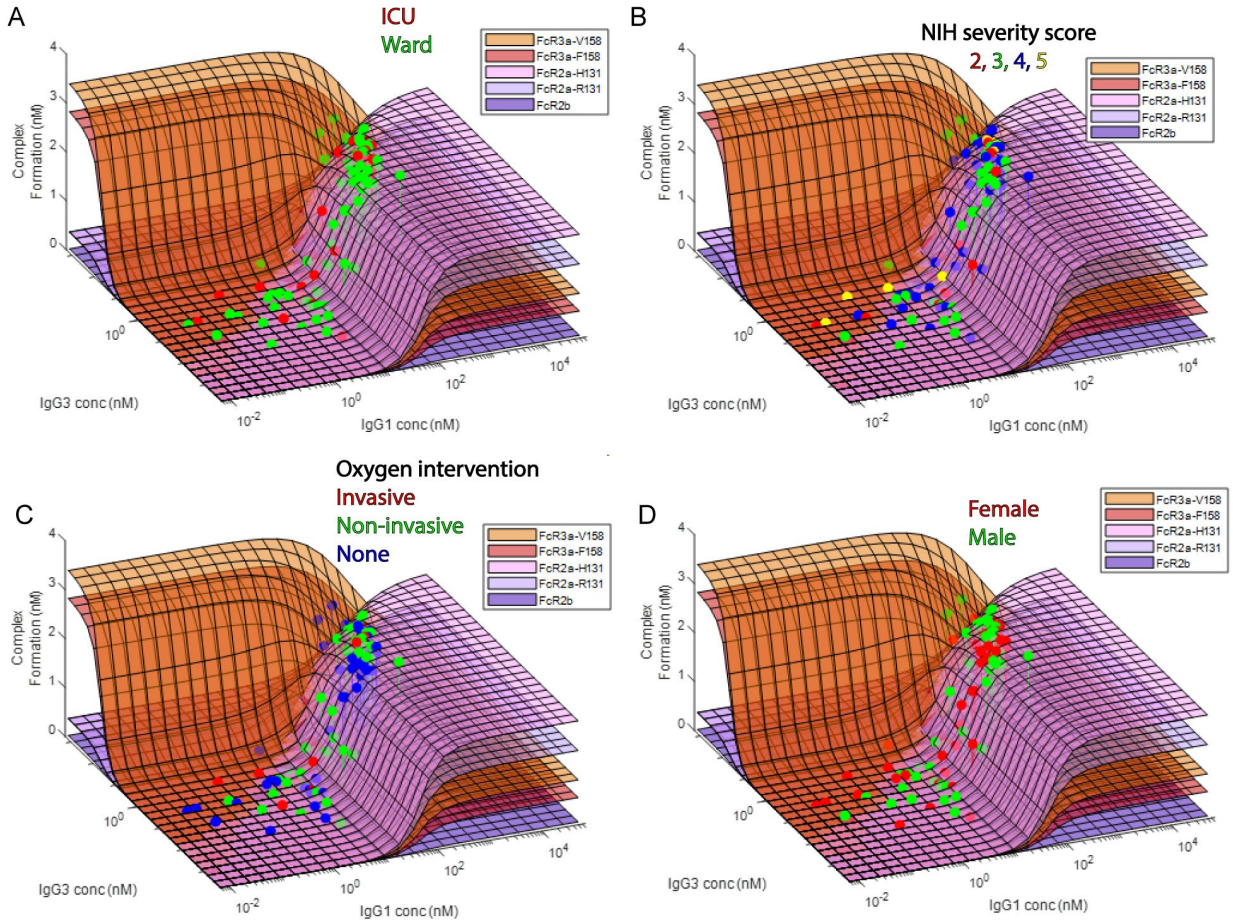

Figure 4-9 IgG1 vs IgG3 initial concentration landscapes

Complex formation landscapes for all five FcRs with the DRASTIC cohort plotted onto the surfaces colored either by ICU and ward (A), NIH severity score (B), oxygen use (C), and gender (D).

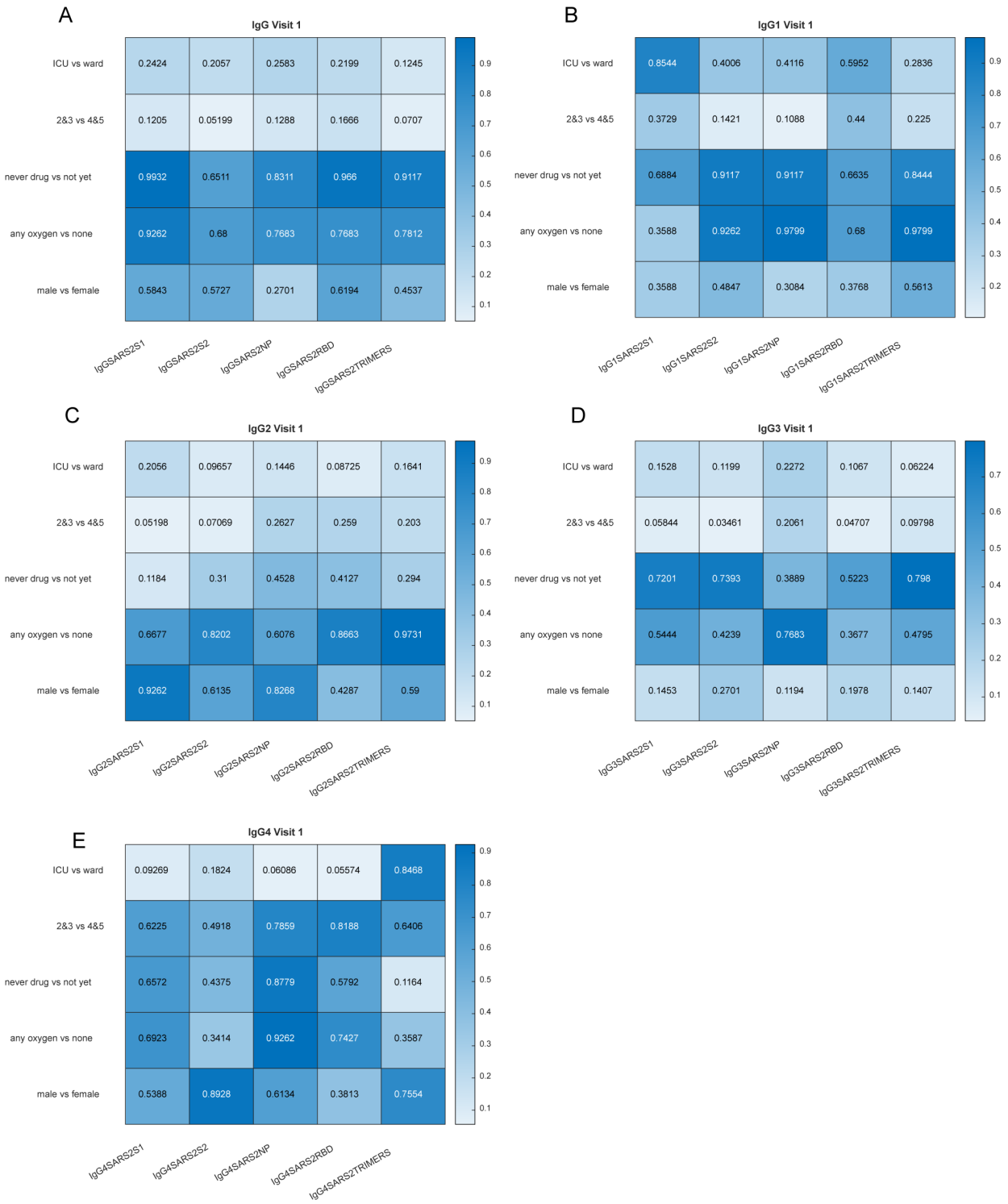

Figure 4-11 P-values from Mann-Whitney tests of IgG concentration data separating groups

p-values from Mann-Whitney tests comparing the IgG concentratrion listed in the panel title in the groups listed on the y axis for five SARS epitopes on the x axis.

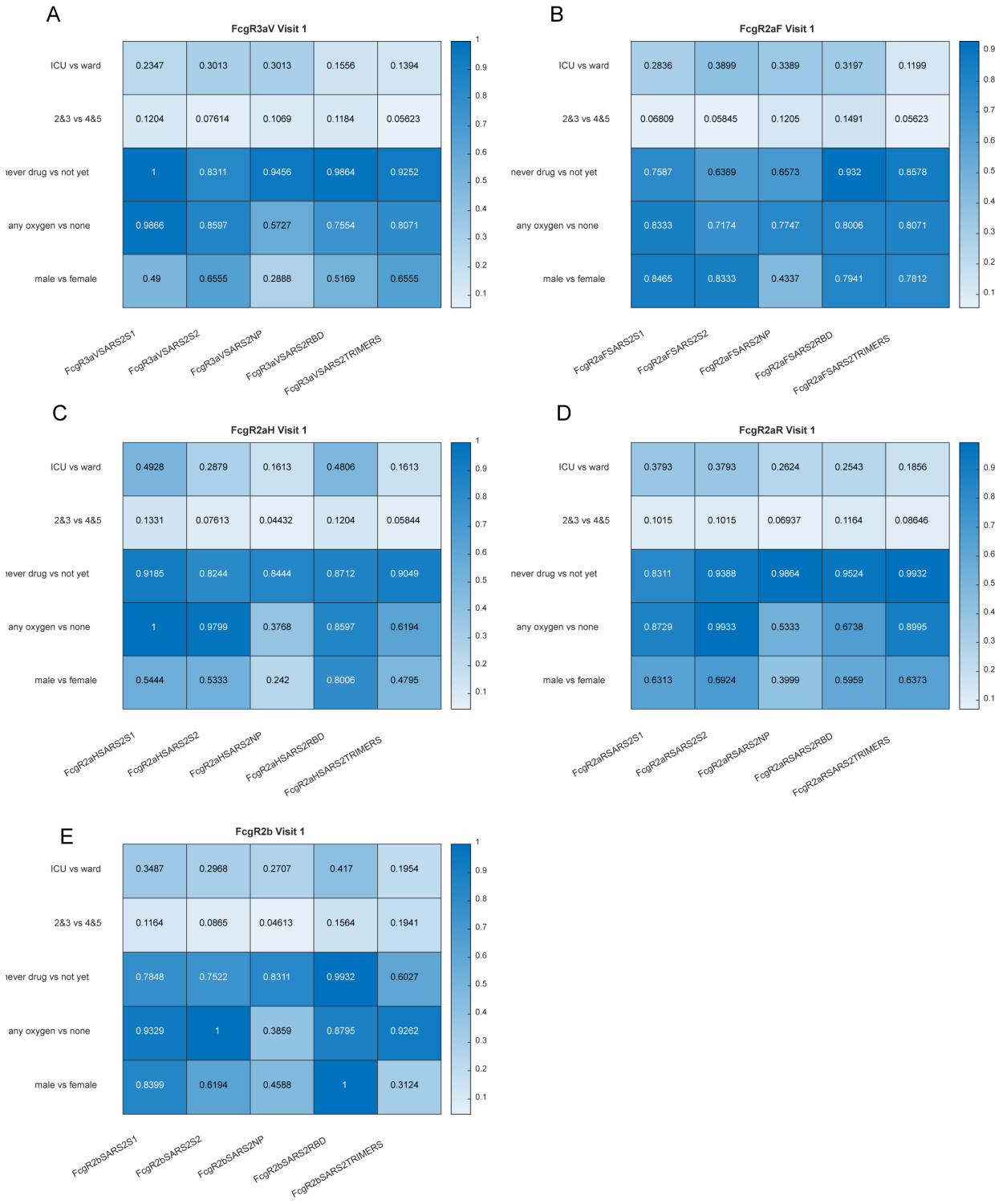

Figure 4-12 P-values from Mann-Whitney tests of experimental FcR complex concentration data separating groups

p-values from Mann-Whitney tests comparing the IgG concentratrion listed in the panel title in the groups listed on the y axis for five SARS epitopes on the x axis.

o consistent significant differences in the input data between groups.

4.3.4 Limitations

The lack of variety or natural separation in the cohort groups to begin with limits the analysis we are capable of performing. If we want to determine the mechanisms that drive a more severe COVID response, we need data from individuals with more severe responses. The DRASTIC cohort data was collected in Australia in the beginning of the pandemic when the disease was under control and hospitals had room to treat mild to moderate cases in the ICU meaning our data is from mostly individuals with more mild cases so separation is difficult to achieve.

4.3.5 Future Directions

We will investigate new COVID datasets with more varied responses as well as apply the methods from chapeter 3 to investigate how genetics impacts COVID-19.

4.4 SARS-CoV-2-specific Neutralizing Antibody Interactions

4.4.1 Introduction

Variants of the SARS-CoV-2 virus are rapidly developing and spreading. Monoclonal antibodies that may be used to combat the infection bind differently to different variants, and specifically have different affinities. We developed a model to rapidly investigate the monoclonal antibody interactions that will lead to protection in the case of differing variants.

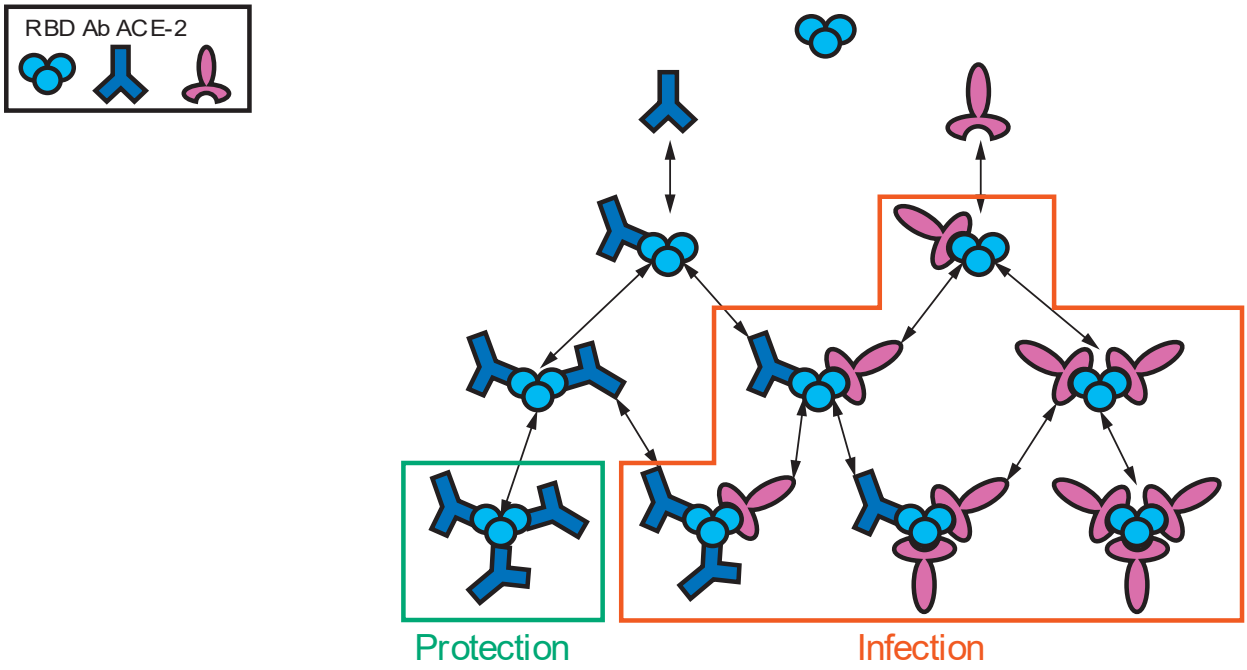

Figure 4-13 Model Schematic

The model depicts ordinary differential equations that were used to predict total HIV ant-IgG-FcγR complexes formed as a function of concentration and binding affinity of RBD antigen, monoclonal IgG antibodies (Ab), and ACE2. Reversible reactions are represented by double-ended arrows. Model output was the sum of all protective or infectious complexes formed (boxed in green and orange respectively) at steady state. Reactions follow mass-action kinetics and consist of a forward reaction (on rate, k_{on}, multiplied by the concentrations of the substrates) and a reverse reaction (off rate, k_{off}, multiplied by the concentration of the product of the forward reaction). Differential equations for change in each complex over time were generated for each complex.

4.4.2 Methods

Table 4-5 Parameter table

k_{on} Ab-RBD ($M^{-1}s^{-1}$)	k_{off} Ab-RBD (s^{-1})	k_{on} ACE2-RBD ($M^{-1}s^{-1}$)	k_{off} ACE2-RBD (s^{-1})	Ab (nM)	ACE2 (nM)	RBD (nM)
depends on variant				0.78	116	2.7

Table 4-6 ACE2-RBD affinities to different variants

ACE2-RBD	Wild type	N501Y	Q483L	N439K	S494P	E484K	E484D

Kon	3.28E-04	1.55E-04	2.46E-04	2.68E-04	2.44E-04	1.97E-04	3.28E-04
Koff	2.10E-03	3.26E-03	6.20E-03	7.00E-03	9.09E-03	2.18E-02	2.10E-03

Table 4-7 Ab-RBD kon affinities to different variants

Ab-RBD k_{on} (nM^{-1s-1})	Wild type	N501Y	Q483L	N439K	S494P	E484K	E484D
COVA2-15	0.001	0.001	0.001	0.001	0.001	0.001	0.001
COVA1-18	0.001	0.001	0.001	0.001	0.001	0.001	0.001
MM43	0.001	0.001	0.001	0.001	0.001	0.001	0.001
REGEN 10987	0.001	0.001	0.001	0.001	0.001	0.001	0.001
REGEN 10933	0.001	0.001	0.001	0.001	0.001	0.001	0.001
C135	0.001	0.001	0.001	0.001	0.001	0.001	0.001
C002	0.001	0.001	0.001	0.001	0.001	0.001	0.001
SAD-35	0.001						
CR3022	0.001						
Flu mAb	1						

Table 4-8 Antibody-RBD koff affinities to different RBD variants

Ab-RBD k_{off} (s^{-1})	Wild type	N501Y	Q483L	N439K	S494P	E484K	E484D
COVA2-15	9.04E-04	1.43E-03	1.72E-03	8.43E-04	7.89E-02	2.86E-03	1.46E-03

COVA1-18	1.14E-03	1.31E-03	9.31E-04	1.28E-03	1.36E-03	7.41E-02	2.23E-03
MM43	1.17E-03	1.49E-03	1.59E-03	2.05E-03	1.44E-03	1.79E-03	1.58E-03
REGEN 10987	1.06E-03	1.34E-03	1.21E-03	3.49E-03	1.44E-03	1.66E-03	1.47E-03
REGEN 10933	7.42E-04	8.86E-04	1.63E-03	6.59E-04	6.78E-04	2.73E-03	1.47E-03
C135	9.85E-04	1.84E-03	1.13E-03	2.36E-03	1.59E-03	1.39E-03	1.28E-03
C002	9.37E-04	1.03E-03	6.54E-02	1.20E-03	9.59E-04	2.18E-03	1.94E-03
SAD-35	7.48E-04						
CR3022	1.43E-03						
Flu mAb	1.64E-03						

4.4.3 Results

The initial validation of the model focuses on the amount of IgG bound, the amount of ACE2 bound, and the percent inhibition of the ACE2. Currently the model is predicting there is less IgG bound than in the assay and the model saturates later (**Figure 4-14**):

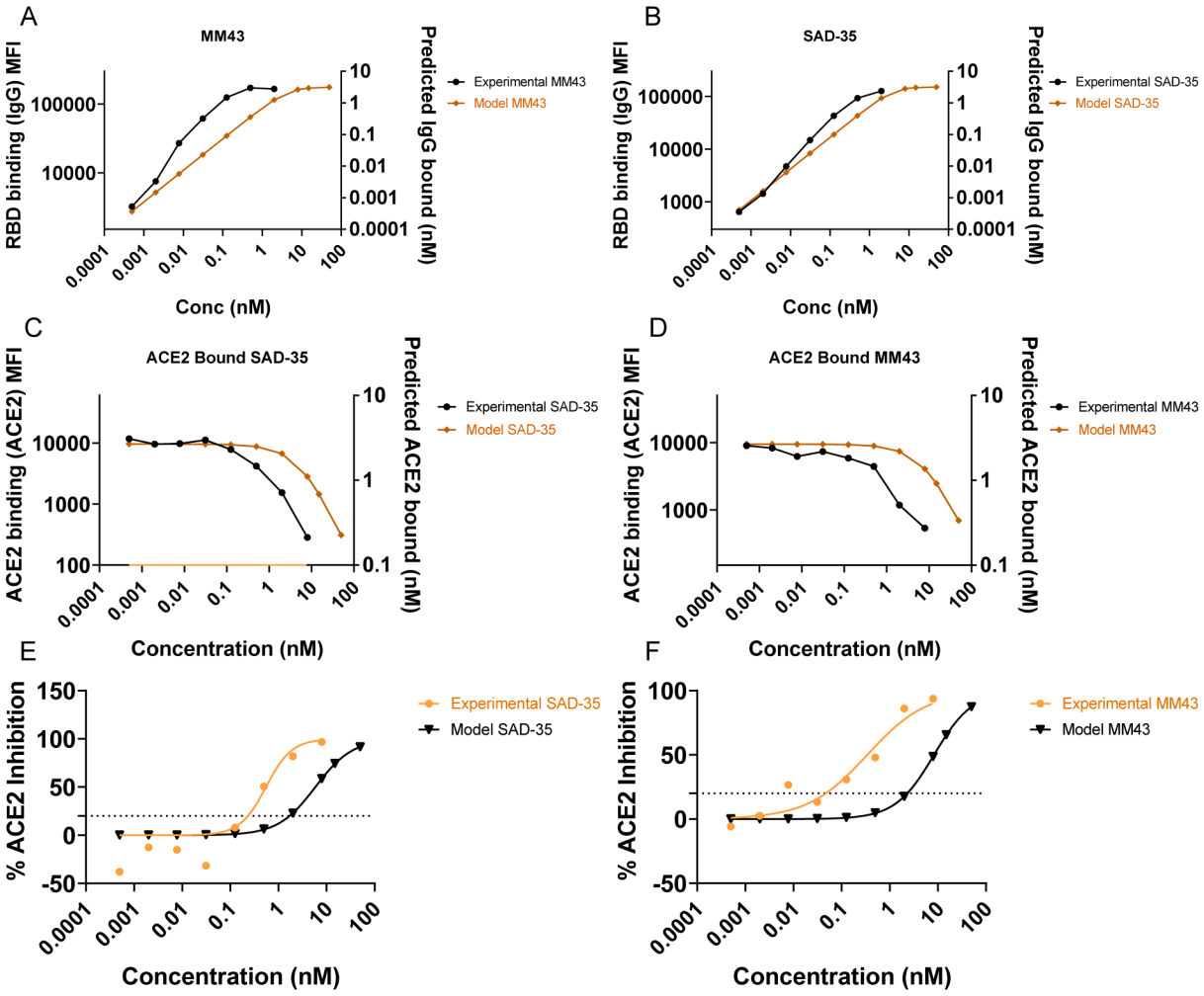

Figure 4-14 Model vs experimental results for two neutralizing antibodies.

(A-B) Model (orange) and experimental (black) IgG binding over various MM43 (A) and SAD-35 (B) antibody concentrations. (C-D) Model (orange) and experimental (black) ACE2 binding over various MM43 (C) and SAD-35 (D) antibody concentrations. (E-F) Model (orange) and experimental (black) percentage of ACE2 inhibition over various MM43 (E) and SAD-35 (F) antibody concentrations. Percentage ACE2 inhibition = (binding w/o IgG – w/ IgG)/binding w/o IgG * 100.

4.4.4 Limitations

The mismatch in data between experimental and model results could be caused by there being more IgG in the experiment than we initially measured. There may also be more RBD in the assay or a higher affinity if IgG to RBD.

4.4.5 Future Directions

We will reinvestigate experimental parameters to determine the flaw is not there. If that does not change, we may need to adjust the structure of the model with things like, a change in the number of binding sites.

Chapter 5 Discussion

5.1 Scientific contributions

In this thesis, I present a cohesive framework for mechanistic analysis of immune complex formation in the activation of Fc receptors and generate and validate hypotheses on how personal and genetic variation affect FcR activation in HIV vaccinees. I constructed an ODE model of immune complex formation representing all IgG subclasses that can predict relative complex formation on a personalized basis. The computational framework developed utilizes personal IgG subclass data from plasma that could be collected in vaccine studies or any biological applications where FcR-antibody interactions are of interest. More broadly, this model can be utilized in any well-mixed system where complexes form in the given structure (i.e., IgA antibodies, other antigens, other dimerized receptors). With currently available data, I used this framework to identify IgG subclasses of the most importance and show how individual variations in subclass concentrations affected potential intervention outcomes. Additionally, I related genetic factors that affect model parameters to identify vulnerable genetic backgrounds. With the future collection of more extensive data, this model could predict vaccine efficacy in different populations and specific individuals and predict ideal intervention scenarios or preferred vaccine recommendations on an individual and population basis.

5.2 Model identified effects of personal variability on FcR activation

Our ODE model, with its ability to take in personal antigen-specific antibody concentrations, showed how the variability in initial IgG subclass concentrations affected the FcR complex formation, how individual IgG subclasses contributed, and the success of a boosting intervention.

5.2.1 Importance and limitations of IgG1 concentration

RV144 follow-up studies identified HIV-specific IgG3 antibodies as correlates of lower infection risk and were higher in RV144 than in the failed predecessor trial, VAX003, and they posited that IgG3 drove a more polyfunctional immune response thought to be protective[52,79]. Additionally, an experimental analysis revealed that depletion of IgG3 antibodies decreased ADCC significantly in a way that mirrored the decrease in IgG3 and protection over time in RV144 vaccinees[57]. IgG3 was identified as the most critical subclass likely due to its high affinity to FcγRIIIa, the FcR leading to ADCC[88]. In contrast, our model brought attention to IgG1 as the most universally important subclass, as although it has an affinity to FcR 5X lower than IgG3, its concentration is typically 28X higher. In our kinetics-based equations, affinity is multiplied by concentration, determining complex formation, and this highlighted the importance of the influence IgG1 has through its high concentration.

A possible explanation for the lack of IgG1 focused results previously is perhaps due to the location of the sensitive regions for IgG1 and IgG3. Figure 2.3 and A.S5A show a surface of complex formation at varying levels of initial IgG1 and IgG3 concentrations. Here there are two main sensitive regions: IgG1 sensitivity is seen in the sloped region on the right side where small changes in IgG1 initial concentration have a significant effect on complex formation; IgG3 sensitivity is seen in the sloped region on the left side where small changes in IgG3 concentration

have an even more significant effect on complex formation. Notably, when vaccinees were evaluated based on their initial IgG concentrations, many were close to, on, or just past the region where FcR complex formation was sensitive to IgG1 sensitive. In contrast, only four vaccinees were in an IgG3 sensitive region. While this shows that IgG1 sensitivity is more likely in a given vaccinee, it also points to more uniformity in IgG1 initial concentration's effect on complex formation in comparison to IgG3.

The steeper slope in the IgG3 dimension means that for those individuals unusually high in IgG3 initial concentrations, complex formation is dramatically different from those with slightly lower IgG3 concentrations. This could easily lead to the conclusion that IgG3 is more important for protection because there is a more distinct subpopulation with very high IgG3 levels and very high complex formation. However, the statistics that have pulled out this relationship while attempting to distinguish between a protective and non-protective response have failed to identify IgG1 as a more universally approachable method to improve complex formation in the majority population. IgG1's more universal effect is illustrated in Figures 2.3D and 2.3F, where a 5X increase in IgG1 alone brought 81 out of 105 vaccinees out of relatively low complex formation, but a 20X increase in IgG3 was needed to affect the same number of vaccinees.

While boosts in IgG1 concentration are more likely to bring an individual out of relatively low complex formation, they have a limited effect on individuals who already have moderately high levels of initial IgG1. This limitation is displayed in a plateau on the surface mentioned above, where further increases in IgG1 no longer increase complex formation. We used the model to identify eight individuals who would benefit from an IgG1 boost (IgG1 responders) and eight

who would not benefit (IgG1 non-responders). Experimentally, we performed two boosts with an IgG1 monoclonal antibody at 34nM and 140 nM, and these 16 individuals behaved as predicted, with a 5 and 7-fold increase in complex formation in the responders and 1.3 and 1.3-fold change non-responders. The non-responders already had initial IgG1 concentrations above 150 nM, while the responders had IgG1 concentrations below 32 nM. If these cutoffs were used to identify responders and non-responders in our 105 vaccinee population, 33% would be non-responders and 27% responders. If we assume that our samples represent the general population, one-third of people may not benefit from a boost in IgG1 concentration, meaning if a vaccine does not already protect these individuals, they will need an intervention that does not rely on boosting IgG1.

Lastly, the IgG1 plateau represents a limit on complex formation that cannot be breached without an increase in the affinity of IgG1 to FcR (increases height of the plateau) or an IgG3 concentration above 20 nM, which only 2% of our population has. Additionally, the model showed how changes in IgG3 concentration must occur while IgG1 concentrations are moderately low since high levels of IgG1 will suppress the positive benefits of high IgG3 concentration. This surprising and novel mechanism could point to a situation where boosts in IgG1 are detrimental in some individuals, especially in boosting situations where IgG3 was high. This mechanism could explain the failure in vaccine trials with extended boosting regimens, but it is impossible to confirm this without direct experimental measurements from individual vaccinees in a trial where boosting was applied. In this case, a model such as the one developed here could be valuable for deconvolving the influence of different IgG subclass concentrations, including changes in subclass profiles towards IgG2 and IgG4 such as those observed in

VAX003[52–55]. However, since we do not know the threshold of complex formation necessary for ADCC or protection, it is unclear whether this IgG1 limit prevents protection or does not interfere.

5.3 Model predicted effects of host genetics on FcR activation

Host genetics can affect IgG-FcγR complex formation in several ways: IgG1 allotype can alter the concentration of all subclasses[90,112,136] and has been linked to ethnicity[118,119]; FcR polymorphisms alter the affinity of each IgG subclass to FcRs[88]. We can easily alter these parameters in our model, and in doing so, we were able to gain new insight into the relative role of host genetics in IgG-FcγR complex formation.

5.3.1 Impacts of synergy between IgG1 concentration and affinity to FcR

The model identified a synergistic relationship between personal IgG subclass concentration and genetics not previously appreciated. After the model identified IgG1 concentration and IgG1 affinity to FcR as critical parameters in complex formation, both affected by genetic and personalized factors, we knew the model would be a valuable tool to predict how simultaneous changes in both parameters affected the system. Our findings indicated a synergistic relationship between concentration and affinity for IgG1 that suggested that the change in one parameter affects the level of impact the other parameter can have. When experimentalists and modelers choose one of these parameters, such as affinity, to focus on for ease of interpretability, it is easy to forget that their conclusions are specifically relevant only for a fixed concentration and vice versa. We used the model to computationally simulate all relevant combinations of these two parameters to assess the role of host genetics, including FcR polymorphism and IgG1 allotype.

FcR polymorphism

After a boost in IgG1 concentration, the model illustrated how FcR polymorphism becomes more impactful, with a more significant difference between complex formation in the high-affinity FcR polymorphism (FcγRIIIa-V^{158}) and the low one (FcγRIIIa-F^{158}). Our simulations indicated that the higher affinity polymorphism always has higher complex formation than the lower affinity polymorphism with any input, but this difference increases with increasing IgG1 concentrations. For example, in RV306, all five arms of the study received the original RV144 vaccine regimen, two arms received an additional 12-month booster, one arm a 15-month booster, one an 18-month booster, and one no additional boost[60]. Since they saw increasing HIV-specific IgG titers with later boosts[60], our model suggests that polymorphism in these vaccinees will impact their protection outcome more the later the boost in this series. If we had access to RV306 plasma samples to measure HIV-specific IgG subclasses, we could test which vaccine arms have significant differences between FcR polymorphisms and validate the differences experimentally. If case vs. control and FcR polymorphism data were also available, we could simulate each individual with their actual genetic profile and group them into case and control to help determine how FcR polymorphism contributes to protection mechanisms.

While high-affinity FcRIIIa-V^{158} has been associated with enhanced ADCC functionality and better outcomes within the mAb cancer field[144,145], it has also been linked with disease progression[146] and a lack of vaccine protection in HIV[125]. The reason for FcγRIIIa-V^{158}'s link to the lack of protection in the VAX004 trial is not explained by our model[125], perhaps due to its all-male cohort, other genetic factors linked to FcR polymorphism (like GM allotype[161,162]) that we are not accounting for, or low overall vaccine efficacy. Our findings, unsurprisingly, do

support FcγRIIIa-V[158]'s association with enhanced ADCC[144,145] as one would expect higher affinity in all areas to increase complex formation. While polymorphism associations with outcomes have been found through statistical analysis, we can use this approach to go beyond and predict the effects of polymorphism affinity differences in different vaccine scenarios with more targeted analysis.

IgG1 allotype

We found that the IgG1 allotype determines whether a boost in IgG1 concentration or affinity to FcR will be most beneficial at any given boosting level. IgG1 allotype, having been linked to changes in all four IgG subclass concentrations[136], is a complex factor to account for intuitively when it is challenging to know which if any or all subclasses drive an allotype's success. Accounting for these complexities with allotype and its synergisms with FcR polymorphism, we simulated six different genotyped populations with each combination of allotype and polymorphism. This data revealed that no matter the FcR polymorphism, concentration boosting was more beneficial than affinity boosting in G1m-1,3 populations in most cases, and the opposite was true for both G1m1,3 (the highest IgG1 allotype) and G1m1 populations. We pinpointed the exact boosting level where affinity became more influential than concentration for G1m-1,3, although likely unattainable at 1000%, the tool we have developed can find thresholds such as this one. This approach was also able to highlight how FcR polymorphism is not essential for determining the best interventions.

Finding that the amount of G1m-1,3 allotype in a given population determines which boosts would increase complex formation most suggests that it is low IgG1 concentrations that drive these boosting differences. The more G1m-1,3 individuals in a population, the more we predict a

concentration boost will be significant. This observation relates to the personalized IgG concentration results where lower IgG1 concentrations bring more people into an IgG1 sensitive region where small changes in IgG1 have a more significant effect. Additionally, it points to the synergy between IgG1 concentration and affinity to FcR as it demonstrates that a boost in affinity to FcR is not going to be very beneficial unless a person has reached a high enough IgG1 concentration.

Allotype alone could be a helpful predictor of a population's success with a particular vaccine regimen. It has a known effect on the concentration of subclasses both generally[136] and for vaccine antigen-specific antibodies[112], and it could be tested before vaccination. Knowing the allotypes of each person in a population would give an estimate of their antigen-specific IgG subclass concentration profile. Whereas if we could only measure antigen-specific IgGs in the plasma, we would not get results until after the vaccination has been completed and the regimen planned. Using measured allotypes to estimate IgG titers could help determine the number and timing of booster immunizations – tuning the increase in IgG1 up to the most beneficial level and not past that when it can deter positive effects IgG3.

If individual allotype measurements are not possible and a new vaccine regimen needs to be tailored to a new genetic population, links between allotype, ethnicity, and population demographics could help estimate vaccine outcomes. Population-based data on which allotypes are prevalent in specific communities, countries, or ethnicities have been explored previously[118,119], but there are gaps in the populations represented and differences in the allotypes tested for in each small study. If further data can be collected on allotypes present in a diverse set

of populations and shows reliable, consistent connections, we can be more confident that we could estimate ideal boosting regimens using population demographics. The utility of this method depends on further validation that allotype affects IgG subclass concentration in the HIV vaccine trials of the future, which would require the collection of allotype data alongside protection and plasma samples. Antigen-specific antibodies can be measured in the plasma Allotype results can be grouped to get a more representative estimate of how allotype affects IgG subclass concentration in a larger sample size.

5.3.2 Vulnerable individuals, populations, and interventions

Our ability to predict the effects of genetics on complex formation allowed us to identify genotypes that would not be responsive to increases in IgG1 titers (concentration). We were also able to simulate heterogeneous populations and identify vulnerabilities there. As expected, when we projected RV144 data into each allotype-polymorphism genotype, we saw significantly different complex formation in each population with FcγRIIIa-V^{158} always having higher complex formation than FcγRIIIa-F^{158} within an allotype, with the high IgG1 allotypes having the highest complex formation. At baseline, this leaves G1m-1,3 allotyped individuals at the greatest risk regardless of their polymorphism.

We can use this approach to simulate nonhomogeneous populations to make broader recommendations for an entire population's protection. While FcR polymorphism will affect the total complex formation achieved, in this scenario, a specific threshold of complex formation is not the goal; instead, it is any increase in complex formation. Therefore, we can disregard polymorphism since it has a limited effect on which parameter boost will most benefit. Testing mixed allotype populations, we found that populations with high levels of G1m-1,3 benefit more

from a concentration boost, especially at low boosting levels. In addition, the amount of G1m-1,3 in a population determined the boosting level at which affinity became more beneficial than concentration. With knowledge of the magnitude of boosts possible, one could use this method to determine which intervention is ideal for increasing complex formation in most of the population.

With the caveat that allotype linkage to ethnicity needs further exploration and confirmation, we were able to provide predictions relevant to the recent failure of the HVTN 702 trial with allotype. HVTN 702 (South Africa) mimicked the regimen of the moderately successful RV144 trial (Thailand), but they altered the antigens to match the strains circulating in South Africa as well as the adjuvant. With multiple alterations to the vaccine itself and the population it was administered to, it will require extensive follow-up to determine all failure mechanisms. One possible contributing factor between the difference in RV144 and HVTN702 was the allotype of the two vaccine populations. Extensive allotype data was not collected in either of these cohorts, and demographic data were not published. However, if they follow previous generalized studies of allotype[118,119] and ethnicity within these countries, RV144 vaccinees likely have high IgG1 allotypes (G1m1,3), and the low IgG1 allotype (G1m-1,3) is more prevalent in the HVTN 702 vaccinees[118].

The ability to simulate heterogeneous populations is helpful due to the difficulties in enrolling and formulating a vaccine in a truly heterogeneous vaccine trial population. In recent COVID-19 vaccine trials, only 11.4% were enrolling in low-middle income countries, and 80% of participants in the Pfizer, Moderna, and AstraZeneca trials were white[163]. Although demographic

data is limited, previous HIV vaccine trials have also been relatively homogenous populations due to the demographics of the regions at high risk chosen for the trial and the logistics of administering a vaccine to multiple regions. For instance, differing circulating HIV subtypes means that the vaccine formulations most likely need to be tailored to each region of interest. Additionally, sociological factors, including historical mistrust of the healthcare system due to previous inequalities, contribute to willingness to participate in vaccine trials and, even after approval, vaccine hesitancy[164]. The ability to simulate underrepresented genetic populations will help expedite the development of optimal vaccines for every population leading to universal and equitable protection against HIV.

5.4 Limitations

The ODE model we developed has formed a framework for analyzing personalized antigen-specific antibody data by predicting FcR complex formation while allowing for exploration of overall system dynamics in combination with targeted simulations of specific genetic and interventional scenarios. The limitations of this approach mainly lie in the availability of data; however model itself served as an identifier of necessary data.

5.4.1 Accuracy of the model

As discussed in Chapter 2, the ODE model was validated for predicting the rank order of FcR complex formation of 30 individuals for two HIV antigens and an influenza antigen.
Of note is the terminology we were careful to use in our results sections: “FcR complex formation” instead of “FcR activation.” This word use is intentional as the measurements we are comparing our model results to are not from cellular assays where the FcRs are being activated and carrying out ADCC. Our experimental output is just the same as our model output, the

number of immune complexes formed in a cell-free environment with antigens, antibodies, and FcR dimers. This complex formation is a highly relevant measure in the systems serology field, where vaccine trial plasma samples are currently being evaluated using this novel high-throughput technology[75–78]. While the dimerized recombinant FcγR and the accompanying assay developed have proven to correlate immune complex formation measurements with cell-based ADCC assay outputs[74], we do not know the mathematical relationship between complex formation and functional cell killing.

There are several critical next steps to translate our model output into predicted ADCC cytotoxicity: (1) obtain actual concentration measurements for personalized antigen-specific IgG subtypes instead of MFIs (2) determine the threshold of complexes formed that would lead to ADCC, and (3) potentially alter the model to include cells where the FcRs reside that eventually carryout ADCC.

Currently, we are calculating personalized IgG concentrations using MFIs and an HIV-specific IgG1 plasma concentration measurement as a reference concentration to calculate a conversion factor[112,147]. Ideally, we would calculate personal HIV-specific IgG subtype concentrations based on a standard curve calculated using reagents of known concentration. The experimental roadblock preventing this currently is the polyclonal nature of the plasma antibodies being measured. A monoclonal antibody could theoretically be used to develop a standard curve in the antibody detection assay. Still, the MFI measurements from a monoclonal antibody that bind one specific site on the antigen may not align well with a set of polyclonal antibodies that can bind several unknown sites of the same antigen. In the future, a standard curve may be developed that

uses polyclonal antibodies purified from plasma, but this may still prove to be time-consuming and unreliable.

Determining a threshold of complexes that must form before downstream signaling leads to ADCC could be accomplished with concurrent cell and cell-free assays where immune complex formation in samples is varied and some samples trigger ADCC while others do not. You could then find the samples with the lowest complex formation that triggered ADCC and the samples with the highest complex formation that did not trigger ADCC and find the threshold or range of complex formation measurements (either relative or actual) where ADCC is being triggered.

Finally, if a simple threshold based on the current model structure is not identifiable, we may need to expand the model structure to include cells. A valuable tool for this endeavor may be a recently developed cellular model of immune complex formation on the surface of cells with multiple FcR types by Robinett et al.[107]. This equilibrium model could be implemented with the same input data we have used in addition to data on the FcR makeup of the NK cells used in the cellular ADCC assay. With this method, the number of activated FcRs on each cell could be counted to determine how many individual cells reach the threshold to trigger ADCC.

Ideally, in the future, we would eventually be able to create a model that would go beyond FcR activation and ADCC and predict protection from infection. Currently, we are limited by the lack of consensus on which mechanisms or collection of mechanisms protect an individual from infection[127,165,166]. A model encompassing all likely protection mechanisms in the plasma would potentially include FcR activation[52,68], alongside anti-protective IgA antibodies[57], the

complement system[167], and neutralizing antibodies[57]. The complexity of this model would require a more significant amount of input data, computational power, and the determination of what quantitatively leads to protection, which could be an infinite number of combinations of the above mechanisms.

5.4.2 Relative personalized concentrations and antibody decay

While the model can identify exact quantitative thresholds and ranges of initial IgG subclass concentrations, it will require exact personalized input measurements to contextualize them. As of now, we are confident in the average affinities input into the model (glycosylation may alter these), but the IgG subclass concentrations, as mentioned above, are calculated indirectly. Due to this calculation method, we can only predict individuals' relative IgG subclass concentration, although we believe them to be in the correct range based on a similar HIV vaccine trial[112]. Additionally, because we know glycosylations affect affinity values, there may be personalized affinity measurements due to differential glycosylation patterns that may affect our personalized predictions.

While we have detailed relative personalized IgG concentrations, these are from one specific timepoint. Antigen-specific antibody titers decay over time [60], and although it would be challenging to collect personalized data over long periods with current technology, we can model antibody decay.

5.4.3 Lack of genetic data and affinity interventions

While we were able to project our data into different genotypes and make predictions on which genetic factors are best or most important, these results should be considered preliminary and

evidence to support the collection of this genetic data in future vaccine trials. FcR polymorphism affinity data is reliable and well-cited88, but it is not easy to make conclusions on how large of an effect it has on protection when we do not know how many immune complexes are necessary. In conjunction, we do not consider vaccinees who may be heterozygous for FcR polymorphism in the current model as we only have one FcR type at a time. Additionally, it is impossible or far less accessible to alter an individual's genetic polymorphism than boost their IgG levels. In this case, glycosylation could be induced using different vaccine adjuvants that influence IgG affinity to FcRs, but the link between adjuvants and specific glycosylation patterns is not well studied[168].

While IgG boosting is more accessible than affinity alterations, the ideal boosting regimen may be determined by allotype, which has less reliable associated data. The way that we determined our allotype projections was based on a very small sample size (n=6) of individuals in a phase I HIV vaccine trial with known allotypes and measured antigen-specific IgG subclasses. Ideally, we would need a larger HIV vaccine trial with a heterogenous allotype population where allotype and IgG subclass data was collected to determine how that exact vaccine regimen would influence antigen-specific IgGs in each allotype. This more reliable data could be used to calculate conversion factors for IgG subclasses between allotypes and simulate individual genetic cases alongside larger mixed allotype populations. The step from allotyping each individual or population specifically to predicting allotype from demographic data needs to be considered carefully regarding its accuracy and usefulness. As mentioned above, data linking allotype to ethnicity may be tempting to utilize, but the data available as of now needs further genetic and regional representation, consistency, and ethical analysis.

5.5 Future directions

5.5.1 Personalized antibodies over time and in competition

We may be able to collect personalized affinity data and accurate IgG subclass concentration data to improve personalized model accuracy in the future. However, we can also explore other potential factors like antibody decay and personalized levels of non-antigen-specific antibodies with data available now.

Measures of antigen-specific antibody decay were measured in the RV306 trial, which included several different boosting regimens that led to further decay profiles [60]. We can use these decay profiles to estimate how the level of antibody decay at a specific time point would affect complex formation and ADCC activation. Individuals and vaccine regimens particularly vulnerable to a rapid decay in antigen-specific IgGs could be identified. This RV306 data does not differentiate between the IgG subclasses, so we need to assume a uniform decay in all subclasses, which may need further revision.

We have also begun to explore how non-antigen-specific antibodies may be interfering with complex formation against HIV antigens. Non-antigen-specific antibodies, in this case, would be any IgG antibody that is not specific to the HIV epitope of interest, meaning all other antibodies in the plasma. These "non-specific" antibodies are much more abundant than HIV-specific antibodies and so may be out competing HIV-specific antibodies for FcRs. When a person is fighting off an unrelated infection like the common cold or has an autoimmune disease, "non-specific" antibody concentrations are likely high[169,170], possibly to the detriment of the HIV-specific antibodies. These antibody concentrations also vary on a personalized basis and may

need to be accounted for when analyzing mechanisms of vaccine efficacy. We can add these to our model using a new species to represent "non-specific" antibodies that can bind to FcRs independently. We can then input personalized measurements of IgG titer alongside personalized antigen-specific antibodies to monitor the predicted competition and potentially identify individuals with beneficial antigen-specific antibody profiles but detrimental non-specific antibodies and vice versa and determine which is more important to address on a personalized basis.

5.5.2 More genetic factors and experimental validation

Without relying on the future collection of allotype and demographic data, the next steps include introducing multiple FcR types and polymorphisms, accounting for allotype effects on affinity values, validation experiments, and other diseases.

The first step to introducing new FcRs to the model would be the addition of a second FcR species into the existing model, which would allow for modeling of vaccinees heterozygous for FcR polymorphism. It could also be used to study competition between FcRIIIa and FcRIIa, which trigger ADCC and ADCP, respectively. Another method to study multiple FcRs would be implementing the multivalent equilibrium model mentioned previously, which can model multiple FcR types and polymorphisms on the same cell surface, mimicking different cell populations[107].

Recent studies indicate that IgG3 allotypes influence binding affinities to FcR[89]. We could use the data presented in the literature to predict the effects of IgG3 allotype alone in just FcγRIIIa-V[158], as well as in combination with different FcR types and polymorphisms. Additionally, we

can assess how IgG1 allotype would contribute to complex formation in concert with IgG3 allotype and FcR polymorphism.

Experimental validation is a critical next step for using genetic data to predict complex formation in a genetic scenario. We have already validated the model in multiple FcR polymorphisms, but only at baseline, and we validated the predicted variable effects of boosting IgG1, but only in FcγRIIIa-V^{158}. One of the most approachable experiments would be to validate our predicted boost in IgG1 in both FcγRIIIa-V^{158} and FcγRIIIa-F^{158} and show the difference between the two using plasma samples and the Luminex based recombinant FcγR based assay used in all previous validations. We have not validated our model against results from the cell-based ADCC assays using the same plasma samples [73–76,78]. Relating our model to cellular assay output may be achieved in two different ways: (1) we develop a formula relating complex formation to cytotoxicity seen in the cell-based assays, which would need to include some form of complex thresholding for ADCC to be triggered as mentioned above, or (2) we implement the equilibrium model with multiple FcRs on cell surfaces with simple thresholding based on the number of activated FcRs on each cell.

5.6 Overall conclusions

Our ODE model was developed in a generalizable format that allows for alterations in concentration and affinity input parameters to represent changes in antigen, antigen epitope, antibody type, FcR type, personal health status, and disease state. Since we do not account for spatial aspects or sizes of molecules in an ODE model, switching between diseases and individual scenarios requires only a change in concentration or affinity. We have begun the development of this model for use in influenza vaccination, HIV-positive progressors and elite

controllers, Sjogren's syndrome, and SARS-CoV-2, and when data is available, there are many other applications for which we can develop personalized immune complex formation models to further universal vaccine protection and disease control.

Appendix

Appendix A Supplemental Materials: A systems approach to elucidate personalized mechanistic complexities of antibody-Fc receptor activation post-vaccination

Table A -1 Affinities of IgG subtypes to FcRIIa and FcRIIIa polymorphisms

related to Figures 2.1, A.S3-5, A.S7, A.S9, and A.S11

K_{eq} (mM^{-1})	**FcγRIIa-H^{131}**	**FcγRIIa-R^{131}**	**FcγRIIIa-F^{158}**	**FcγRIIIa-V^{158}**
K_{eq}-IgG1-FcR	5,200	3,500	1,170	2,000
K_{eq}-IgG2-FcR	450	100	30	70
K_{eq}-IgG3-FcR	890	910	7,700	9,800
K_{eq}-IgG4-FcR	170	210	200	250

K_{eq} values measured in Bruhns et al., 2009[88]. FcγRIIIa V^{158} values are used for all baseline analyses.

Table A-2 Fold change in IgG affinity to FcR with changes in Fc glycosylation, related to Figure 2.7.

	FcγRIIa-H^{131}	**FcγRIIa-R^{131}**	**FcγRIIIa-F^{158}**	**FcγRIIIa-V^{158}**
	0.4X[123]		19.7X[123]	
	1.5X[122]	1.73X[122]	130X[122]	60X[122]
	1.1X[121]	0.92X[121]	13.7X[121]	5.2X[121]
	1.5X[148]	2X[148]	42X[148]	31X[148]
Max	1.5X	2X	130X	60X
Avg	1.1X	1.3X	51X	29X
Min	0.4X	0.4X	13.7X	5.2X

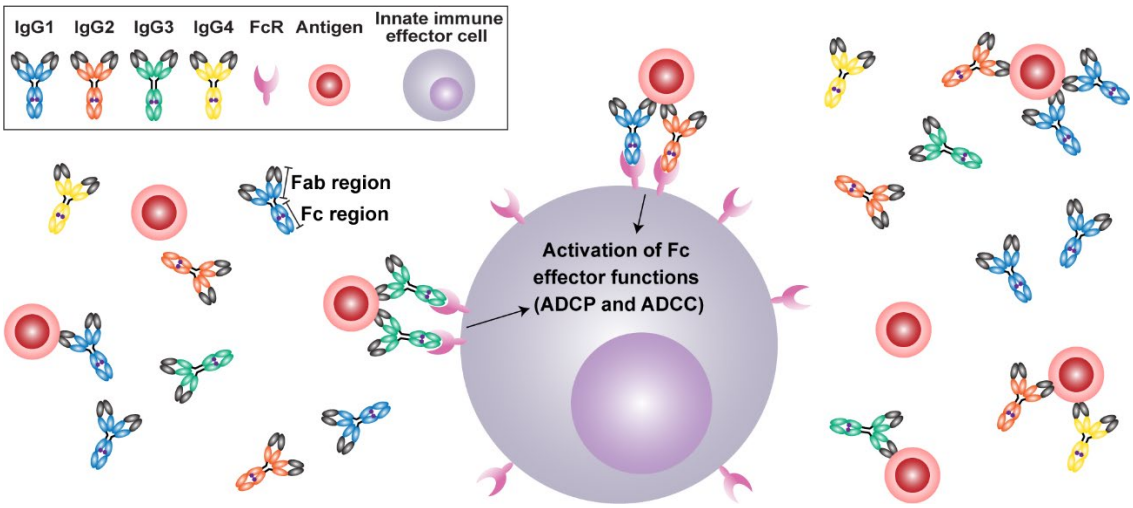

Figure A-1 Extracellular IgGs activate Fc effector functions via FcRs

Related to Figure 2.1. IgGs form activating complexes with antigen (via the Fab region) and FcRs on innate immune cells (via the Fc region) to trigger Fc effector functions including ADCC and ADCP. IgG subclasses (1-4) engage Fc receptors with varying affinities, and IgG subclass concentration distribution varies across individuals. Glycosylation to the IgG Fab and Fc regions may alter binding of IgGs to both antigen and FcRs, respectively. FcR polymorphisms alter binding of IgGs to FcRs.

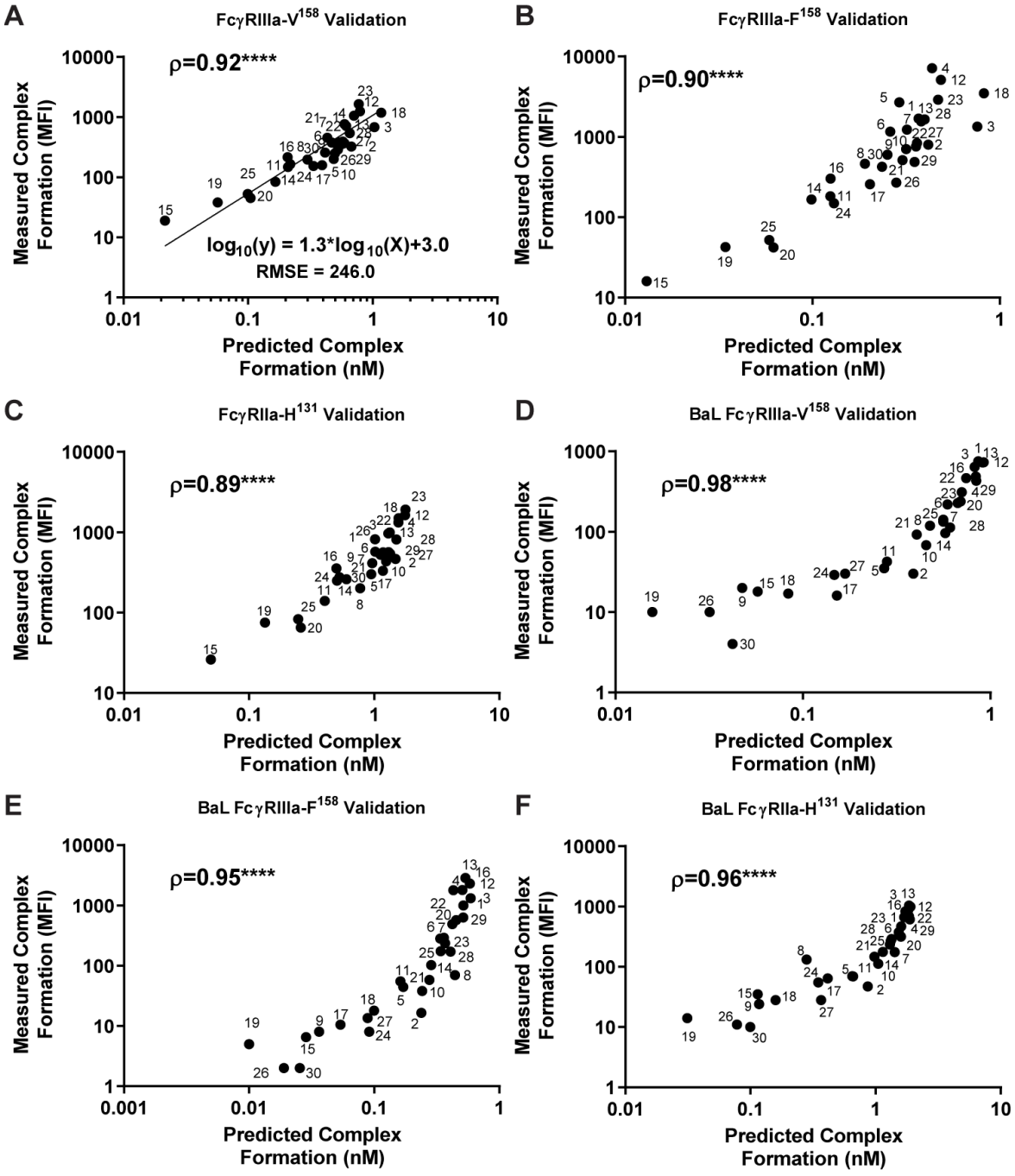

Figure A-2 Model validation with log-log least-squares fit (A). Model validation for A244 in FcγRIIIa-F158 and FcγRIIa-H131 (B-C), and BaL in FcγRIIIa-V158, FcγRIIIa-F158 and FcγRIIa-H131 (D-F).

Related to Figure 2. (A) Model predictions for dimeric FcγRIIIa-V^{158} complex formation were compared to rsFcγRIIIa-V^{158} multiplex experimental measurements converted from MFIs to nM (see methods) for 30 RV144 vaccinee samples (labeled 1-30) with an added least-squares fit line (Spearman correlation coefficient of 0.92, $p<0.0001$; log-log least-squares fit, RMSE = 246.0). Model predictions for A244 (B) FcγRIIIa-F^{158} and (C) FcγRIIa-H^{131} complex formation; and BaL (D) FcγRIIIa-V^{158}, (E) FcγRIIIa-F^{158} and (F) FcγRIIa-H^{131} complex formation

were compared to FcR multiplex experimental measurements in 30 RV144 vaccinee samples (labelled 1-30) (Spearman correlation coefficient of 0.90, 0.89, 0.98, 0.95, and 0.96 respectively, $p<0.0001$ for all).

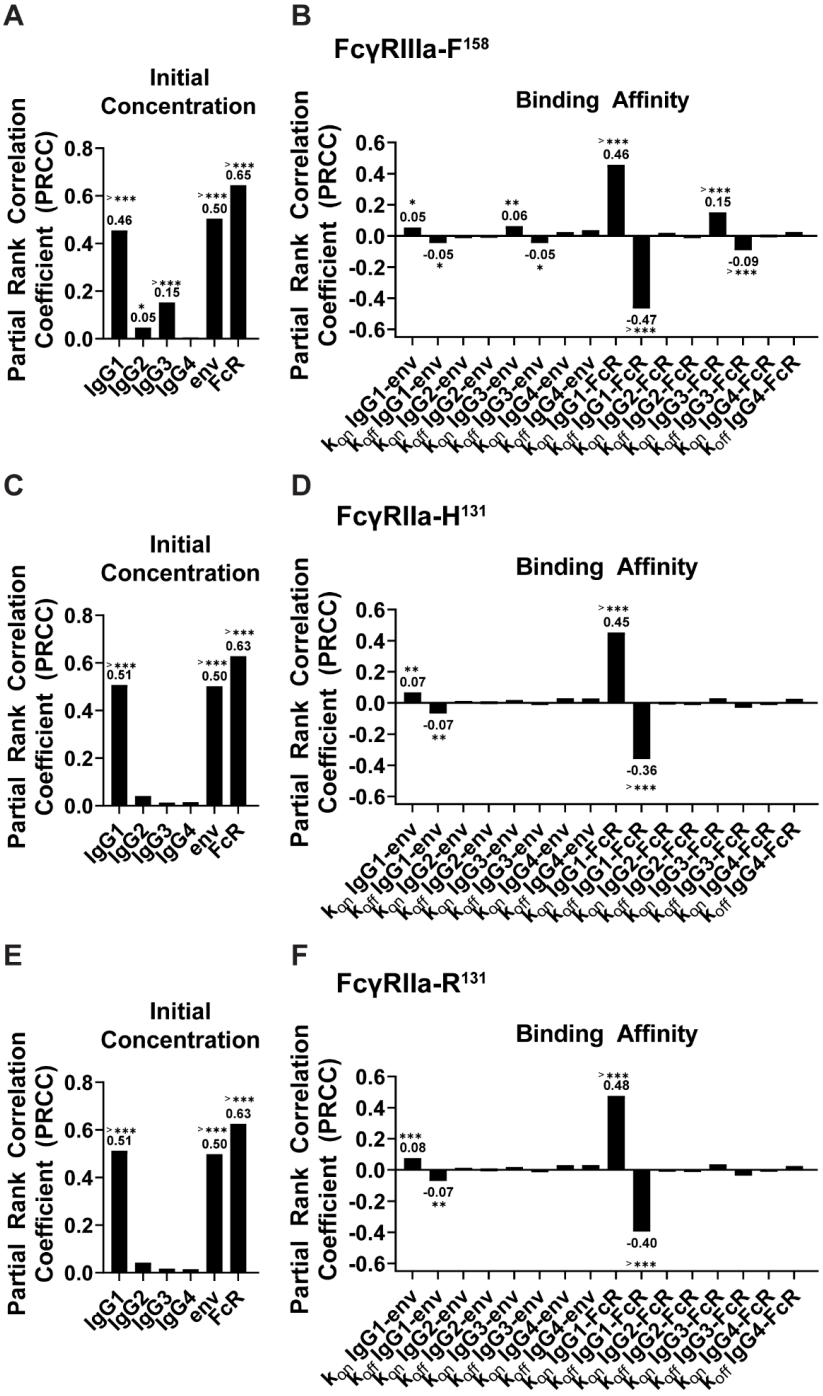

Figure A-3 Global sensitivity analysis for FcγRIIIa-F158 (A-B), FcγRIIa-H131 (C-D), and FcγRIIa-R131 (E-F)

Related to Figure 2. Global uncertainty and sensitivity analysis[133] of initial concentration for FcγRIIIa-F^{158} (A), FcγRIIa-H^{131} (C), and FcγRIIa-R^{131} (E) and binding parameters for FcγRIIIa-F^{158} (B), FcγRIIa-H^{131} (D), and FcγRIIa-R^{131} (F), where partial rank correlation coefficient (PRCC) indicates output sensitivity to parameters. 2000 unique parameter sets were created by sampling

from uniform pdfs for each parameter ranging from 0.004X to 20X baseline. PRCC and significance were calculated using the output from these 2000 simulations. The significance of each PRCC value is tested by comparing its T value, which accounts for the number of other parameters and number of samples, to a critical t-value giving a p-value used to determine if the PRCC is significantly different from zero. k_{on} indicates forward reaction rates and k_{off} indicates reverse reaction rates (>*** indicates $p < 0.0001$, *** indicates $p < 0.001$, ** indicates $p < 0.01$, *indicates $p < 0.05$).

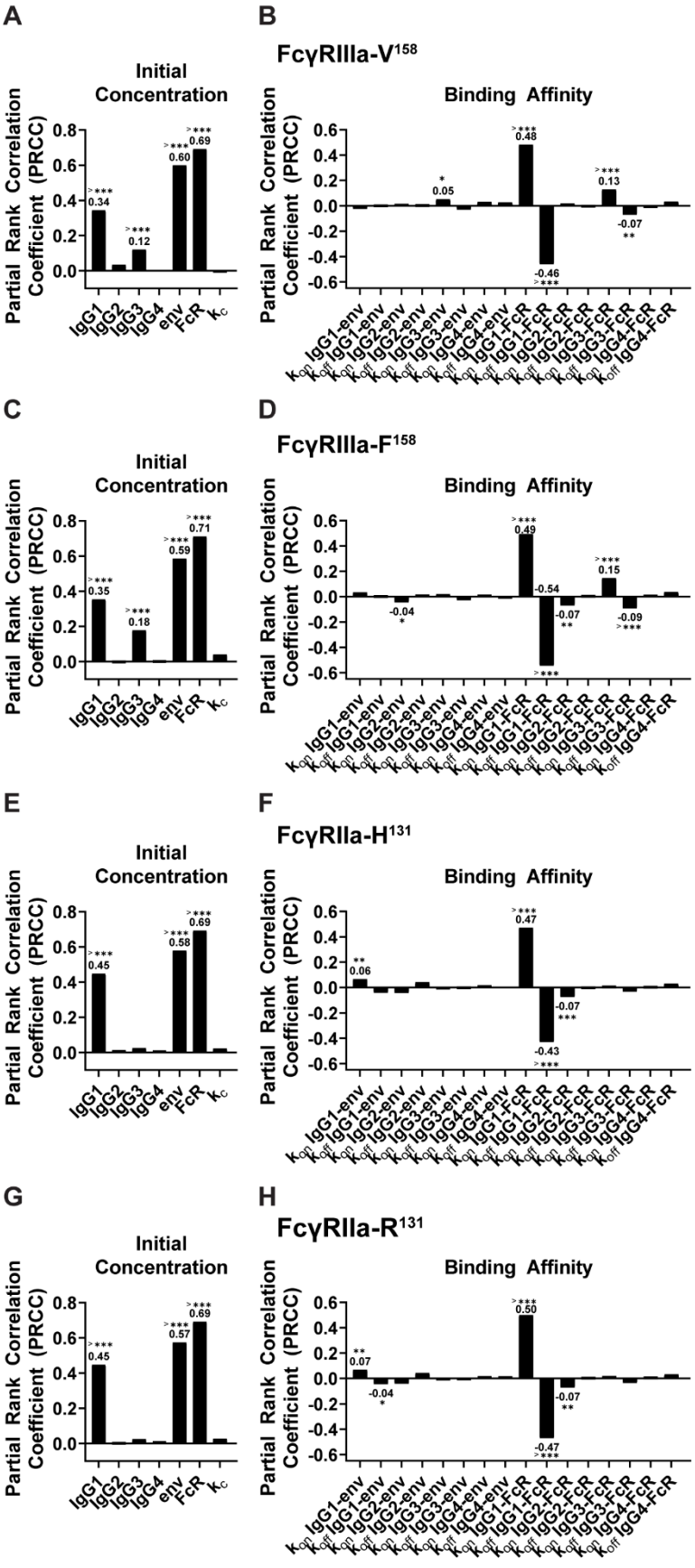
A
Initial Concentration
Partial Rank Correlation Coefficient (PRCC)
IgG1
IgG2
IgG3
IgG4
env
FcR
Kc
B
FcγRIIIa-V158
Binding Affinity
C
Initial Concentration
D
FcγRIIIa-F158
Binding Affinity
E
Initial Concentration
F
FcγRIIa-H131
Binding Affinity
G
Initial Concentration
H
FcγRIIa-R131
Binding Affinity

Figure A-4 Global sensitivity analysis with a cooperativity constant for FcγRIIIa-V158 (A-B), FcγRIIIa-F158 (C-D), FcγRIIa-H131 (E-F), and FcγRIIa-R131 (G-H).

Related to Figures 1 and 2. Global uncertainty and sensitivity analysis with the addition of a cooperativity constant (k_c)[133] of initial concentration for FcγRIIIa-V^{158} (A), FcγRIIIa-F^{158} (C), FcγRIIa-H^{131} (E), and FcγRIIa-R^{131} (G) and binding parameters for FcγRIIIa-V^{158} (B), FcγRIIIa-F^{158} (D), FcγRIIa-H^{131} (F), and FcγRIIa-R^{131} (H), where partial rank correlation coefficient (PRCC) indicates output sensitivity to parameters. 2000 unique parameter sets were created by sampling from uniform pdfs for each parameter ranging from 0.01-100 for k_c and 0.004X to 20X baseline for all other parameters. The cooperativity constant was applied to each reaction where a second IgG was binding to env. PRCC and significance were calculated using the output from these 2000 simulations. The significance of each PRCC value is tested by comparing its T value, which accounts for the number of other parameters and number of samples, to a critical t-value giving a p-value used to determine if the PRCC is significantly different from zero. k_{on} indicates forward reaction rates and k_{off} indicates reverse reaction rates (~*** indicates $p < 0.0001$, *** indicates $p < 0.001$, ** indicates $p < 0.01$, *indicates $p < 0.05$).

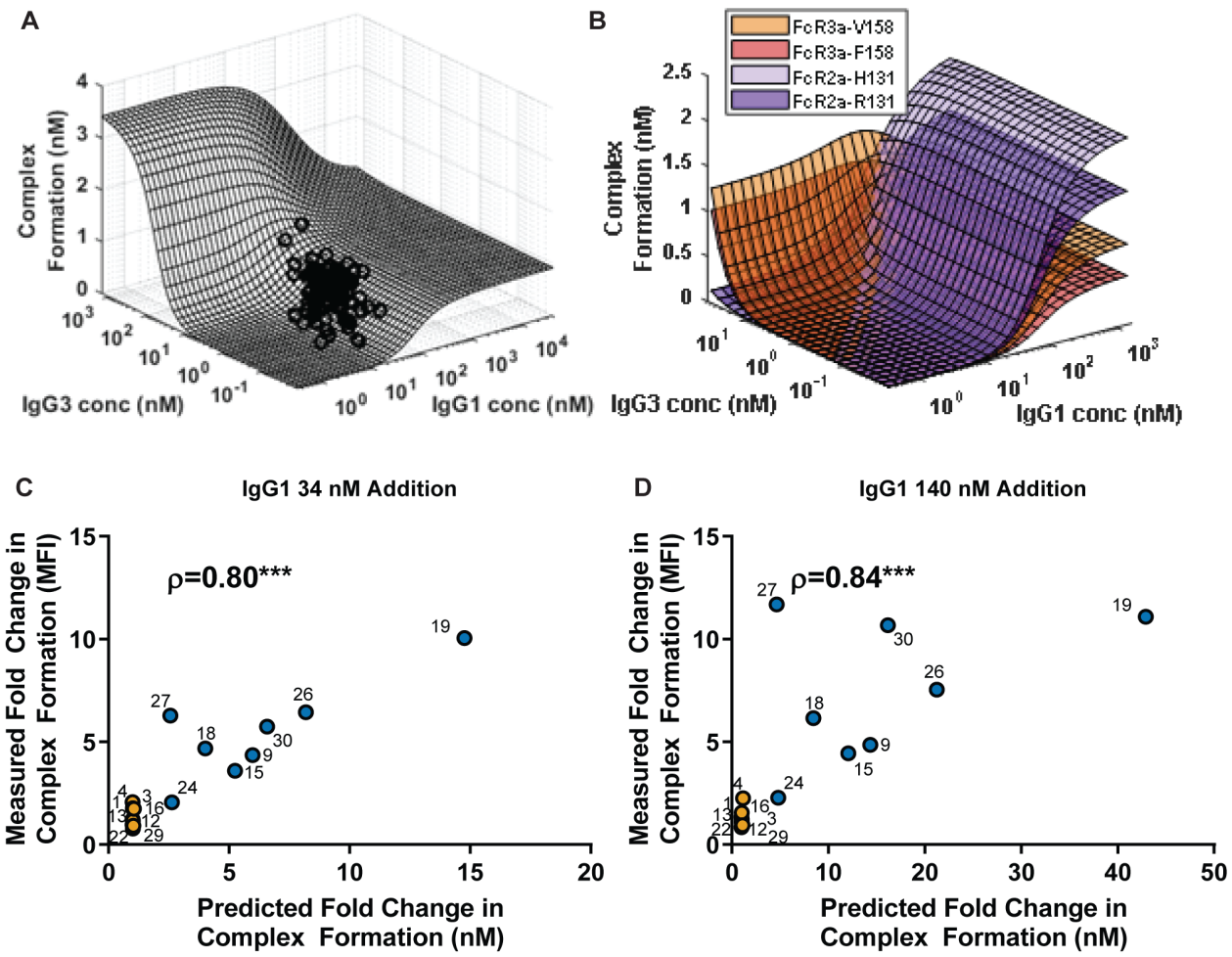

Figure A-5 Alternative IgG1 vs IgG3 landscapes (A-B), and direct comparison of the predicted and measured fold change in complex formation after addition of IgG1 (C-D).

Related to Figure 3 and 4. (A) Model predictions for env:IgG:IgG:FcγRIIIa:FcγRIIIa complex formation at steady state (z-axis) for 2500 simulations over an extended range (0.004X-500X) of IgG1 and IgG3 baseline initial concentration combinations (x and y-axis). RV144 vaccinee samples (n=105) were plotted (black circles) at their corresponding individual env-specific IgG1 & IgG3, and complex formation concentrations. (B) Model predictions for env:IgG:IgG:FcγRIIIa:FcγRIIIa complex formation at steady state (z-axis) for 2500 simulations over a range (0.004X-20X) of IgG1 and IgG3 baseline initial concentration combinations (x and y-axis) for FcγRIIIa-V^{158} (light orange), FcγRIIIa-F^{158} (dark orange), FcγRIIa-H^{131} (light purple) and FcγRIIa-R^{131} (dark purple). Model predictions for a change in complex formation after a (C) 34 nM addition and (D) 140 nM addition of IgG1 were compared to change in FcR multiplex experimental measurements in 8 RV144 responders (blue) and 8 non-responders (orange) after the respective addition of IgG (labelled with their respective vaccinee ID) (Spearman correlation coefficient of 0.80 and 0.84 respectively, p = 0.0003 and p = 0.0001 respectively).

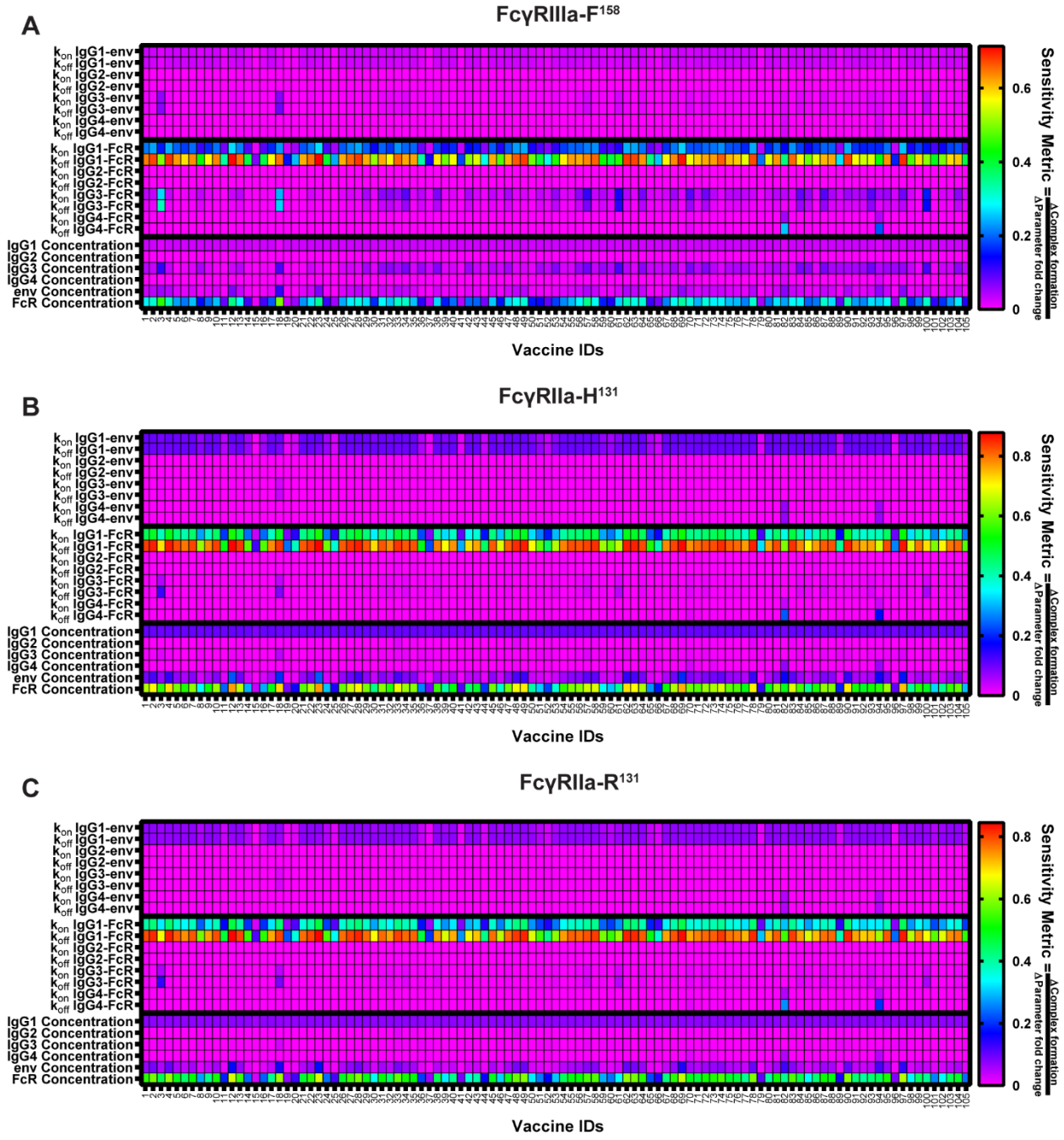

Figure A-6 Personalized single-parameter sensitivity analyses for FcγRIIIa-F158 (A), FcγRIIa-H131 (B), and FcγRIIa-R131 (C).

Related to Figure 6. For each vaccinee (x-axis, labeled 1-105), we predicted sensitivity to each parameter (y-axis) one at a time from 0.004X-20X baseline for FcγRIIIa-F^{158} (A), FcγRIIa-H^{131} (B), FcγRIIa-R^{131} (C). The sensitivity metric was calculated by dividing the change in complex formation by the change in the parameter multiplier. A high sensitivity metric (red) indicates a large change in complex formation with changes in the given parameter. A low sensitivity metric (purple) indicates very little change in complex formation with changes in the given parameter.

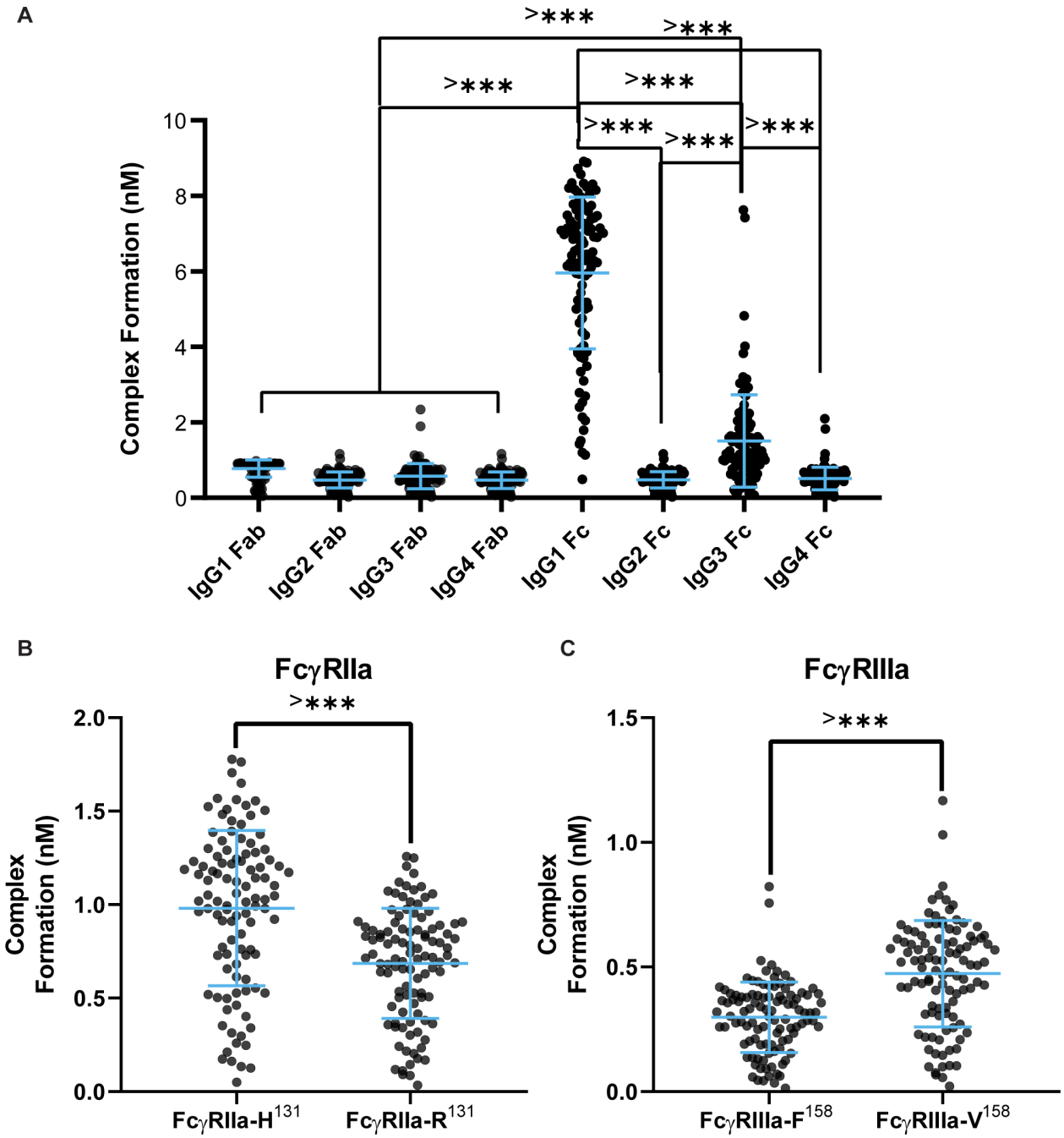

Figure A-7 Comparison of IgG subtypes and glycosylation regions and complex formation at baseline in different FcγR classes and polymorphism.

Related to Figure 6. (A) The model predicted change in complex formation with glycosylation of each IgG subtype and each region (Fc region alters IgG-FcR affinity; Fab region alters IgG-env affinity). Each respective affinity value is multiplied by the maximum fold change seen in Dekkers et al. for FcγRIIIa-V^{158} (31X) individually[148]. (B) Complex formation in 105 RV144 vaccinee samples projected into each FcγRIIa polymorphism (FcγRIIa-H^{131} and FcγRIIa-R^{131}). A two-tailed Wilcoxon matched-

pairs signed-rank test indicated FcγRIIa-H^{131} complex formation was significantly greater than FcγRIIa-R^{131} complex formation; $p < 0.0001$. (C) Complex formation in 105 RV144 vaccinee samples projected into each FcγRIIIa polymorphism (FcγRIIIa-F^{158} and FcγRIIIa-V^{158}). A two-tailed Wilcoxon matched-pairs signed-rank test indicated FcγRIIIa-V^{158} complex formation was significantly greater than FcγRIIIa-F^{158} complex formation; $p < 0.0001$.

Bibliography

1. WHO. Vaccination Data. *WHO Coronavirus (COVID-19) Dashboard* https://covid19.who.int/table (2021).
2. Sullivan, S. Challenges in reducing influenza-associated mortality. *The Lancet* **391**, 1242–1244 (2018).
3. WHO. HIV/AIDS Key Facts. https://www.who.int/news-room/fact-sheets/detail/hiv-aids (2021).
4. Roth, G. A. *et al.* Global, regional, and national age-sex-specific mortality for 282 causes of death in 195 countries and territories, 1980–2017: a systematic analysis for the Global Burden of Disease Study 2017. *The Lancet* **392**, 1736–1788 (2018).
5. UNAIDS. Global HIV & AIDS statistics — Fact sheet. https://www.unaids.org/en/resources/fact-sheet (2021).
6. S. Lucas & AM. Nelson. HIV and the spectrum of human disease. *The Journal of pathology* **235**, 229–241 (2015).
7. MS. Cohen *et al.* Prevention of HIV-1 infection with early antiretroviral therapy. *The New England journal of medicine* **365**, 493–505 (2011).
8. MS. Cohen *et al.* Antiretroviral Therapy for the Prevention of HIV-1 Transmission. *The New England journal of medicine* **375**, 830–839 (2016).

9. MS. Saag *et al.* Antiretroviral Drugs for Treatment and Prevention of HIV Infection in Adults: 2018 Recommendations of the International Antiviral Society-USA Panel. *JAMA* **320**, 379–396 (2018).

10. Prabhu, S., Harwell, J. I. & Kumarasamy, N. Advanced HIV: diagnosis, treatment, and prevention. *The Lancet HIV* vol. 6 (2019).

11. Ghosn, J., Taiwo, B., Seedat, S., Autran, B. & Katlama, C. HIV. *The Lancet* **392**, 685–697 (2018).

12. L. Gazzola, C. Tincati, GM. Bellistrì, Ad. Monforte & G. Marchetti. The absence of CD4+ T cell count recovery despite receipt of virologically suppressive highly active antiretroviral therapy: clinical risk, immunological gaps, and therapeutic options. *HIV/AIDS* **48**, 328–337 (2009).

13. M. Massanella, E. Negredo, B. Clotet & J. Blanco. Immunodiscordant responses to HAART--mechanisms and consequences. *Expert review of clinical immunology* **9**, 1135–1149 (2013).

14. D. Nakanjako *et al.* Frequency and impact of suboptimal immune recovery on first-line antiretroviral therapy within the International Epidemiologic Databases to Evaluate AIDS in East Africa. *AIDS* **30**, 1913–1922 (2016).

15. P, C. & J, R. Immune reconstitution under antiretroviral therapy: the new challenge in HIV-1 infection. *Blood* **117**, 5582–5590 (2011).

16. M. Battegay, R. Nüesch, B. Hirschel & GR. Kaufmann. Immunological recovery and antiretroviral therapy in HIV-1 infection. *The Lancet. Infectious diseases* **6**, 280–287 (2006).

17. Yang, X. *et al.* Incomplete immune reconstitution in HIV/AIDS patients on antiretroviral therapy: Challenges of immunological non-responders. *Journal of Leukocyte Biology* **107**, 597–612 (2020).

18. Chesney, M. Adherence to HAART Regimens. *AIDS PATIENT CARE and STDs* **17**, 169–177 (2003).

19. Iacob, S. A., Iacob, D. G. & Jugulete, G. Improving the Adherence to Antiretroviral Therapy, a Difficult but Essential Task for a Successful HIV Treatment—Clinical Points of View and Practical Considerations. *Frontiers in Pharmacology* **0**, 831 (2017).

20. Mantsios, A. *et al.* "I feel empowered": women's perspectives on and experiences with long-acting injectable antiretroviral therapy in the USA and Spain. *Culture, Health & Sexuality* **23**, 1066–1078 (2020).

21. Anderson, P. L. *et al.* Emtricitabine-tenofovir concentrations and pre-exposure prophylaxis efficacy in men who have sex with men. *Science Translational Medicine* **4**, (2012).

22. Grant, R. M. *et al.* Preexposure Chemoprophylaxis for HIV Prevention in Men Who Have Sex with Men. *The New England Journal of Medicine* **363**, 2587–2599 (2010).

23. MC. Thigpen *et al.* Antiretroviral preexposure prophylaxis for heterosexual HIV transmission in Botswana. *The New England journal of medicine* **367**, 423–434 (2012).

24. Baeten, J. M. *et al.* Antiretroviral Prophylaxis for HIV Prevention in Heterosexual Men and Women. *The New England Journal of Medicine* **367**, 399–410 (2012).

25. K. Choopanya *et al.* Antiretroviral prophylaxis for HIV infection in injecting drug users in Bangkok, Thailand (the Bangkok Tenofovir Study): a randomised, double-blind, placebo-controlled phase 3 trial. *Lancet* **381**, 2083–2090 (2013).

26. McFarland, W. *et al.* Low PrEP Awareness and Use Among People Who Inject Drugs, San Francisco, 2018. *AIDS and Behavior 2019 24:5* **24**, 1290–1293 (2019).

27. Celum, C. & Baeten, J. PrEP for HIV Prevention: Evidence, Global Scale-up, and Emerging Options. *Cell Host & Microbe* **27**, 502–506 (2020).

28. Fonner, V. A. *et al.* Effectiveness and safety of oral HIV preexposure prophylaxis for all populations. *AIDS* **30**, (2016).

29. Patterson, K. B. *et al.* HIV. Penetration of tenofovir and emtricitabine in mucosal tissues: Implications for prevention of HIV-1 transmission. *Science Translational Medicine* **3**, (2011).

30. Hendrix, C. W. *et al.* Dose Frequency Ranging Pharmacokinetic Study of Tenofovir-Emtricitabine after Directly Observed Dosing in Healthy Volunteers to Establish Adherence Benchmarks (HPTN 066). *AIDS Research and Human Retroviruses* **32**, (2016).

31. Cottrell, M. L. *et al.* A Translational Pharmacology Approach to Predicting Outcomes of Preexposure Prophylaxis Against HIV in Men and Women Using Tenofovir Disoproxil Fumarate With or Without Emtricitabine. *The Journal of Infectious Diseases* **214**, 55–64 (2016).

32. Cheu, R. K. *et al.* Impact of vaginal microbiome communities on HIV antiretroviral-based pre-exposure prophylaxis (PrEP) drug metabolism. *PLOS Pathogens* **16**, e1009024 (2020).

33. Lee, C. Y. *et al.* Quantitative modeling predicts mechanistic links between pre-treatment microbiome composition and metronidazole efficacy in bacterial vaginosis. *Nature communications* **11**, 6147 (2020).

34. Klatt, N. R. *et al.* Vaginal bacteria modify HIV tenofovir microbicide efficacy in African women. *Science* **356**, 938–945 (2017).

35. Obón-Azuara B, Gasch-Gallén A, Gutiérrez-Cía I & -Aznar C, T. Commentary Obón Azuara et al Women who have sex with women (WSW) and women who have sex with women and men (WSWM) in the HIV/AIDS prevention campaigns. *Journal of Allergy and Infectious Diseases* **2**, 39–41 (2021).

36. Cloete, A., Sanger, N. & Simbayi, L. C. Are HIV positive women who have sex with women (WSW) an unrecognized and neglected HIV risk group in South Africa? *Journal of AIDS and HIV Research* **3**, 1–5 (2011).

37. Abubakari, G. M. *et al.* Intersectional stigma and its impact on HIV prevention and care among MSM and WSW in sub-Saharan African countries: a protocol for a scoping review. *BMJ Open* **11**, e047280 (2021).

38. UNAIDS. Ending AIDS: Progress towards the 90-90-90 targets. *GLOBAL AIDS UPDATE* (2017).

39. Petersen, M. *et al.* Association of Implementation of a Universal Testing and Treatment Intervention With HIV Diagnosis, Receipt of Antiretroviral Therapy, and Viral Suppression in East Africa. *JAMA* **317**, 2196–2206 (2017).

40. UNAIDS. Snapshot #HLM2016AIDS – HIV investments. . (2016).

41. Medlock, J. *et al.* Effectiveness of UNAIDS targets and HIV vaccination across 127 countries. *Proceedings of the National Academy of Sciences* **114**, 4017–4022 (2017).

42. Berkley, S. F. & Koff, W. C. Scientific and policy challenges to development of an AIDS vaccine. *Lancet* vol. 370 (2007).

43. Fauci, A. S. An HIV Vaccine Is Essential for Ending the HIV/AIDS Pandemic. *JAMA* **318**, 1535–1536 (2017).

44. Ahmed, Y., Tian, M. & Gao, Y. Development of an anti-HIV vaccine eliciting broadly neutralizing antibodies. *AIDS Research and Therapy* **14**, 50 (2017).

45. Wang, H.-B., Mo, Q.-H. & Yang, Z. HIV Vaccine Research: The Challenge and the Way Forward. *Journal of Immunology Research* **2015**, (2015).

46. Rerks-Ngarm, S. *et al.* Vaccination with ALVAC and AIDSVAX to Prevent HIV-1 Infection in Thailand. *New England Journal of Medicine* **361**, 2209–2220 (2009).

47. Robb, M. L. *et al.* Risk behaviour and time as covariates for efficacy of the HIV vaccine regimen ALVAC-HIV (vCP1521) and AIDSVAX B/E: A post-hoc analysis of the Thai phase 3 efficacy trial RV 144. *The Lancet Infectious Diseases* **12**, 531–537 (2012).

48. Hutchinson, E. C. Influenza Virus. *Trends in Microbiology* **26**, 809–810 (2018).

49. Sah, P. *et al.* Future epidemiological and economic impacts of universal influenza vaccines. *Proceedings of the National Academy of Sciences* **116**, 20786–20792 (2019).

50. Boutwell, C. L., Rolland, M. M., Herbeck, J. T., Mullins, J. I. & Allen, T. M. Viral Evolution and Escape during Acute HIV-1 Infection. *The Journal of infectious diseases* **202**, S309 (2010).

51. Hargrave, A., Mustafa, A. S., Hanif, A., Tunio, J. H. & Hanif, S. N. M. Current Status of HIV-1 Vaccines. *Vaccines 2021, Vol. 9, Page 1026* **9**, 1026 (2021).

52. Chung, A. W. *et al.* Polyfunctional Fc-effector profiles mediated by IgG subclass selection distinguish RV144 and VAX003 vaccines. *Science Translational Medicine* **6**, (2014).

53. Forthal, D. N. *et al.* IgG2 inhibits HIV-1 internalization by monocytes, and IgG subclass binding is affected by gp120 glycosylation. *AIDS* **25**, (2011).

54. Smith, D. J., Forrest, S., Ackley, D. H. & Perelson, A. S. Variable efficacy of repeated annual influenza vaccination. *Proceedings of the National Academy of Sciences of the United States of America* **96**, (1999).

55. Skowronski, D. M. *et al.* Serial vaccination and the antigenic distance hypothesis: Effects on influenza vaccine effectiveness during A(H3N2) epidemics in Canada, 2010-2011 to 2014-2015. *Journal of Infectious Diseases* **215**, 1059–1069 (2017).

56. Balasubramanian, P. *et al.* Functional Antibody Response Against V1V2 and V3 of HIV gp120 in the VAX003 and VAX004 Vaccine Trials. *Scientific Reports* **8**, 1–14 (2018).

57. Haynes, B. F. *et al.* Immune-Correlates Analysis of an HIV-1 Vaccine Efficacy Trial. *New England Journal of Medicine* **366**, 1275–1286 (2012).

58. Rerks-Ngarm, S. *et al.* Randomized, Double-Blind Evaluation of Late Boost Strategies for HIV-Uninfected Vaccine Recipients in the RV144 HIV Vaccine Efficacy Trial. *The Journal of Infectious Diseases* **215**, 1255 (2017).

59. Easterhoff, D. *et al.* Boosting with AIDSVAX B/E Enhances Env Constant Region 1 and 2 Antibody-Dependent Cellular Cytotoxicity Breadth and Potency. *Journal of Virology* **94**, (2020).

60. Pitisuttithum, P. *et al.* Late boosting of the RV144 regimen with AIDSVAX B/E and ALVAC-HIV in HIV-uninfected Thai volunteers: a double-blind, randomised controlled trial. *The Lancet HIV* **7**, e238–e248 (2020).

61. Bekker, L. G. *et al.* Subtype C ALVAC-HIV and bivalent subtype C gp120/MF59 HIV-1 vaccine in low-risk, HIV-uninfected, South African adults: a phase 1/2 trial. *The Lancet HIV* **5**, e366–e378 (2018).

62. Cohen, J. Combo of two HIV vaccines fails its big test. *Science* vol. 367 (2020).

63. National Institutes of Health. Experimental HIV Vaccine Regimen Ineffective in Preventing HIV. *Www.Nih.Gov* (2020).

64. Plotkin, S. A. Correlates of protection induced by vaccination. *Clinical and Vaccine Immunology* **17**, 1055–1065 (2010).

65. Pulendran, B. & Ahmed, R. Immunological mechanisms of vaccination. *Nature Immunology* **12**, 509–517 (2011).

66. Jegaskanda, S., Vanderven, H. A., Wheatley, A. K. & Kent, S. J. Fc or not Fc; that is the question: Antibody Fc-receptor interactions are key to universal influenza vaccine design. *Human Vaccines & Immunotherapeutics* **13**, 1288–1296 (2017).

67. van Schooten, J. & van Gils, M. J. HIV-1 immunogens and strategies to drive antibody responses towards neutralization breadth. *Retrovirology* **15**, 1–11 (2018).

68. Arnold, K. B. & Chung, A. W. Prospects from systems serology research. *Immunology* **153**, 279–289 (2018).

69. Lu, L. L. *et al.* A Functional Role for Antibodies in Tuberculosis. *Cell* **167**, 433-443.e14 (2016).

70. Gunn, B. M. *et al.* A Role for Fc Function in Therapeutic Monoclonal Antibody-Mediated Protection against Ebola Virus. *Cell Host & Microbe* **24**, 221-233.e5 (2018).

71. Dilillo, D. J., Tan, G. S., Palese, P. & Ravetch, J. v. Broadly neutralizing hemagglutinin stalk-specific antibodies require FcR interactions for protection against influenza virus in vivo. *Nature Medicine* **20**, 143–151 (2014).

72. Chung, A. W. *et al.* Activation of NK Cells by ADCC Responses During Early HIV Infection. *VIRAL IMMUNOLOGY* **24**, 171–175 (2011).

73. Wines, B. D. *et al.* Dimeric FcγR Ectodomains as Probes of the Fc Receptor Function of Anti-Influenza Virus IgG. *The Journal of Immunology* **197**, 1507–1516 (2016).

74. McLean, M. R. *et al.* Dimeric Fcγ Receptor Enzyme-Linked Immunosorbent Assay To Study HIV-Specific Antibodies: A New Look into Breadth of Fcγ Receptor Antibodies Induced by the RV144 Vaccine Trial. *The Journal of Immunology* **199**, 816–826 (2017).

75. Parsons, M. S. *et al.* Partial efficacy of a broadly neutralizing antibody against cell-associated SHIV infection. *Science Translational Medicine* **9**, (2017).

76. Anand, S. P. *et al.* Two Families of Env Antibodies Efficiently Engage Fc-Gamma Receptors and Eliminate HIV-1-Infected Cells. *Journal of Virology* **93**, (2019).

77. Kurtovic, L. *et al.* Multifunctional Antibodies Are Induced by the RTS,S Malaria Vaccine and Associated With Protection in a Phase 1/2a Trial. *The Journal of Infectious Diseases* (2020) doi:10.1093/infdis/jiaa144.

78. Vanderven, H. A. *et al.* Antibody-Dependent Cellular Cytotoxicity Responses to Seasonal Influenza Vaccination in Older Adults. *The Journal of Infectious Diseases* **217**, 12–23 (2018).

79. Yates, N. L. *et al.* Vaccine-induced Env V1-V2 IgG3 correlates with lower HIV-1 infection risk and declines soon after vaccination. *Science Translational Medicine* **6**, (2014).

80. Benedict, K. F. & Lauffenburger, D. A. Insights into Proteomic Immune Cell Signaling and Communication via Data-Driven Modeling. *Life Science Journal* **6**, 23–27 (2012).

81. Vaccari, M. *et al.* Adjuvant-dependent innate and adaptive immune signatures of risk of SIVmac251 acquisition. *Nature Medicine* **22**, 762–770 (2016).

82. Choi, I. *et al.* Machine learning methods enable predictive modeling of antibody feature:function relationships in RV144 vaccinees. *PLoS Computational Biology* **11**, (2015).

83. Chung, A. W. *et al.* Dissecting Polyclonal Vaccine-Induced Humoral Immunity against HIV Using Systems Serology. *Cell* **163**, 988–998 (2015).

84. Parsons, M. S., Chung, A. W. & Kent, S. J. Importance of Fc-mediated functions of anti-HIV-1 broadly neutralizing antibodies. *Retrovirology* vol. 15 (2018).

85. Asokan, M. *et al.* Fc-mediated effector function contributes to the in vivo antiviral effect of an HIV neutralizing antibody. *Proceedings of the National Academy of Sciences* **117**, 18754–18763 (2020).

86. Vidarsson, G., Dekkers, G. & Rispens, T. IgG Subclasses and Allotypes: From Structure to Effector Functions. *Frontiers in Immunology* 520 (2014) doi:10.3389/FIMMU.2014.00520.

87. Schur, P. H. IgG subclasses. A historical perspective. *Monographs in Allergy* **23**, 1–11 (1988).

88. Bruhns, P. *et al.* Specificity and affinity of human Fcγ receptors and their polymorphic variants for human IgG subclasses. *Blood* **113**, 3716–3725 (2009).

89. de Taeye, S. W. *et al.* FcγR Binding and ADCC Activity of Human IgG Allotypes. *Frontiers in Immunology* **11**, 740 (2020).

90. Kratochvil, S. *et al.* Immunoglobulin G1 Allotype Influences Antibody Subclass Distribution in Response to HIV gp140 Vaccination. *Frontiers in Immunology* **8**, 1883 (2017).

91. Castiglione, F., Pappalardo, F., Bernaschi, M. & Motta, S. Optimization of HAART with genetic algorithms and agent-based models of HIV infection. *Bioinformatics* **23**, 3350–3355 (2007).

92. Bauer, A. L., Beauchemin, C. A. A. & Perelson, A. S. Agent-based modeling of host–pathogen systems: The successes and challenges. *Information Sciences* **179**, 1379–1389 (2009).

93. Marinho, E. B. S., Bacelar, F. S. & Andrade, R. F. S. A model of partial differential equations for HIV propagation in lymph nodes. *Physica A: Statistical Mechanics and its Applications* **391**, 132–141 (2012).

94. Graw, F. & Perelson, A. S. Spatial Aspects of HIV Infection. *Mathematical Methods and Models in Biomedicine* 3–31 (2013) doi:10.1007/978-1-4614-4178-6_1.

95. Joshi, H. R. Optimal control of an HIV immunology model. *Optimal Control Applications and Methods* **23**, 199–213 (2002).

96. Perelson, A. S. & Nelson, P. W. Mathematical Analysis of HIV-1 Dynamics in Vivo. *SIAM Review* **41**, 3–44 (2006).

97. Perelson, A. S. Modelling viral and immune system dynamics. *Nature Reviews Immunology 2002 2:1* **2**, 28–36 (2002).

98. Miao, H., Dykes, C., Demeter, L. M. & Wu, H. Differential Equation Modeling of HIV Viral Fitness Experiments: Model Identification, Model Selection, and Multimodel Inference. *Biometrics* **65**, 292–300 (2009).

99. Perelson, A. S., Kirschner, D. E. & de Boer, R. Dynamics of HIV infection of CD4+ T cells. *Mathematical Biosciences* **114**, 81–125 (1993).

100. Cardozo-Ojeda, E. F. & Perelson, A. S. Modeling HIV-1 Within-Host Dynamics After Passive Infusion of the Broadly Neutralizing Antibody VRC01. *Frontiers in Immunology* **12**, (2021).

101. Ferl, G. Z., Wu, A. M. & DiStefano, J. J. A Predictive Model of Therapeutic Monoclonal Antibody Dynamics and Regulation by the Neonatal Fc Receptor (FcRn). *Annals of Biomedical Engineering 2005 33:11* **33**, 1640–1652 (2005).

102. Ng, C. M., Loyet, K. M., Iyer, S., Fielder, P. J. & Deng, R. Modeling approach to investigate the effect of neonatal Fc receptor binding affinity and anti-therapeutic antibody on the pharmacokinetic of humanized monoclonal anti-tumor necrosis factor-α IgG antibody in cynomolgus monkey. *European Journal of Pharmaceutical Sciences* **51**, 51–58 (2014).

103. Kendrick, F., Harding, S., Chappell, M. J. & Evans, N. D. Immunoglobulin G (IgG) and neonatal Fc-receptor (FcRn) dynamics in IgG multiple myeloma. *IFAC-PapersOnLine* **48**, 106–111 (2015).

104. Zhao, L., Ji, P., Li, Z., Roy, P. & Sahajwalla, C. G. The Antibody Drug Absorption Following Subcutaneous or Intramuscular Administration and Its Mathematical Description by Coupling Physiologically Based Absorption Process with the Conventional Compartment Pharmacokinetic Model. *The Journal of Clinical Pharmacology* **53**, 314–325 (2013).

105. Chen, Y. & Balthasar, J. P. Evaluation of a Catenary PBPK Model for Predicting the In Vivo Disposition of mAbs Engineered for High-Affinity Binding to FcRn. *The AAPS Journal* **14**, 850–859 (2012).

106. Kendrick, F. *et al.* Analysis of a Compartmental Model of Endogenous Immunoglobulin G Metabolism with Application to Multiple Myeloma. *Frontiers in Physiology* **0**, 149 (2017).

107. Robinett, R. A. *et al.* Dissecting FcγR Regulation through a Multivalent Binding Model. *Cell Systems* **7**, 41-48.e5 (2018).

108. Tan, Z. C. & Meyer, A. S. A general model of multivalent binding with ligands of heterotypic subunits and multiple surface receptors. *Mathematical Biosciences* **342**, 108714 (2021).

109. Robb, M. L. Failure of the Merck HIV vaccine: an uncertain step forward. *The Lancet* **372**, 1857–1858 (2008).

110. Hessell, A. J. *et al.* Fc receptor but not complement binding is important in antibody protection against HIV. *Nature* **449**, 101–104 (2007).

111. Rouphael, N. G. *et al.* DNA priming and gp120 boosting induces HIV-specific antibodies in a randomized clinical trial. *Journal of Clinical Investigation* **129**, 4769–4785 (2019).

112. Kratochvil, S. *et al.* A phase 1 human immunodeficiency virus vaccine trial for cross-profiling the kinetics of serum and mucosal antibody responses to CN54gp140 modulated by two homologous prime-boost vaccine regimens. *Frontiers in Immunology* **8**, 595 (2017).

113. Marino, S., Hogue, I. B., Ray, C. J. & Kirschner, D. E. A methodology for performing global uncertainty and sensitivity analysis in systems biology. *Journal of Theoretical Biology* **254**, 178–196 (2008).

114. Santillán, M. On the use of the hill functions in mathematical models of gene regulatory networks. *Mathematical Modelling of Natural Phenomena* **3**, 85–97 (2008).

115. Lloyd, S. B. *et al.* Exploration of broadly neutralizing antibody fragments produced in bacteria for the control of HIV. *Human Vaccines and Immunotherapeutics* **13**, 2726–2737 (2017).

116. Parsons, M. S. *et al.* Fc-dependent functions are redundant to efficacy of anti-HIV antibody PGT121 in macaques. *Journal of Clinical Investigation* **129**, (2019).

117. Cai, H. *et al.* Synthetic HIV V3 Glycopeptide Immunogen Carrying a N334 N-Glycan Induces Glycan-Dependent Antibodies with Promiscuous Site Recognition. *Journal of Medicinal Chemistry* **61**, 10116–10125 (2018).

118. Jefferis, R. & Lefranc, M. P. Human immunoglobulin allotypes: Possible implications for immunogenicity. *mAbs* **1**, 332–338 (2009).

119. Johnson, W. E., Kohn, P. H. & Steinberg, A. G. Population genetics of the human allotypes Gm, Inv, and A2m: An analytical review. *Clinical Immunology and Immunopathology* **7**, 97–113 (1977).

120. Dekkers, G. *et al.* Multi-level glyco-engineering techniques to generate IgG with defined Fc-glycans. *Scientific Reports* **6**, (2016).

121. Bruggeman, C. W. *et al.* Enhanced Effector Functions Due to Antibody Defucosylation Depend on the Effector Cell Fcγ Receptor Profile. *The Journal of Immunology* **199**, 204–211 (2017).

122. Li, T. *et al.* Modulating IgG effector function by Fc glycan engineering. *Proceedings of the National Academy of Sciences of the United States of America* **114**, 3485–3490 (2017).

123. Subedi, G. P. & Barb, A. W. The immunoglobulin G1 N-glycan composition affects binding to each low affinity Fc γ receptor. *mAbs* **8**, 1512–1524 (2016).

124. Chung, A. W. *et al.* Identification of antibody glycosylation structures that predict monoclonal antibody Fc-effector function. *AIDS* **28**, (2014).

125. Forthal, D. N., Gabriel, E. E., Wang, A., Landucci, G. & Phan, T. B. Association of Fcγ receptor IIIa genotype with the rate of HIV infection after gp120 vaccination. *Blood* **120**, 2836–2842 (2012).

126. Mahan, A. E. *et al.* Antigen-Specific Antibody Glycosylation Is Regulated via Vaccination. *PLoS Pathogens* **12**, (2016).

127. Chung, A. W. & Alter, G. Systems serology: Profiling vaccine induced humoral immunity against HIV. *Retrovirology* vol. 14 (2017).

128. Dugast, A. S. *et al.* Virus-driven inflammation is associated with the development of bNAbs in spontaneous controllers of HIV. *Clinical Infectious Diseases* **64**, 1098–1104 (2017).

129. Tosif, S. *et al.* Immune responses to SARS-CoV-2 in three children of parents with symptomatic COVID-19. *Nature Communications* **11**, 1–8 (2020).

130. Selva, K. J. *et al.* Systems serology detects functionally distinct coronavirus antibody features in children and elderly. *Nature Communications 2021 12:1* **12**, 1–14 (2021).

131. Madhavi, V. *et al.* HIV-1 Env- and Vpu-Specific Antibody-Dependent Cellular Cytotoxicity Responses Associated with Elite Control of HIV. *Journal of Virology* **91**, (2017).

132. Raedler, M. D. *et al.* Serologic assay to quantify human immunoglobulin G antibodies to the Staphylococcus aureus iron surface determinant B antigen. *Clinical and Vaccine Immunology* **16**, (2009).

133. Marino, S., Hogue, I. B., Ray, C. J. & Kirschner, D. E. A methodology for performing global uncertainty and sensitivity analysis in systems biology. *Journal of Theoretical Biology* **254**, 178–196 (2008).

134. Adeniji, O. S. *et al.* Covid-19 severity is associated with differential antibody fc-mediated innate immune functions. *mBio* **12**, (2021).

135. Aitken, E. H. *et al.* Developing a multivariate prediction model of antibody features associated with protection of malaria-infected pregnant women from placental malaria. *eLife* **10**, (2021).

136. Pandey, J. P. & French, M. A. H. GM phenotypes influence the concentrations of the four subclasses of immunoglobulin G in normal human serum. *Human Immunology* **51**, 99–102 (1996).

137. Webster, C. I. *et al.* A comparison of the ability of the human IgG1 allotypes G1m3 and G1m1,17 to stimulate T-cell responses from allotype matched and mismatched donors. *mAbs* **8**, 253–263 (2016).

138. Hogarth, P. M. & Pietersz, G. A. Fc receptor-targeted therapies for the treatment of inflammation, cancer and beyond. *Nature Reviews Drug Discovery 2012 11:4* **11**, 311–331 (2012).

139. Hirvinen, M. *et al.* Fc-gamma receptor polymorphisms as predictive and prognostic factors in patients receiving oncolytic adenovirus treatment. *Journal of Translational Medicine 2013 11:1* **11**, 1–12 (2013).

140. Hussain, K. *et al.* Impact of Human FcγR Gene Polymorphisms on IgG-Triggered Cytokine Release: Critical Importance of Cell Assay Format. *Frontiers in Immunology* **0**, 390 (2019).

141. Tamura, K. *et al.* FcγR2A and 3A polymorphisms predict clinical outcome of trastuzumab in both neoadjuvant and metastatic settings in patients with HER2-positive breast cancer. *Annals of Oncology* **22**, 1302–1307 (2011).

142. Sanders, L. A. M. *et al.* Human immunoglobulin G (IgG) Fc receptor IIA (CD32) polymorphism and IgG2- mediated bacterial phagocytosis by neutrophils. *Infection and Immunity* **63**, 73–81 (1995).

143. Forthal, D. N. *et al.* FcγRIIa Genotype Predicts Progression of HIV Infection. *The Journal of Immunology* **179**, 7916–7923 (2007).

144. Wang, W., Erbe, A. K., Hank, J. A., Morris, Z. S. & Sondel, P. M. NK Cell-Mediated Antibody-Dependent Cellular Cytotoxicity in Cancer Immunotherapy. *Frontiers in Immunology* **0**, 368 (2015).

145. Cartron, G. *et al.* Therapeutic activity of humanized anti-CD20 monoclonal antibody and polymorphism in IgG Fc receptor FcγRIIIa gene. *Blood* **99**, 754–758 (2002).

146. Poonia, B., Kijak, G. H. & Pauza, C. D. High Affinity Allele for the Gene of FCGR3A Is Risk Factor for HIV Infection and Progression. *PLOS ONE* **5**, e15562 (2010).

147. Lemke, M. M. *et al.* A systems approach to elucidate personalized mechanistic complexities of antibody-Fc receptor activation post-vaccination. *Cell Reports Medicine* **2**, 100386 (2021).

148. Dekkers, G. *et al.* Decoding the human immunoglobulin G-glycan repertoire reveals a spectrum of Fc-receptor- and complement-mediated-effector activities. *Frontiers in Immunology* **8**, (2017).

149. Lee, W. S. *et al.* Decay of Fc-dependent antibody functions after mild to moderate COVID-19. *Cell Reports Medicine* **2**, 100296 (2021).

150. Pozzetto, B. *et al.* Immunogenicity and efficacy of heterologous ChadOx1/BNT162b2 vaccination. *Nature 2021* 1–9 (2021) doi:10.1038/s41586-021-04120-y.

151. Mestecky, J. *et al. Paucity of Antigen-Specific IgA Responses in Sera and External Secretions of HIV-Type 1-Infected Individuals*. *AIDS RESEARCH AND HUMAN RETROVIRUSES* vol. 20 www.liebertpub.com (2004).

152. Nguyen-Contant, P. *et al.* S protein-reactive IGG and memory B cell production after human SARS-CoV-2 infection includes broad reactivity to the S2 subunit. *mBio* **11**, 1–11 (2020).

153. Walls, A. C. *et al.* Elicitation of Potent Neutralizing Antibody Responses by Designed Protein Nanoparticle Vaccines for SARS-CoV-2. *Cell* **183**, 1367-1382.e17 (2020).

154. Zhao, Z. *et al.* New Insights from Chemical Biology: Molecular Basis of Transmission, Diagnosis, and Therapy of SARS-CoV-2. *CCS Chemistry* 1501–1528 (2020) doi:10.31635/ccschem.020.202000322.

155. Vogel, A. B. *et al.* BNT162b vaccines are immunogenic and protect non-human primates against SARS-CoV-2. *bioRxiv* 27 (2020) doi:10.1101/2020.12.11.421008.

156. Shi, R. *et al.* A human neutralizing antibody targets the receptor-binding site of SARS-CoV-2. *Nature* **584**, 120–124 (2020).

157. Huo, J. *et al.* Neutralization of SARS-CoV-2 by Destruction of the Prefusion Spike. *Cell Host and Microbe* **28**, 445-454.e6 (2020).

158. Tian, X. *et al.* Potent binding of 2019 novel coronavirus spike protein by a SARS coronavirus-specific human monoclonal antibody. *Emerging Microbes and Infections* vol. 9 382–385 (2020).

159. Huo, J. *et al.* Neutralizing nanobodies bind SARS-CoV-2 spike RBD and block interaction with ACE2. *Nature Structural and Molecular Biology* **27**, 846–854 (2020).

160. Seydoux, E. *et al.* Analysis of a SARS-CoV-2-Infected Individual Reveals Development of Potent Neutralizing Antibodies with Limited Somatic Mutation. (2020) doi:10.1016/j.immuni.2020.06.001.

161. Cocklin, S. L. & Schmitz, J. E. The role of Fc receptors in HIV infection and vaccine efficacy. *Current opinion in HIV and AIDS* **9**, 257 (2014).

162. Pandey, J. P. *et al.* Immunoglobulin genes and the acquisition of HIV infection in a randomized trial of recombinant adenovirus HIV vaccine. *Virology* **441**, 70–74 (2013).

163. Pepperrell, T. *et al.* Making a COVID-19 vaccine that works for everyone: ensuring equity and inclusivity in clinical trials. *Global Health Action* **14**, (2021).

164. Newman, P. A. *et al.* HIV Vaccine Trial Participation Among Ethnic Minority Communities: Barriers, Motivators, and Implications for Recruitment. *JAIDS Journal of Acquired Immune Deficiency Syndromes* **41**, (2006).

165. Pitisuttithum, P. & Marovich, M. A. Prophylactic HIV vaccine: vaccine regimens in clinical trials and potential challenges. *Expert Review of Vaccines* **19**, 133–142 (2020).

166. Tomaras, G. D. & Plotkin, S. A. Complex immune correlates of protection in HIV-1 vaccine efficacy trials. *Immunological Reviews* **275**, 245–261 (2017).

167. Mayr, L. M., Su, B. & Moog, C. Non-neutralizing antibodies directed against HIV and their functions. *Frontiers in Immunology* **8**, 1590 (2017).

168. Alter, G., Ottenhoff, T. H. M. & Joosten, S. A. Antibody glycosylation in inflammation, disease and vaccination. *Seminars in Immunology* **39**, 102–110 (2018).

169. Johnson, P. M. & Faulk, W. P. Rheumatoid factor: Its nature, specificity, and production in rheumatoid arthritis. *Clinical Immunology and Immunopathology* **6**, 414–430 (1976).

170. Wat, D. The common cold: a review of the literature. *European Journal of Internal Medicine* **15**, 79–88 (2004).